Title

Utilizing Biogeochemical and Genetic Tools to Understand and Support Clam Populations in a Changing Ocean

Author

Kempf, Hannah

Publication Date

2024

Utilizing Biogeochemical and Genetic Tools to Understand and Support Clam Populations in a Changing Ocean

By

HANNAH L. KEMPF
DISSERTATION

Submitted in partial satisfaction of the requirements for the degree of

DOCTOR OF PHILOSOPHY

in

Earth and Planetary Sciences

in the

OFFICE OF GRADUATE STUDIES

of the

UNIVERSITY OF CALIFORNIA

DAVIS

Approved:

_____

David Gold, Co-Chair

_____

Sandra Carlson, Co-Chair

_____

Tessa Hill

Committee in Charge

2024

Table of Contents

Abstract

Marine bivalves are at risk due to anthropogenic climate change. This poses a threat to commercial aquaculture, and the communities that depend on bivalves for food security. Ocean acidification, the lowering of seawater pH, is of particular concern for marine calcifiers, including bivalves. Ocean acidification occurs as carbon dioxide enters the atmosphere at a rate faster than natural geologic processes can buffer. It is energetically costly for marine calcifiers like clams, mussels, and oysters, to mineralize under acidic conditions, and low pH leads to the dissolution of calcium carbonate shells and skeletons. This problem warrants research on acidification adaptation strategies that will keep coastal populations healthy. Adding calcium carbonate shell hash to coastal sediments may mitigate negative effects of acidification on infaunal shellfish by altering the chemistry of pore fluids, thus providing a potential mitigation strategy for local populations, including species like the Pacific littleneck clam (*Leukoma staminea*).

Here, I present the first in-depth description of the shell mineralogy, microstructure, body size variability, and geochemical properties of modern *L. staminea*, a common eastern Pacific, shallow, infaunal bivalve. Additionally, I document the impact of ocean acidification on the shell growth and gene expression of *L. staminea*, and test whether adding shell hash to its infaunal environement can promote growth under acidified conditions. Juvenile clams were raised in four experimental conditions for 90 days: control seawater, acidified seawater, control seawater with shell hash, and acidified seawater with shell hash. Clam shell weight, soft tissue weight, and new shell growth were measured. The presence of shell hash increased the pH, alkalinity and aragonite saturation state of pore fluids across all treatments, and increased shell

growth on average, although growth metrics were variable across and within treatments. Lastly, RNA-sequencing revealed the impacts of experimental acidification on juvenile clam gene expression. Clams grown in the presence of shell hash had gene expression profiles more similar to those grown in control (non-acidified) conditions. In all, this research suggests that adding shell hash to coastal sediments alters the chemistry of pore fluids and buffers against acidic conditions that deleteriously affects clam mineralization.

Acknowledgements

Finishing this dissertation would not have been possible without the support of some incredible people. Thank you to my co-advisors, Drs. Sandy Carlson and David Gold. When I applied to UC Davis, I thought I wanted to study deep-time paleoecology questions. When I started to re-evaluate my research goals during my first year, Sandy and David encouraged me to explore new topics, and allowed space for me to learn and change course (a couple of times). I'm very grateful to have had mentors that trusted me, while also providing much needed guidance and perspective along the way. Also, thank you to Drs. Tessa Hill, Tsim Schneider and Alyssa Griffin for your support, feedback, and encouragement throughout my time at UC Davis and the Bodega Marine Lab. I'm so thankful to work with such bright and passionate professors, all of whom were integral to this project.

To my dear friends from home, especially Harry. I would not be finishing this degree without you. You continue to be one of my biggest cheerleaders, and I am so thankful. Thank you to my sweet pup, Luna, who makes every day better. To all my friends in Davis, especially Meghan Z., Chris, Noemie, Liyu, Tessa, Elizabeth, Kaitlyn, Elaine, and Becky – graduate school would have been way less fun without you. Becky, your passion for the Earth and all its strangeness is contagious in the best possible way. You make me want to be a better human and a better scientist. I will always be thankful that graduate school brought us together.

Most of all, I want to thank my parents, Barb and Rich Kempf. They've fostered my love for the outdoors since I was a little kid. They've encouraged my nerdiness without pushing me too hard or expecting me to perform perfectly. They took us camping and to see national parks. They thought my rock collection was cool. My dad read *Hamlet* with me in high school and made it fun. My mom never got mad when I brought home a lunchbox full of trash that I

collected on the playground as a weird little kindergartner. I am so grateful to have parents like them. To my sisters, Emma and Attie, you two are the people I look up to the most. I'm constantly in awe of your abilities to "do it all" – have successful careers, be amazing mothers and partners, and continue caring for your little sister even when we're thousands of miles apart.

Chapter 1.

Investigating the relationship between growth rate, shell morphology, and trace element composition of the Pacific littleneck clam (*Leukoma staminea*): implications for paleoclimate reconstructions

minerals

MDPI

Article

Investigating the Relationship between Growth Rate, Shell Morphology, and Trace Element Composition of the Pacific Littleneck Clam (*Leukoma staminea*): Implications for Paleoclimate Reconstructions

Hannah L. Kempf *, David A. Gold and Sandra J. Carlson

Department of Earth and Planetary Sciences, University of California, Davis, CA 95616, USA; dgold@ucdavis.edu (D.A.G.); sjcarlson@ucdavis.edu (S.J.C.)
* Correspondence: hlkempf@ucdavis.edu

Abstract: Due to their robust preservation and widespread nature, marine bivalve shells are increasingly used as informative, high-resolution records of past environmental conditions. Unfortunately, few studies have investigated variability amongst individuals in a genetic cohort and throughout their ontogeny. We measured several morphological properties and the element patterning of 200-day-old juvenile *Leukoma staminea* (Conrad, 1837) grown in identical conditions from the same reproductive cohort. We hypothesized that slower shell growth would correspond to the reduced incorporation of trace/minor elements (Sr, Mg, and S) in the aragonite lattice, as has been documented in other biomineralizing marine invertebrates. Microprobe analyses of adult shells revealed higher levels of S, Sr, and Mg in the dark, slower-growing growth lines compared to the light, faster-growing increments, particularly in the inner shell layer, thus refuting our hypothesis. Moreover, elemental count variation within single adult shells generally tracked changes in shell microstructure (i.e., higher counts in prismatic microstructures) and growth line patterns, and these differences are detectable on a micrometer scale. Juvenile shells of different sizes showed variation in S, Sr, and Mg counts as well, but it was unclear whether the variability closely tracked changes in microstructure, body size, and/or growth line patterns. In all individuals, regardless of life stage, the outermost shell layer showed higher Sr and S count values, and these elements closely mirrored each other within individual shells. The results presented herein represent the first in-depth description of the shell mineralogy, microstructure, body size variability, and geochemical properties of modern *L. staminea*, a common eastern Pacific, shallow, infaunal bivalve, allowing for the rigorous evaluation of *L. staminea* shells as recorders of past environmental and biological change. Significant intraspecific variation in the young body size, growth band patterning, and elemental composition of individuals of the same age and genetic stock complicates the use of size alone as a proxy for age in historical studies. Additionally, elemental composition shifted from high to low values (for example, Sr ranging from ~190 to 100 counts) at a very fine (micrometer) scale within single shells, as evidenced by visible correlations between microstructure and elemental composition. While young *L. staminea* shells are likely not useful as archives of (paleo)environmental conditions, adult *L. staminea* shells are likely suitable if micrometer-scale variability in shell structure and chemistry is accounted for.

Keywords: biomineralization; paleoclimate; microstructure

Citation: Kempf, H.L.; Gold, D.A.; Carlson, S.J. Investigating the Relationship between Growth Rate, Shell Morphology, and Trace Element Composition of the Pacific Littleneck Clam (*Leukoma staminea*): Implications for Paleoclimate Reconstructions. *Minerals* **2023**, *13*, 814. https://doi.org/10.3390/min13060814

Academic Editors: Chiara Lombardi, Paul D. Taylor and Frédéric Marin

Received: 8 May 2023
Revised: 10 June 2023
Accepted: 12 June 2023
Published: 14 June 2023

1. Introduction

Readily preserved in a wide range of conditions due to their hard, mineralized calcium carbonate shells, bivalve molluscs are increasingly used as high-resolution records of both distant and recent past oceanographic conditions [1–4]. Despite a growing body of knowledge, few studies have investigated variability amongst individuals in a genetic cohort. To test the influence of growth rate on aragonitic biomineralization, we investigated

the shell morphology, microstructure and chemical composition of Pacific littleneck clams, *Leukoma staminea* (Conrad, 1837), of multiple sizes and life stages. We hypothesized that periods of slower growth correspond to lower values of trace/minor elements (Sr, Mg, and S) in the shell because slower calcification can allow for the exclusion of "impurities" from the $CaCO_3$ crystal lattice [5–7]. Interestingly, though, as calcification rate increases in *Arctica islandica* (Linnaeus, 1767), another marine bivalve, the Ba, Mg, and Sr/Ca ratios *decrease* in a nonlinear fashion, and patterns vary across individuals studied and locations of collection [5]. This highlights the need to study species-specific relationships between growth and trace/minor element shell chemistry. To test our hypothesis, we evaluated various morphological properties and element patterning of 200-day-old juvenile *L. staminea* clams grown in identical conditions from the same reproductive cohort. Additionally, we analyzed the parent individuals from Bodega Bay, CA to make comparisons across life stages of individuals from a common genetic stock. We then used this information to rigorously evaluate the utility of *L. staminea* shells as records of historical environments. By examining animals from multiple life stages, we captured both pre-sexual maturity and post-sexual maturity shell features and made comparisons among and within individuals. We provide the first in-depth description of the shell mineralogy, microstructure, body size variability, and geochemical properties of *L. staminea*, and we determine whether and how differences in growth rate and life stage correspond to changes in shell structure and trace element patterns.

Bivalve shell morphology, body size variability, and chemistry have been analyzed to infer historical patterns of shellfish harvesting by humans [6–8], as well as recent and paleo-oceanographic conditions [1–4]. To use shells as records of environmental and climatic trends, biominerals and the complex interplay between physiology and the environment from which they arise must be understood. Biomineralized calcite and aragonite from corals [9], foraminifera [10–12], and marine bivalves [1,13,14] can serve as records of past oceanographic conditions when evaluated with stable isotopes, and trace and/or minor elements. These organisms actively incorporate molecules present in seawater into their shells and skeletons and therefore can capture the chemical properties of seawater and record changes throughout their development. Some trace and minor elements, including Sr, Mg, Na, B, and Ba, can record properties such as seawater temperature and salinity at the time of calcification [10,14,15]. However, how element concentrations in the shell change as body size increases and shell shape changes is not always straightforward and is complicated by ontogeny, "vital" or other biological effects, and environmental conditions [15–17].

During abiotic crystallization, Sr ions can be incorporated into the aragonite lattice at concentrations approaching twice as high as in calcite due to (1) the structure of the crystal lattice and the larger size of the Sr ion and (2) because Sr is strongly precipitation-rate-dependent in inorganic calcite (but not aragonite), with slower growth leading to less incorporation [18,19]. Furthermore, inorganic aragonite shows an inverse relationship between temperature and Sr concentration [18] and is independent of precipitation rate [20]. Although metal-Ca ratios show predictable correlations with temperature in inorganic aragonite and calcite [18,20,21], the relationships show little consistency across biomineralized species and often deviate from elemental equilibrium due to several co-varying "vital effects" [22–24]. During biomineralization, vital effects, including metabolic rate, ontogenetic age, genetic variability, and growth rate, are known to affect the incorporation of elemental impurities into shells, causing discrepancies across (and within) species [23–25]. Differences in species-specific organism development may translate to some species having more dramatic vital effects than others, and some are likely more influenced by their ambient chemical environment than others. Because of these complexities, studies investigating these relationships are necessary to further document species' variability.

Across bivalve species, immense variability in shell trace element incorporation exists. For example, the middle layer of the aragonitic venerid clam *Mercenaria campechiensis* (Gmelin, 1791) exhibits Sr/Ca ratios negatively correlated with seawater temperature [26],

while the outer layer of another venerid, *Saxidomus gigantea* (Deshayes, 1839), exhibits Sr/Ca ratios positively correlated to temperature [27]. Additionally, metal-Ca ratios can vary significantly throughout the ontogeny of a single individual, as was demonstrated in the large Mediterranean clam, *Pinna nobilis* (Linnaeus, 1758), which is a member of the more distantly related Pteriomorphia [28,29]. Such variation throughout ontogeny can impact metal-Ca ratios among individuals within a population. For example, slower-growing *Arctica islandica* individuals maintained lower Mg- and Sr-to-Ca ratios in their aragonitic shells than faster growing individuals of the same population, complicating its use as a species-specific paleo-archive and illustrating the importance of incorporating intraspecific growth rate variation into sclerochronological analyses [25]. Given these complexities, paleoclimate reconstruction using chemical proxies of biogenic materials requires a deep understanding of biomineralization mechanisms across species, among populations, and within single individuals.

In addition to chemical proxies, microstructural changes within a shell may reflect organisms' response to shifts in environment throughout development [30]. Like trace elements, though, the precise relationships between microstructure and environment are underexplored, potentially species-specific, and could vary within populations due to genetic variability. During biomineralization, the molecules needed to produce $CaCO_3$ microstructures are transported into and out of the calcifying fluid from the ambient environment via potentially energetically costly transport processes [31,32]. The degree to which the site of calcification is isolated from the environment varies by species [15], and the mechanisms underlying element partitioning in shells are complex and variable. In bivalve molluscs, biomineralization occurs extracellularly on organic templates, the diverse array of which are hypothesized to determine the species-specific mineralogy and shell microstructure [15,33–35]. Recent work suggests minor elements, such as Mg^{+2}, play an important role in the transformation of the amorphous calcium carbonate precursor to organized calcite and aragonite crystals [36,37]. Furthermore, despite the small amounts of proteinaceous material in bivalve shells, researchers have documented a diverse array of amino acid compositions across species as well as within-single species' microstructurally distinct layers [33,38], supporting the hypothesis that microstructural changes within a shell may reflect changes in organic composition at the site of calcification throughout development [35]. Clearly, both the final shell microstructure and trace/minor element geochemistry result from a complex interplay of whole-organism biological and environmental processes. While a thorough understanding of shell microstructure, growth patterning, and geochemistry is not always straightforward, it is necessary to (1) understand the mechanisms involved in element partitioning in biogenic minerals; (2) characterize the variability among individuals, conspecific populations, and among species; and (3) accurately interpret shells of marine organisms as archives of historical conditions.

Leukoma Staminea as a Study Organism

The Pacific littleneck clam, *L. staminea*, is an excellent focal species because it is geographically widespread, abundant, easily collected, and ecologically and culturally significant [39–42]. *L. staminea* is an infaunal marine bivalve (Veneridae) that burrows 5–15 cm beneath the sediment surface and is found along nearly the entire coast of western North America, ranging from Baja California, Mexico to Alaska [39,43]. Found in a variety of habitats ranging from exposed rocky beaches to low-energy mudflats, *L. staminea* is a suspension feeder that feeds on a variety of plankton [39]. Sexual maturity occurs at around 2–3 years, and spawning takes place in late-spring and early summer [39,44]. *L. staminea* have been harvested for millennia by Indigenous peoples across the northeastern Pacific coast [40,41] and remain commonly collected and eaten today. Recent research has documented *L. staminea* population decline in some areas, likely due to competition with invasive species [45].

L. staminea produces aragonitic shells that contain light and dark banding patterns in the outer layers [39,46] (Figures 1 and 2). Until this study, the fine-scale shell structure,

growth patterning, relationship between dark/light patterns and chemical properties of the shell, and patterns of ontogenetic variation in individual size and shape had not been studied extensively [46]. Generally, though, under reflected light, bivalve shell sections often exhibit patterns of light and dark banding, where light increments correspond to fast growth in optimal conditions, and dark bands to slow (or nearly ceased) growth in stressful conditions [4,47–49]. The well-studied, long-lived bivalve species *A. islandica* documents high resolution environmental trends via daily and annual growth lines that closely follow differences in shell stable isotope and elemental chemistry [2,14,50]. While the extensive research on *A. islandica* demonstrates its utility as a record of past climate and seasonal trends, research on additional bivalve species (particularly common, temperate zone species) aimed at evaluating their utility as a record of environmental change is limited [4].

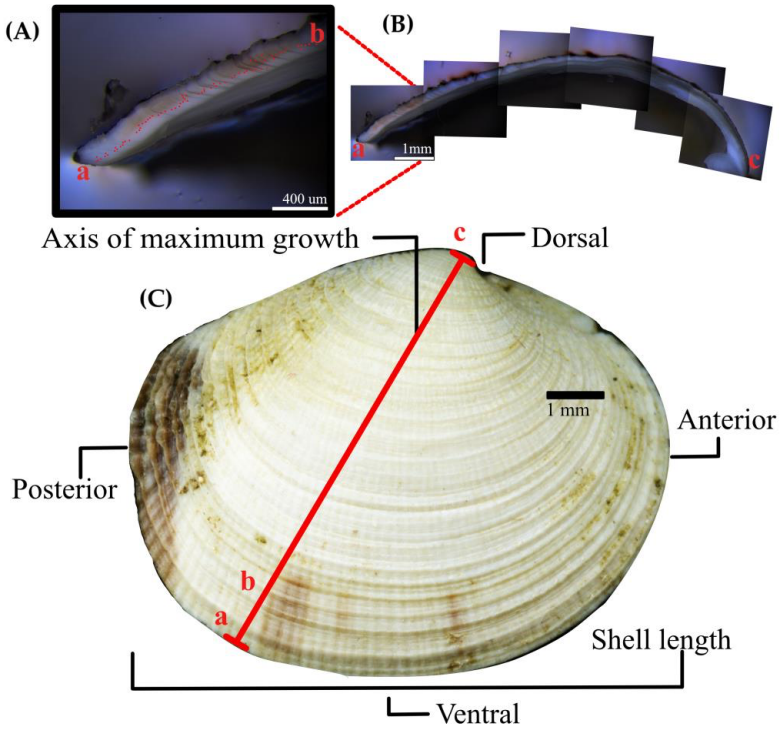

Figure 1. *L. staminea* anatomy. (**A**) ventral margin of juvenile; red dots within the cross section mark sub-annual growth bands; scale = 400 um. (**B**) entire cross sectional view of juvenile shell; scale = 1 mm. (**C**) Whole-shell image and shell cross section are from a 200-day-old juvenile. Red line denotes the axis of maximum growth along the shell; scale = 1 mm.

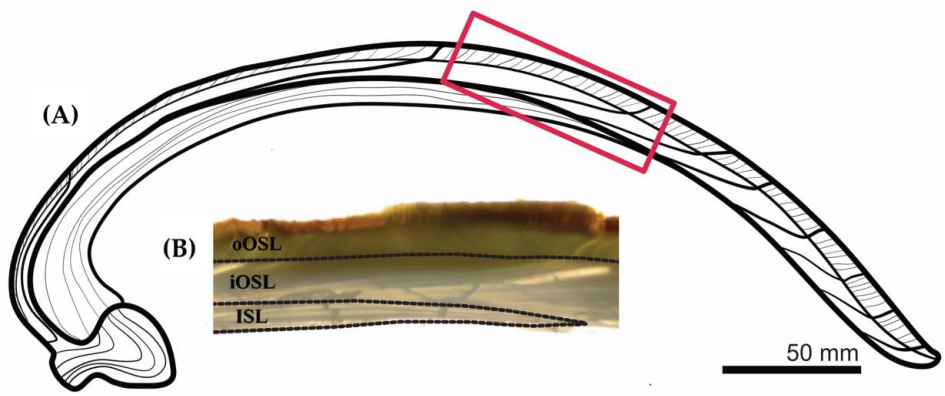

Figure 2. (A) Drawing of an *L. staminea* shell cross section showing microstructurally distinct layers. Red box denotes approximate area of the shell imaged in below in 2B. Scale: 50 mm. (**B**) Transmitted light microscopy image showing microstructurally distinct shell sublayers in an adult *L. staminea* shell. Scale: 50 mm.

2. Materials and Methods

2.1. Oceanographic Setting of Broodstock Sampling Location

Bodega Bay is located approximately 60 miles north of San Francisco on the central coast of California. The area sits within the California Current System, which is composed of various currents that create the complex mosaic of oceanographic conditions off the California coast [51,52]. Coastal waters around Bodega Bay experience seasonal upwelling during the spring-early summer months associated with strong alongshore winds and Ekman transport, with temperatures from ~10 to 12 °C, followed by autumn relaxation periods with temperatures around ~13 to 15 °C, and wet, moderate winters with seawater temperatures ~11 °C [53,54]. Average seawater pH varies widely from ~7.6 to ~8.0 throughout the region due to seasonally influenced physical processes, including wind stress and upwelling, which lower pH, as well as diel cycles of photosynthesis and respiration [54–57].

2.2. Sample Collection and Preparation

We analyzed a total of 41 *L. staminea* specimens, including 36 juvenile clams (ranging from ~5 mm–12 mm) and five broodstock adults (~3 cm). Adult broodstock were collected from Bodega Harbor in Bodega Bay, CA in the winter of 2021. Adults underwent a controlled mass spawn in the laboratory, which produced the juveniles used in this study (Supplemental Information). All juvenile specimens were kept in identical, consistent conditions for 200 days before they were collected from group culture in November 2021. Due to the fragility of the juvenile shells, these samples were immediately frozen in −80 °C and allowed to thaw to open the valves. Adult individuals were carefully opened using a shucking knife. Shells were cleaned by gently scraping out the soft tissues, which were then frozen in −80 °C, subsequently rinsed in water-free ethyl alcohol, and air–dried.

2.3. Shell Morphology and Growth Banding

Shell morphology was examined to identify the precise relationships between juvenile body size, growth rate, shell chemistry, and structure. Morphological characteristics measured included shell length, the length of axis of maximum growth, shell mass, and the number of internal dark growth lines visible in the entire shell (Figure 1). The whole valve shell length and axis of maximum growth of each individual was measured using digital calipers (0.1 mm accuracy), and shell mass (g) was measured using a Mettler Toledo M140E scale (Mettler-Toledo, LLC, Columbus, OH, USA) (0.0001 g).

To quantify growth banding patterns in juveniles of the same age from a genetic cohort, 18 juvenile shell cross sections were prepared and imaged using light and stereoscopic microscopes to count growth lines. The fragility of the juvenile shells made it infeasible to produce high quality polished thin sections. Therefore, juveniles were embedded in 1-inch epoxy rounds, cut in half, polished, and imaged using an Olympus SZX10 stereoscope (Olympus Corporation, Tokyo, Japan) with PRECiV software. Growth lines were counted manually on images in Affinity Designer 2 (Figure 1; Supplemental Information).

2.4. Microstructual Properties: SEM Analyses

Scanning electron microscopy (SEM) was used to generate two-dimensional images of shell microstructural textures at a very fine scale in cross-section. To document the shell microstructure and crystal orientation of each shell layer and throughout ontogeny, two broodstock adults were examined with a high-resolution scanning electron microscope (Philips XL30 SEM) (SEMTech Solutions, Inc., North Billerica, MA, USA). To prepare samples for SEM, shell thin sections along the axis of maximum growth were prepared by gluing whole valves to a plexiglass cube, which was then covered with a layer of epoxy resin and dried overnight. A low speed Buehler Isomet saw was used to cut 200-µm sections along the axis of maximum growth for each valve. Sections were ground using Buehler silicon carbide papers of different grit sizes and mounted on a grinder-polisher machine. After each grinding step, the blocks were rinsed in an ultrasonic bath for two minutes and observed with transmitted light to check for the quality of the polish. For SEM, sections were etched in 1 vol% HCl for 10 s and bleached in 6 vol% NaOCl for 30 min. After air-drying for at least 24 h, samples were attached to SEM stubs using double-sided tape and coated with gold using a sputter coater. To identify ontogenetic variability in microstructural fabrics, micrographs were taken at or near the thickest part of the shell to capture the microstructural properties of all mineralogical layers, as well as within both growth lines and increments in two broodstock adults. Images were taken at the same sections of the shell as the electron microprobe (EMP) analyses described below and ranged from 65× to 2500× magnification.

2.5. Trace Element Composition: EMP Analyses

EMP is a non-destructive method to evaluate fine-scale element patterns in solid materials, where samples are bombarded with a condensed electron beam, which then produces X-rays characteristic of an element. To identify the precise relationships between body size; growth rate; shell structure; and the incorporation of Mg, Sr, and S, we produced two dimensional elemental maps using a JEOL JXA-8230 electron microprobe (JEOL Ltd., Tokyo, Japan) at the Stanford University Mineral and Microchemical Analysis Facility. We produced maps of S, Sr, and Mg for four individuals (one ~35 mm adult, and three juveniles ranging from 5–12 mm in length). We imaged the entire cross section for each juvenile shell and produced maps showing the section of interest in the adult shell, capturing all of the shell sublayers (Figure 2).

EMP maps were produced using wavelength-dispersive spectroscopy for high precision, highly sensitive elemental mapping at 2-µm resolution. The electron beam was regulated at a current of 400 nA with a dwell time in 100 ms in all samples. X-rays are generated at the main element peak (element k-alpha) when the shell is bombarded by electrons. Each map illustrates the relative intensity of X-ray counts along the cross section of the shell, which are reflected by a color scale indicative of the relative amount of each element (see Section 3). Beam conditions were kept constant across runs, allowing us to qualitatively compare element incorporation across different samples as well as within each sample.

2.6. Statistical Analyses

Morphological variability and relationships among growth parameters in juveniles (n = 18) were analyzed with linear and exponential regression. All regression analyses

were performed in R (version 4.3.0). Furthermore, in addition to a qualitative analysis of microprobe count values, we utilized Fiji to calculate the minimum, maximum, mean, and standard deviation of gray-scale values (i.e., the average of the three component colors (R, B, and G)) along line profiles of the shell [58]. This analysis was performed to quantitatively confirm element variation between structurally distinct layers in adult specimens.

3. Results

3.1. Shell Morphology and Growth Banding

Adult *L. staminea* shells exhibit three microstructurally distinct aragonitic layers. This finding differs from previous studies, which only described two distinct layers [46]. Somewhat similar to well-studied *A. islandica*, *L. staminea* shells consist of an outer shell layer with two sublayers, which we refer to as the inner (iOSL) and outer-outer shell layer (oOSL) and an inner shell layer (ISL) [50] (Figure 2). Thin sections cut to a 200-µm uniform thickness and viewed under transmitted light reveal growth banding (i.e., dark and light sections of shell) present in the outer shell sublayers (iOSL and oOSL) (Figure 2). These growth patterns demonstrate that *L. staminea* lengthens its shell via ventral margin extension of these layers. The innermost layer contains growth lines/increments that run approximately parallel to the shell surface. This layer thickens, rather than lengthens, the shell, likely after the first shell is deposited very early in ontogeny between 6–11 mm in length (see Section 3.3), thus strengthening the shell. Furthermore, the ISL tapers off near the middle of the shell (Figure 2). Viewed under a stereoscope, juvenile shells from the same reproductive cohort also exhibited layered shells but lacked a clear boundary between the oOSL and iOSL. Further, juveniles exhibited highly variable body sizes despite rearing in identical conditions (Table 1; Figure 3). In general, greater shell length and weight correlated with more visible internal growth bands in the outer shell layer, and this relationship is statistically significant ($p < 0.001$) (Figure 3).

Table 1. Shell metrics (mm) (mean ± standard deviation) of juvenile clams raised in identical conditions.

Shell Weight (mg) (n = 36)	Shell Length (mm) (n = 36)	Axis of Maximum Growth (mm) (n = 36)	Number of Dark Growth Lines (n = 18)
121.7 ± 151.2	10.8 ± 3.3	9.3 ± 2.6	91 ± 46

3.2. Microstructural Properties: SEM Analyses

SEM micrographs reveal three microstructurally distinct layers in the shells of adult *L. staminea*. In the iOSL and oOSL, annual and semiannual growth lines and increments all exhibited homogeneous microstructures with crystals of various sizes and orientations (Figure 4). When viewed qualitatively, the oOSL showed slightly smaller crystal sizes and more distinct boundaries between dark cessation lines and adjacent increments than the iOSL (Figure 4). Growth lines are characterized by slight textural changes in the shell cross sectional surface, but the microstructure appears to remain homogenous (Figure 4). However, there is not a clear, systematic microstructural boundary observed between a growth line and an adjacent growth increment in the SEM images in the two outer shell layers (Figure 4). The ISL was dominated by increments composed of well-organized cross acicular microstructure, and growth lines running approximately parallel to the direction of growth composed of prismatic microstructures (Figure 4). The observed growth patterns of *L. staminea* mirrored other bivalve species in some ways, including the well-studied species *Arctica islandica* [25,35,47,50,59]. For example, *A. islandica* also contains an OSL with two microstructurally different sublayers (an oOSL and an iOSL) [60]. Despite similarities to *A. islandica*, it is important to note that these two genera are classified in different families, and microstructures are incredibly variable across Bivalvia, with paleontologists, or anyone studying sclerochronological patterns in bivalves, sometimes using them as discerning characters in identifying fossils [38].

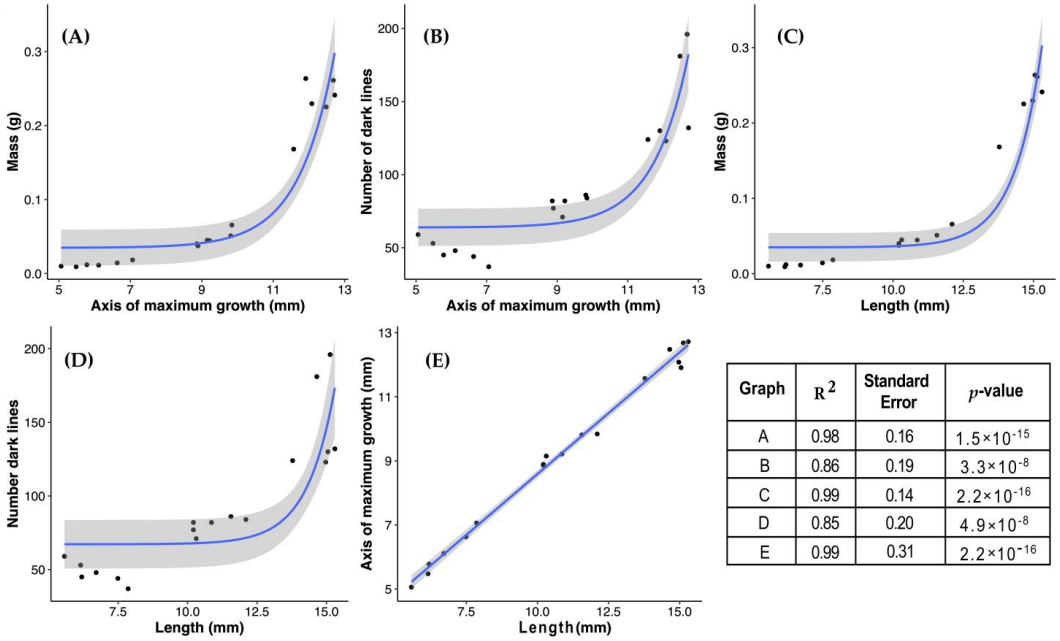

Graph	R^2	Standard Error	*p*-value
A	0.98	0.16	1.5×10^{-15}
B	0.86	0.19	3.3×10^{-8}
C	0.99	0.14	2.2×10^{-16}
D	0.85	0.20	4.9×10^{-8}
E	0.99	0.31	2.2×10^{-16}

Figure 3. Morphological variability and relationships among growth parameters in juveniles (n = 18). Variables were compared using linear and exponential regression analyses in R. Data shown in (**A**–**D**) are fit with exponential regression, while (**E**) is a linear regression. All regression analyses were performed in R. Shaded gray shows 95% CI for regression.

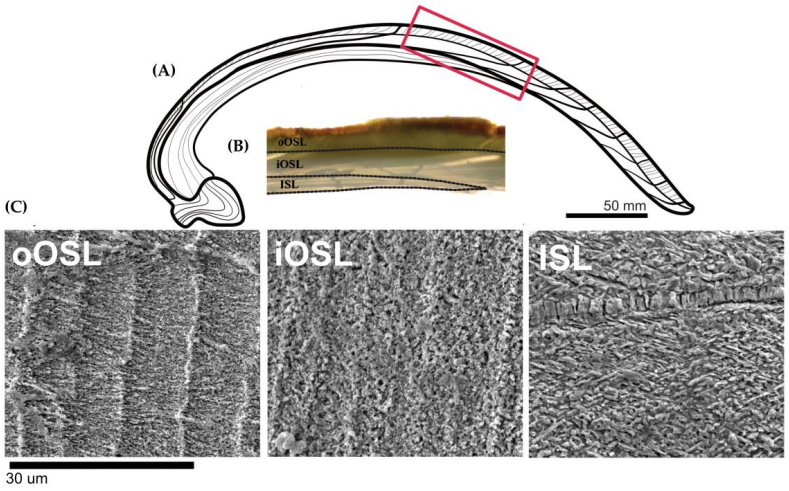

Figure 4. (**A**) Drawing of an *L. staminea* shell cross section showing microstructurally distinct layers, as shown in Figure 2, scale bar: 50 mm. (**B**) Transmitted light microscopy image showing microstructurally distinct shell sublayers in an adult *L. staminea* shell, scale bar: 50 mm. (**C**) SEM images of microstructures present in adult *L. staminea* shell layers; scale bar: 30 µm. oOSL = outer shell layer; ISL = inner shell layer; and iOSL = inner outer shell layer. The structure in the oOSL appears to respond more clearly to periodicities in the environment, and the ISL less clearly.

3.3. Trace Element Composition: EMP Analyses

Microprobe analyses show that Sr, S, and Mg concentrations vary throughout the shells of all analyzed shells (n = 4). When viewed qualitatively, all individuals clearly contain chemically distinct layers of the shell that correspond to the structurally distinct layers visible under stereoscopic and transmitted light, deposited over time during ontogeny. In the adult specimens, the area of interest captured all microstructurally distinct layers (Figure 5). The oOSL and iOSL show evidence of dark growth lines that are relatively enriched in Sr (~190 counts) and S (~50 counts) when compared to growth increments, which are distinguished by thickness (Figure 5). Growth increments, on the other hand, contain Sr values of ~100 counts and S values of ~15 counts. In the same individual, the ISL shows markedly higher Sr, with count values ranging from ~190–218. Mg varied throughout the shell in a similar manner to Sr and S, but the differences between the growth lines and increments are less distinct. Generally, Mg values ranged from ~20–40 counts throughout the entire shell section analyzed (Figure 5). Additionally, the average gray-scale values of each layer varied significantly between the ISL, iOSL, and oOSL (Figure S1; Table S1). As mentioned previously, the microstructure of the growth increments differs from that of the growth lines in the adult specimen, particularly in the inner shell layer, which corresponds closely with changes in shell elemental chemistry (Figure 6).

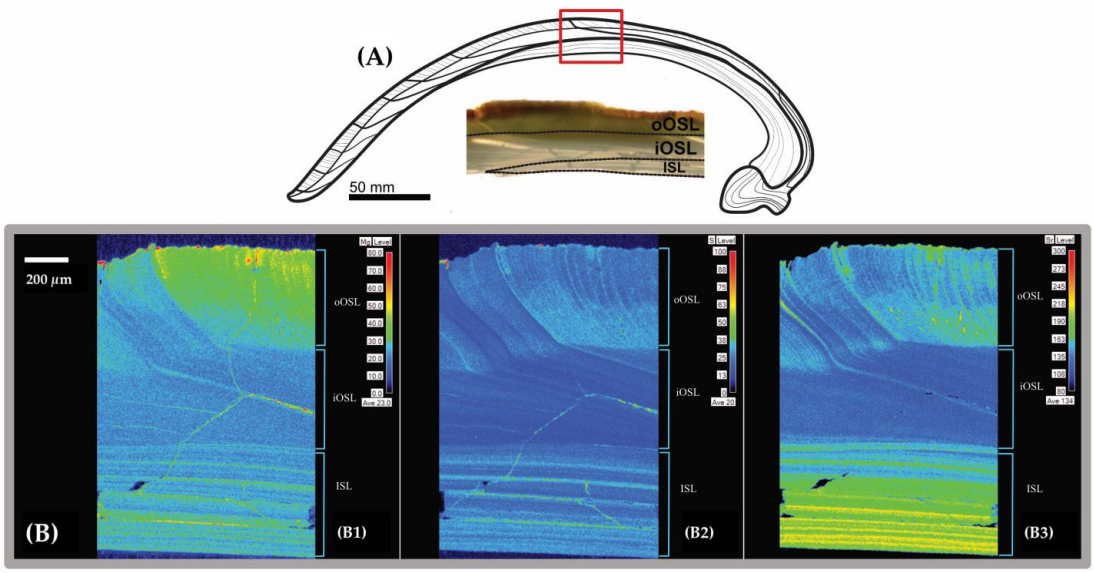

Figure 5. Element maps of adult *L. staminea*. (**A**) drawing of shell section and transmitted light cross sectional view of microstructurally distinct layers; red box: area of interest for element maps. (**B**) Element maps. B1. Mg, B2. S, B3. Sr. Scale bar: 200 µm. oOSL = outer shell layer; ISL = inner shell layer; and iOSL = inner outer shell layer.

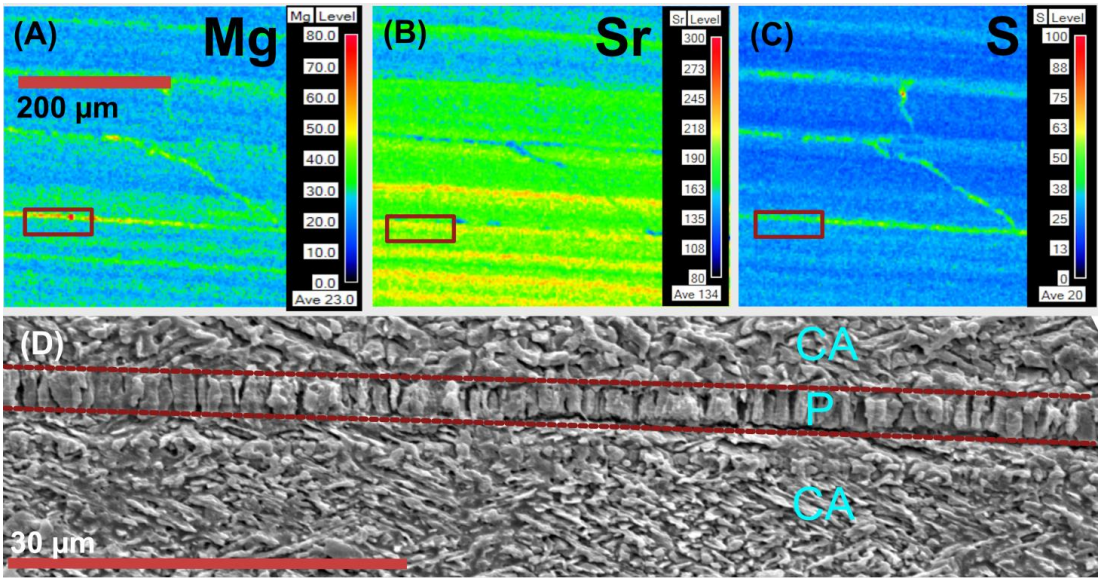

Figure 6. Inner shell layer of adult *L. staminea*. (**A**–**C**) element maps. Red boxes on maps indicate the area of interest highlighted in the SEM image. Color scales show x-ray counts from microprobe analyses. (**D**) SEM image in area of interest showing the correlation between microstructures and trace element counts. P = prismatic microstructure; CA = cross acicular microstructure. Dotted red line indicates boundary between growth line and growth increment in the ISL.

Juvenile shells showed variation in Sr, S, and Mg counts as well (Figure 7). In all individuals, the oOSL showed higher Sr and S values (Figure 7). In the outer layers of the juveniles, the smallest individual had the highest count values for Sr (~190 counts), followed by the largest juvenile (~170 counts) and then the medium-sized juvenile (~15 counts). For S, the smallest juvenile OSL had values ~50 counts, followed by the medium and largest juvenile, both of which had similar counts of ~42. Mg was highest in the smallest and largest juvenile OSL, with values of ~40 counts, followed by the medium juvenile, with values of ~15 counts. The medium juvenile showed little to no variation in Mg levels throughout the shell, which may be related to differences in microstructure that were not captured in this study. Interestingly, the juvenile individuals did not show clear evidence of an inner shell layer (ISL) enriched in S and Sr (Figure 7). However, we hypothesize that this pattern is observed due to the fragility of the shell and potential loss of shell material during the polishing process.

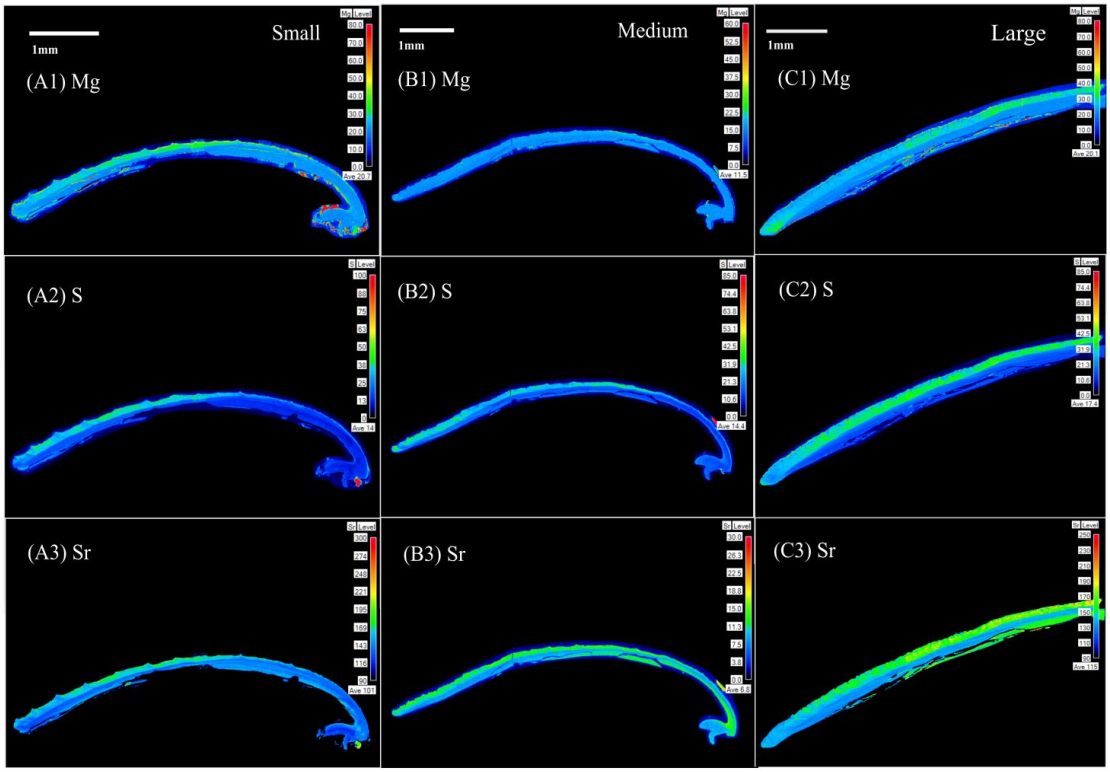

Figure 7. Microprobe analysis of juvenile *L. staminea*. (**A1**–**A3**) = small (6 mm); (**B1**–**B3**) = medium (11 mm); and (**C1**–**C3**) = large (15 mm) juvenile *L. staminea* Mg, S, and Sr values, respectively. (**C1**–**C3**) show only the ventral margin of the largest individual. Scales show relative X-ray counts for each element. Note differences in color scales between scans. EMP analyses do not allow for direct comparisons among different elemental maps. For example, if the Mg map shows more counts than the Sr map that does not indicate more Mg than Sr in the sample, i.e., Mg maps can only be compared to other Mg maps.

4. Discussion

4.1. Ontogenetic Influences on Shell Microstructure and Geochemistry

In this study, we consider the shell growth rate on two distinct temporal scales: (1) growth increments (faster and thicker) vs. growth lines (slower and thinner), and (2) early ontogeny (faster) vs. late ontogeny (slower). We hypothesized that slow shell growth would correspond to lower EMP X-ray count values of trace element incorporation in the shell, due to individuals having more time to exclude elemental "impurities" from the crystal lattice during biomineralization. Our results reject this hypothesis and suggest that the fast growth (i.e., growth increments) of aragonite in *L. staminea* leads to a depletion of Mg, Sr, and S compared to periods of slow growth (i.e., growth lines) in adult growth (Figure 5). When comparing average trace element count values of juveniles vs. adults, the outer shell layers were generally comparable. However, juveniles lacked an ISL enriched in Sr, ensuring that the average shell chemistry of the overall faster-growing juveniles contained less Mg, Sr, and S. Lastly, when comparing different sections of the adult shells, we found no detectable differences between the umbo-ward sections of the shell (earlier ontogeny, faster growth) vs. the ventral margin (most recent growth). However, the X-ray maps of the umbo and ventral margin were not complete due to irregular textures in the

shell (see Figure S2). Due to the nature of our approach, it is important to note that we did not calculate Sr/Ca ratios but instead based our results on high-resolution X-ray maps and count values, which are more qualitative in nature but allow for an extremely fine-scale investigation of element patterns. Interestingly, these results counter the previous limited work on *L. staminea* using LA-ICP-MS, which linked the faster growth rate to higher element: Ca ratios [46]. Takesue and Van Geen (2004) only analyzed the outer shell layers, which clearly document growth reduction over ontogeny as annual lines become more closely spaced [46]. However, the ISL, which they did not study, appears to be mineralized at a rate distinct from the outer layer(s), as indicated by the higher Sr levels (Figures 5 and 6). This supports the idea that different regions of the mantle mineralize at different rates and different times throughout ontogeny. We also add finer-scale images of element patterns, as well as descriptions of shell microstructure, and provide useful information on juveniles and their variability in size and growth during the same, known period, from an extant population living further south than previously studied.

EMP count values for S correlated to those for Sr, and to a lesser extent Mg in *L. staminea* shells. We suspect that this pattern is a manifestation of the organisms' modulation of insoluble and soluble organic matrices, which often contain sulfur, throughout development [35,61–66]. Interestingly, however, when comparing the life stages of our samples, not all juvenile individuals show clear evidence of an ISL enriched in S and Sr, suggesting that the trace elemental incorporation of these elements in the thickening portion of the shell may occur later in ontogeny. In our juvenile samples, inner layers relatively enriched in Sr start to form between 6–11 mm in length, but the smallest individual lacks evidence of an ISL, and it is not until the juveniles are closer to 11 mm in length that the Sr values in the ISL approach values akin to the adult ISL (Figure 7). The thick, Sr-rich ISL present in our adult samples may indicate that this inner layer grows later and more slowly than the oOSL and iOSL, which are not as enriched in Sr (Figure 5). Additionally, within Veneridae, microstructural variation between the myostracum and underlying shell in the ISL exists [67]. This warrants further investigation of the ISL to identify precise relationships between microstructure, geochemistry, and how these vary between the myostracum and the underlying shell.

Juvenile *L. staminea* showed, like the adults, clear microstructural evidence of ventral margin extension via growth lines/increments in the shells and a structurally distinct thickening inner shell when viewed under a stereoscope. While these internal growth band patterns could not be directly correlated to our microprobe data, we suspect that the microprobe resolution of 2 µm, while very fine, may have still been too coarse to detect even-finer scale patterns of elemental variation that may be present in juvenile shells. One potential reason for this observation could be that the shell crystal size was too small (sub-micrometer size). Another possibility is that the juvenile shell contained significant amounts of amorphous calcium carbonate (ACC) in its structure. Although the transformation mechanisms of ACC to crystalline material are elusive, several recent studies have investigated the role of ACC in biomineralization and documented its presence in bivalve shells using novel imaging techniques [36,68–71]. Interestingly, precipitation experiments involving inorganic calcium carbonate from seawater have shown that ACC can differ chemically quite significantly from crystalline $CaCO_3$ [72], which could explain the lack of clear elemental patterns in our juvenile samples.

Although we could not identify precise correlations in elemental and growth line patterns in 200-day-old individuals, juveniles exhibited notable differences in trace and minor element composition within single shells, which varied across individuals of different sizes and the same age. In the outer shell layer, the large and medium-sized (i.e, faster-growing) individuals showed the lowest count values for S (~42), while the smallest individual had only slightly higher counts of ~50. For Sr, the medium sized (moderately fast growing) individuals had the lowest count value for Sr (~15 counts), which was significantly lower than both the fastest and slowest growing individuals (190 and 170 for Sr, respectively). Growth rate differences early in ontogeny may have some relationship to the

elemental incorporation of Sr into the shell biomineral; however, the different expressions of element incorporation in juvenile *L. staminea* are perhaps a result of other physiological and/or genetic variation present within the population. In all, these results suggest that ontogenetic and microstructural biases must be considered when using *L. staminea* for paleoclimate reconstructions and proxy development, particularly if one is interested in the ISL [73].

4.2. Population-Level Variability in Growth and Studying Biomineralization through Time

The mineralized shell developed early on in mollusc evolution and was subsequently lost in some lineages, making variability in shell structure a point of interest for those studying morphological change, phylogenetic histories, heterochrony, and macroevolutionary trends through time [2,38,48,74,75]. In some studies, shell size is used as a proxy for age, and annually precipitated growth patterns can provide age-at-size information and document life history [75]. Often, researchers must distinguish annual lines from "disturbance lines," which can occur from storms, predation attempts, and/or abnormal environmental events and are in many ways morphologically like annual lines [31]. One way that researchers distinguish these lines is via close examination of the "microincrements," or subannual lines, which precede the darker/thicker annual lines in shells [46]. Microincrements supposedly decrease uniformly in width leading up to an annual line, while disturbance lines occur more abruptly amid regularly spaced microincrements [48].

Microincrements in bivalve shells have been empirically linked to a variety of environmental processes, including tidal cycles, nutrient availability, and dark/light cycles [48,76–85]. The production of microincrements may stem from endogenous rhythms controlled by "biological clocks" [77]. Biological clocks exist across the tree of life, ranging from cyanobacteria, to fungi, mammals, and molluscs [86–89]. These systems are composed of (1) a central molecular oscillator that tracks time; (2) environmental cues that measure time; and (3) rhythms of physiological, biochemical, or behavioral activities of an organism, such as gape (opening) patterns in marine bivalves [90,91]. Biological clocks are ultimately under genetic, rather than environmental, control and serve to optimize the energetic balance of organisms by obtaining nutrients and using energy when it is available [77]. Aschoff (1981) argued that biological clocks can be "auto-entertained," meaning that the observed physiological oscillations can continue even if the organism is kept under constant conditions, similar to what we observed in *L. staminea* juveniles [92]. These patterns are observable, likely because the biological clock is highly conserved [93]. Biological clocks have been documented in several bivalve species, mainly at the daily and tidal frequencies, and posited as responsible for growth line/increment patterns [17,77,84]. Further, in recent years, homologous clock genes have been studied in the mussels *Mytilus edulis* [86] and *Mytilus californianu* [94], the oyster *Magallana* gigas [95], and the scallops *Argopecten irradians* [96] and *Chlamys islandica* [97].

Interestingly, though, microincrements within the juvenile shells of *L. staminea* did not present in a regular, predictable pattern but occurred somewhat haphazardly throughout all the analyzed individuals (Figure S3). This also occurs in many oysters, making them a less common study group in sclerochronology studies [98,99]. Variability in the observed gross morphology and growth banding patterns may reflect inherent intrapopulation genetic variability present in the sample. Additionally, distinct environmental drivers of the biological clock system beyond those classically studied (i.e., photoperiod and/or temperature), such as food availability, should be considered and further evaluated and may shed light on *L. staminea* growth banding. It is likely that size variability within the juvenile cohort corresponds to variability in their feeding habits (i.e., larger individuals may have been feeding more and therefore may have produced larger shells with more growth lines/increments). While we did not measure feeding rate in our juvenile samples, further studies in controlled laboratory studies should investigate the role of food availability/consumption on shell growth patterning.

Marine bivalves, including *L. staminea*, typically decrease their shell growth rate throughout ontogeny, and species-specific ontogenetic patterns can affect the duration

and timing of the growing season (i.e., when increments are formed vs. when lines are formed) [100–102]. We suspect this may also vary within species with large geographic ranges, such as *L. staminea*, where local adaptation and population genetic variation can occur. Additionally, how the variability in growth rate, growth banding, and elemental composition observed in our young, juvenile population grown in the lab would scale throughout their ontogeny is unknown and warrants further study. To better understand these questions, more data on adult populations of the same, known age, and location are necessary. Lastly, a deeper investigation into the genetic mechanisms of the biological clock in *L. staminea* and the role of the feeding rate could yield important information regarding the timing and tempo of their growth line and trace and minor element incorporation patterns.

4.3. Potential of L. staminea to Document (Paleo)Environmental Conditions

As biomineralization mechanisms vary both across and within species, we argue that both morphological and geochemical measurements must be leveraged to accurately use bivalve shells as a record of paleoenvironmental conditions, growth rate, and/or lifespan [103]. In addition to trace elements, the stable oxygen isotope composition of bivalve shell carbonate, which typically varies along the axis of maximum growth, can and should be used since it is highly temperature-dependent [23,104] and therefore responds to seasonal trends in temperature. Oxygen isotopes, when coupled with clear growth band patterns, can thus reveal chronological environmental information from the shell. Early research demonstrated that the oxygen isotope composition of bivalve shell carbonate is precipitated at, or near, isotopic equilibrium with the seawater in which the organism builds its shell and therefore reflects the oxygen-isotope composition of the seawater (δ^{18}O w) and ambient temperature [104]. Since then, δ^{18}O of both aragonitic and calcitic bivalve shells has been used as a record of past seawater temperatures [3,105–109]. However, kinetic effects during biomineralization can cause species-specific deviations from isotopic equilibrium [100,109–111]. Owen et al. (2002) documented a relationship between low shell growth rate and shell δ^{18}O that was more positive (differing by ~0.4‰, corresponding to an offset of 1.9 °C) than the predicted values of inorganic calcite in isotopic equilibrium with seawater [100]. Additionally, Cusack et al. (2008) found significant differences in isotopic composition (differing by ~0.4‰), depending on whether the outer prismatic or inner nacreous section of the shell was sampled, similar to our results with Sr incorporation differences between the inner and outer shell layers [33]. As is the case with trace/minor elements, we suspect ontogenetic and population-level variability in growth rate and other physiological properties may also obscure recorded isotope values.

Because elemental composition changed significantly at the very fine (micrometer) scale within single shells in our study, as evidenced by visible correlations between microstructure and elemental composition, we argue that adult *L. staminea* shells are only suitable for further proxy-development if micrometer-scale variability in the shell structure and chemistry is accounted for to minimize time-averaging. To do so, researchers should use both electron microprobe mapping tools, SEM, and quantitative analyses such as fine-scale LA-ICP-MS or stable isotope sampling. Although previous work documented in situ trace element measurements of Sr and Mg in the outer shell layer of *L. staminea* [46], these results were based on samples ablated from 90–100 µm diameter spots, which comprise an overly coarse resolution to accurately capture the elemental variability present in the shell. LA-ICP-MS typically requires the sampling of at least ~50 µm spot size [112], but new high-resolution LA-ICP-MS technologies allow for elemental analysis at ~10 µm resolution [113]. Additionally, correlations between crystal microstructure and elemental chemistry in adult specimens point to the need for the detailed mapping of the crystal fabrics in addition to analyses of stable isotopes and/or trace elements, due to the close relationships among them [60,114]. These various shell characteristics must be accounted for and necessitate the rigorous evaluation of modern, local populations prior to (paleo)environmental analyses. In all, our results highlight the biological influences underlying the shell charac-

teristics of *L. staminea*, demonstrating the importance of accounting for both ontogenetic and population-level variability. These issues likely affect species other than *L. staminea* and are particularly problematic for extinct species. In all, the best way forward for (paleo)environmental reconstructions using *L. staminea*, or any aragonitic bivalve, is to take a multi-proxy approach drawing upon morphological and geochemical properties, and account for micrometer-scale variability that occurs throughout the organism's lifespan.

5. Conclusions

We provide the first detailed description of shell mineralogy, microstructure, body size variability, and geochemical properties of modern *L. staminea*. We measured various morphological properties and element patterning of 200-day-old juveniles grown in identical conditions from the same reproductive cohort, as well as their parent individuals.

5.1. Morphology and Growth Rate

We hypothesized that slow shell growth yields lower trace/minor element incorporation in the shell, due to individuals having more time to exclude elemental "impurities" from the biomineral. Our results refute our hypothesis. In adults, growth increments (fast growth) were relatively depleted in Mg, Sr, and S compared to growth lines (i.e., slow growth) (Figure 5). When comparing different ontogenetic sections of the adult shells, we found no detectable differences in count values between the umbo (earlier ontogeny, faster growth), the middle, and the ventral margin (most recent growth). However, microprobe maps of the umbo and ventral margin were not complete due to irregular textures in the shell, thus warranting further examination.

5.2. Microstructure and Trace Elements

Growth lines and increments showed distinct microstructural and geochemical properties. Microprobe analyses revealed higher levels of S, Sr, and Mg in the prismatic growth lines, particularly in the inner shell layer, suggesting a link between microstructure and trace element chemistry. Further, we provide the first structural and geochemical description of the inner shell layer, which appears to mineralize at a slower rate than the outer layers and only once the shell length reaches between ~6–11 mm, demonstrating that different regions of the mantle mineralize at distinct rates and times throughout ontogeny. While juvenile shells of different sizes also showed variation in S, Sr, and Mg, we could not link elemental patterns clearly to microstructure, body size, and/or growth line patterns. Significant intraspecific variation in the body size, growth band patterning, and elemental composition of individuals of the same age and genetic stock nevertheless complicates the use of size as a proxy for age in historical studies. Juvenile *L. staminea* shells are likely not useful for paleontological and/or (paleo)environmental research due to these issues as well as to potential diagenetic alteration. Lastly, because elemental composition changed significantly at the micrometer scale within single shells, we argue that *L. staminea* shells are only suitable if micrometer-scale variability in the shell structure and chemistry is accounted for to minimize time-averaging and if a multi-proxy approach to environmental reconstruction is adopted. Further studies examining the role of the biological clock and vital effects on biomineralization, and how these processes vary throughout ontogeny and across populations, are warranted to further rigorously evaluate the utility of *L. staminea*, and other bivalve species, in paleoenvironmental studies.

Supplementary Materials: The following supporting information can be downloaded at https://www.mdpi.com/article/10.3390/min13060814/s1, Figure S1: Line profiles for gray-scale variance; Figure S2: Irregular textures in adult shell; Figure S3: Haphazard expression of growth banding within a single juvenile shell; and Table S1: Mean, standard deviation, maximum, and minimum gray-scale values.

Author Contributions: Conceptualization, H.L.K. and S.J.C.; methodology, H.L.K. and S.J.C.; formal analysis, H.L.K.; investigation, H.L.K.; resources, H.L.K., S.J.C. and D.A.G.; data curation, H.L.K.; writing—original draft preparation, H.L.K.; writing—review and editing, H.L.K., S.J.C. and D.A.G.; visualization, H.L.K.; supervision, H.L.K., S.J.C. and D.A.G.; and funding acquisition, H.L.K. and D.A.G. All authors have read and agreed to the published version of the manuscript.

Funding: This research was supported by a California Sea Grant Graduate Research Fellowship (Grant NA22OAR4170106) to H.L.K.

Data Availability Statement: The data presented in this study are available in the Supplementary Materials. Unprocessed data are available upon request from the authors.

Acknowledgments: Thank you to Joe Newman and the Bodega Marine Lab Aquatic Resources Group for their help developing a spawn protocol for *L. staminea*. All the thin sections and epoxy rounds were prepared by Greg Baxter. Thank you to Sarah Roeske for helping us interpret our microprobe data.

Conflicts of Interest: The authors declare no conflict of interest. The funders had no role in the design of the study; in the collection, analyses, or interpretation of data; in the writing of the manuscript; or in the decision to publish the results.

References

1. Schöne, B.R.; Pfeiffer, M.; Pohlmann, T.; Siegismund, F. A Seasonally Resolved Bottom-Water Temperature Record for the Period AD 1866–2002 Based on Shells of Arctica Islandica (Mollusca, North Sea). *Int. J. Climatol.* **2005**, *25*, 947–962. [CrossRef]
2. Schöne, B.R.; Gillikin, D.P. Unraveling Environmental Histories from Skeletal Diaries—Advances in Sclerochronology. *Palaeogeogr. Palaeoclimatol. Palaeoecol.* **2013**, *373*, 1–5. [CrossRef]
3. Trofimova, T.; Andersson, C.; Bonitz, F.G.W.; Pedersen, L.-E.R.; Schöne, B.R. Reconstructing Early Holocene Seasonal Bottom-Water Temperatures in the Northern North Sea Using Stable Oxygen Isotope Records of Arctica Islandica Shells. *Palaeogeogr. Palaeoclimatol. Palaeoecol.* **2021**, *567*, 110242. [CrossRef]
4. Vriesman, V.P.; Carlson, S.J.; Hill, T.M. Investigating Controls of Shell Growth Features in a Foundation Bivalve Species: Seasonal Trends and Decadal Changes in the California Mussel. *Biogeosciences* **2022**, *19*, 329–346. [CrossRef]
5. Cannarozzi, N.R.; Kowalewski, M. Seasonal Oyster Harvesting Recorded in a Late Archaic Period Shell Ring. *PLoS ONE* **2019**, *14*, e0224666. [CrossRef]
6. Eerkens, J.W.; Byrd, B.F.; Spero, H.J.; Fritschi, A.K. Stable Isotope Reconstructions of Shellfish Harvesting Seasonality in an Estuarine Environment: Implications for Late Holocene San Francisco Bay Settlement Patterns. *J. Archaeol. Sci.* **2013**, *40*, 2014–2024. [CrossRef]
7. Jenkins, J.A. Methods for Inferring Oyster Mariculture on Florida's Gulf Coast. *J. Archaeol. Sci.* **2017**, *80*, 74–82. [CrossRef]
8. Allison, N.; Finch, A.A. High-Resolution Sr/Ca Records in Modern Porites Lobata Corals: Effects of Skeletal Extension Rate and Architecture. *Geochem. Geophys. Geosys.* **2004**, *5*, 1–10. [CrossRef]
9. Eggins, S.; De Deckker, P.; Marshall, J. Mg/Ca Variation in Planktonic Foraminifera Tests: Implications for Reconstructing Palaeo-Seawater Temperature and Habitat Migration. *Earth Planet. Sci. Lett.* **2003**, *212*, 291–306. [CrossRef]
10. Sadekov, A.Y.; Eggins, S.M.; De Deckker, P. Characterization of Mg/Ca Distributions in Planktonic Foraminifera Species by Electron Microprobe Mapping. *Geochem. Geophys. Geosyst.* **2005**, *6*, 1–14. [CrossRef]
11. Spero, H.J.; Lea, D.W. Experimental Determination of Stable Isotope Variability in Globigerina Bulloides: Implications for Paleoceanographic Reconstructions. *Mar. Micropaleontol.* **1996**, *28*, 231–246. [CrossRef]
12. Poulain, C.; Gillikin, D.P.; Thébault, J.; Munaron, J.M.; Bohn, M.; Robert, R.; Paulet, Y.-M.; Lorrain, A. An Evaluation of Mg/Ca, Sr/Ca, and Ba/Ca Ratios as Environmental Proxies in Aragonite Bivalve Shells. *Chem. Geol.* **2015**, *396*, 42–50. [CrossRef]
13. Schöne, B.R.; Zhang, Z.; Radermacher, P.; Thébault, J.; Jacob, D.E.; Nunn, E.V.; Maurer, A.-F. Sr/Ca and Mg/Ca Ratios of Ontogenetically Old, Long-Lived Bivalve Shells (Arctica Islandica) and Their Function as Paleotemperature Proxies. *Palaeogeogr. Palaeoclimatol. Palaeoecol.* **2011**, *302*, 52–64. [CrossRef]
14. Ulrich, R.N.; Guillermic, M.; Campbell, J.; Hakim, A.; Han, R.; Singh, S.; Stewart, J.D.; Román-Palacios, C.; Carroll, H.M.; De Corte, I.; et al. Patterns of Element Incorporation in Calcium Carbonate Biominerals Recapitulate Phylogeny for a Diverse Range of Marine Calcifiers. *Front. Earth Sci.* **2021**, *9*, 1–26. [CrossRef]
15. Markulin, K.; Peharda, M.; Mertz-Kraus, R.; Schöne, B.R.; Uvanović, H.; Kovač, Ž.; Janeković, I. Trace and Minor Element Records in Aragonitic Bivalve Shells as Environmental Proxies. *Chem. Geol.* **2019**, *507*, 120–133. [CrossRef]
16. Warter, V.; Erez, J.; Müller, W. Environmental and Physiological Controls on Daily Trace Element Incorporation in Tridacna Crocea from Combined Laboratory Culturing and Ultra-High Resolution LA-ICP-MS Analysis. *Palaeogeogr. Palaeoclimatol. Palaeoecol.* **2018**, *496*, 32–47. [CrossRef]
17. Kinsman, D.J.J.; Holland, H.D. The Co-Precipitation of Cations with CaCO3—IV. The Co-Precipitation of Sr2+ with Aragonite between 16° and 96 °C. *Geochim. Cosmochim. Acta* **1969**, *33*, 1–17. [CrossRef]

18. Tesoriero, A.J.; Pankow, J.F. Solid Solution Partitioning of Sr^{2+}, Ba^{2+}, and Cd^{2+} to Calcite. *Geochim. Cosmochim. Acta* **1996**, *60*, 1053–1063. [CrossRef]
19. Zhong, S.; Mucci, A. Calcite and Aragonite Precipitation from Seawater Solutions of Various Salinities: Precipitation Rates and Overgrowth Compositions. *Chem. Geol.* **1989**, *78*, 283–299. [CrossRef]
20. Oomori, T.; Kaneshima, H.; Maezato, Y.; Kitano, Y. Distribution Coefficient of Mg^{2+} Ions between Calcite and Solution at 10–50 °C. *Mar. Chem.* **1987**, *20*, 327–336. [CrossRef]
21. Schleinkofer, N.; Raddatz, J.; Evans, D.; Gerdes, A.; Flögel, S.; Voigt, S.; Büscher, J.V.; Wisshak, M. Compositional Variability of Mg/Ca, Sr/Ca, and Na/Ca in the Deep-Sea Bivalve Acesta Excavata (Fabricius, 1779). *PLoS ONE* **2021**, *16*, e0245605. [CrossRef] [PubMed]
22. Urey, H.C.; Lowenstam, H.A.; Epstein, S.; McKinney, C.R. Measurement of Paleotemperatures and Temperatures of the Upper Cretaceous of England, Denmark and the Southeastern United States. *Bull. Geol. Soc. Am.* **1951**, *62*, 399–416. [CrossRef]
23. Weiner, S.; Dove, P.M. An Overview of Biomineralization Processes and the Problem of the Vital Effect. *Rev. Mineral. Geochem.* **2003**, *54*, 1–29. [CrossRef]
24. Ballesta-Artero, I.; Zhao, L.; Milano, S.; Mertz-Kraus, R.; Schöne, B.R.; van der Meer, J.; Witbaard, R. Environmental and Biological Factors Influencing Trace Elemental and Microstructural Properties of Arctica Islandica Shells. *Sci. Total Environ.* **2018**, *645*, 913–923. [CrossRef]
25. Surge, D.; Walker, K.J. Geochemical Variation in Microstructural Shell Layers of the Southern Quahog (Mercenaria Campechiensis): Implications for Reconstructing Seasonality. *Palaeogeogr. Palaeoclimatol. Palaeoecol.* **2006**, *237*, 182–190. [CrossRef]
26. Gillikin, D.P.; Lorrain, A.; Navez, J.; Taylor, J.W.; André, L.; Keppens, E.; Baeyens, W.; Dehairs, F. Strong Biological Controls on Sr/Ca Ratios in Aragonitic Marine Bivalve Shells. *Geochem. Geophys. Geosyst.* **2005**, *6*, 1–16. [CrossRef]
27. Freitas, P.S.; Clarke, L.J.; Kennedy, H.; Richardson, C.A.; Abrantes, F. Environmental and Biological Controls on Elemental (Mg/Ca, Sr/Ca and Mn/Ca) Ratios in Shells of the King Scallop Pecten Maximus. *Geochim. Cosmochim. Acta* **2006**, *70*, 5119–5133. [CrossRef]
28. Richardson, C.A.; Peharda, M.; Kennedy, H.; Kennedy, P.; Onofri, V. Age, Growth Rate and Season of Recruitment of Pinna Nobilis (L) in the Croatian Adriatic Determined from Mg:Ca and Sr:Ca Shell Profiles. *J. Exp. Mar. Biol. Ecol.* **2004**, *299*, 1–16. [CrossRef]
29. Milano, S.; Schöne, B.R.; Witbaard, R. Changes of Shell Microstructural Characteristics of Cerastoderma Edule (Bivalvia)—A Novel Proxy for Water Temperature. *New Res. Methods Appl. Sclerochronol.* **2017**, *465*, 395–406. [CrossRef]
30. Clark, G.R. Growth Lines in Invertebrate Skeletons. *Annu. Rev. Earth Planet. Sci.* **1974**, *2*, 77–99. [CrossRef]
31. McConnaughey, T. Biomineralization Mechanisms. In *Origin, Evolution, and Modern Aspects of Biomineralization in Plants and Animals*; Crick, R.E., Ed.; Springer: Boston, MA, USA, 1989; pp. 57–73. [CrossRef]
32. Cusack, M.; Freer, A. Biomineralization: Elemental and Organic Influence in Carbonate Systems. *Chem. Rev.* **2008**, *108*, 4433–4454. [CrossRef]
33. Falini, G.; Albeck, S.; Weiner, S.; Addadi, L. Control of Aragonite or Calcite Polymorphism by Mollusk Shell Macromolecules. *Science* **1996**, *271*, 67–69. [CrossRef]
34. Shirai, K.; Schöne, B.R.; Miyaji, T.; Radarmacher, P.; Krause, R.A.; Tanabe, K. Assessment of the Mechanism of Elemental Incorporation into Bivalve Shells (Arctica Islandica) Based on Elemental Distribution at the Microstructural Scale. *Geochim. Cosmochim. Acta* **2014**, *126*, 307–320. [CrossRef]
35. Evans, D.; Gray, W.R.; Rae, J.W.B.; Greenop, R.; Webb, P.B.; Penkman, K.; Kröger, R.; Allison, N. Trace and Major Element Incorporation into Amorphous Calcium Carbonate (ACC) Precipitated from Seawater. *Geochim. Cosmochim. Acta* **2020**, *290*, 293–311. [CrossRef]
36. Mergelsberg, S.T.; De Yoreo, J.J.; Miller, Q.R.S.; Marc Michel, F.; Ulrich, R.N.; Dove, P.M. Metastable Solubility and Local Structure of Amorphous Calcium Carbonate (ACC). *Geochim. Cosmochim. Acta* **2020**, *289*, 196–206. [CrossRef]
37. Marin, F. The Formation and Mineralization of Mollusk Shell. *Front. Biosci.* **2012**, *4*, 1099–1125. [CrossRef]
38. Fraser, C.M.; Smith, G.M. Notes on the Ecology of the Little Neck Clam. Paphia Staminea Conrad. *Trans. R. Soc. Can. Ser.* **1928**, *3*, 249–269.
39. Lepofsky, D.; Smith, N.; Cardinal, N.; Harper, J.; Morris, M.; Elroy White, G.; Bouchard, R.; Kennedy, D.; Solomon, A.; Puckett, M.; et al. Ancient Shellfish Mariculture on the Northwest Coast of North America. *Am. Antiq.* **2015**, *80*, 236–259. [CrossRef]
40. Schneider, T.; DeAntoni, G.; Hill, A.; Apodaca, A. Indigenous Persistence and Foodways at the Toms Point Trading Post (CA-MRN-202), Tomales Bay, California. *J. Calif. Gt. Basin Anthropol.* **2018**, *38*, 51–73.
41. Smith, G.M. Food Material as a Factor in Growth Rate of Some Pacific Clams. *Trans. R Soc. Can Ser.* **1928**, *3*, 287–291.
42. Harrington, R.J. Skeletal Growth Histories of Protothaca Staminea Conrad and Protothaca Grata Say throughout Their Geographic Ranges Northeastern Pacific. *Veliger* **1987**, *30*, 148–158.
43. Feder, H.M.; Hendee, J.C.; Holmes, P.; Mueller, G.J.; Paul, A.J. Examination of a Reproductive Cycle of Protothaca Staminea Using Histology, We Weight-Dry Weight Ratios, and Condition Indices. *Veliger* **1979**, *22*, 182–187.
44. Bendell, L.I. Evidence for Declines in the Native Leukoma Staminea as a Result of the Intentional Introduction of the Non-Native Venerupis Philippinarum in Coastal British Columbia, Canada. *Estuaries Coasts* **2014**, *12*, 369–380. [CrossRef]

45. Takesue, R.K.; van Geen, A. Mg/Ca, Sr/Ca, and Stable Isotopes in Modern and Holocene Protothaca Staminea Shells from a Northern California Coastal Upwelling Region. *Geochim. Cosmochim. Acta* **2004**, *68*, 3845–3861. [CrossRef]
46. Schöne, B.R.; Dunca, E.; Fiebig, J.; Pfeiffer, M. Mutvei's Solution: An Ideal Agent for Resolving Microgrowth Structures of Biogenic Carbonates. *Palaeogeogr. Palaeoclimatol. Palaeoecol.* **2005**, *228*, 149–166. [CrossRef]
47. Schöne, B.; Surge, D. *Bivalve Sclerochronology and Geochemistry*; Paleontological Institute: Moscow, Russia, 2012; pp. 1–24.
48. Strasser, C.A.; Mullineaux, L.S.; Walther, B.D. Growth Rate and Age Effects on Mya Arenaria Shell Chemistry: Implications for Biogeochemical Studies. *J. Exp. Mar. Biol. Ecol.* **2008**, *355*, 153–163. [CrossRef]
49. Schöne, B.R. Arctica Islandica (Bivalvia): A Unique Paleoenvironmental Archive of the Northern North Atlantic Ocean. *Glob. Planet. Chang.* **2013**, *111*, 199–225. [CrossRef]
50. Hickey, B.M.; Banas, N.S. Oceanography of the U.S. Pacific Northwest Coastal Ocean and Estuaries with Application to Coastal Ecology. *Estuaries* **2003**, *26*, 1010–1031. [CrossRef]
51. Largier, J.L. Upwelling Bays: How Coastal Upwelling Controls Circulation, Habitat, and Productivity in Bays. *Annu. Rev. Mar. Sci.* **2020**, *12*, 415–447. [CrossRef] [PubMed]
52. García-Reyes, M.; Largier, J. Observations of Increased Wind-Driven Coastal Upwelling off Central California. *J. Geophys. Res. Oceans* **2010**, *115*, 1–8. [CrossRef]
53. García-Reyes, M.; Largier, J.L. Seasonality of Coastal Upwelling off Central and Northern California: New Insights, Including Temporal and Spatial Variability. *J. Geophys. Res. Oceans* **2012**, *117*, 1–17. [CrossRef]
54. Arp, A.J.; Hansen, B.M.; Julian, D. Burrow Environment and Coelomic Fluid Characteristics of the Echiuran Worm Urechis Caupo from Populations at Three Sites in Northern California. *Mar. Biol.* **1992**, *113*, 613–623. [CrossRef]
55. Ricart, A.M.; Ward, M.; Hill, T.M.; Sanford, E.; Kroeker, K.J.; Takeshita, Y.; Merolla, S.; Shukla, P.; Ninokawa, A.T.; Elsmore, K.; et al. Coast-Wide Evidence of Low pH Amelioration by Seagrass Ecosystems. *Glob. Chang. Biol.* **2021**, *27*, 2580–2591. [CrossRef]
56. Silbiger, N.J.; Sorte, C.J.B. Biophysical Feedbacks Mediate Carbonate Chemistry in Coastal Ecosystems across Spatiotemporal Gradients. *Sci. Rep.* **2018**, *8*, 796. [CrossRef] [PubMed]
57. Kindeberg, T.; Bates, N.R.; Courtney, T.A.; Cyronak, T.; Griffin, A.; Mackenzie, F.T.; Paulsen, M.-L.; Andersson, A.J. Porewater Carbonate Chemistry Dynamics in a Temperate and a Subtropical Seagrass System. *Aquat. Geochem.* **2020**, *26*, 375–399. [CrossRef]
58. Schindelin, J.; Arganda-Carreras, I.; Frise, E.; Kaynig, V.; Longair, M.; Pietzsch, T.; Preibisch, S.; Rueden, C.; Saalfeld, S.; Schmid, B.; et al. Fiji: An Open-Source Platform for Biological-Image Analysis. *Nat. Methods* **2012**, *9*, 676–682. [CrossRef]
59. Brosset, C.; Höche, N.; Shirai, K.; Nishida, K.; Mertz-Kraus, R.; Schöne, B.R. Strong Coupling between Biomineral Morphology and Sr/Ca of Arctica Islandica (Bivalvia)—Implications for Shell Sr/Ca-Based Temperature Estimates. *Minerals* **2022**, *12*, 500. [CrossRef]
60. Schöne, B.R.; Radermacher, P.; Zhang, Z.; Jacob, D.E. Crystal Fabrics and Element Impurities (Sr/Ca, Mg/Ca, and Ba/Ca) in Shells of Arctica Islandica—Implications for Paleoclimate Reconstructions. *Palaeogeogr. Palaeoclimatol. Palaeoecol.* **2013**, *373*, 50–59. [CrossRef]
61. Arias, J.L.; Fernández, M.S. Polysaccharides and Proteoglycans in Calcium Carbonate-Based Biomineralization. *Chem. Rev.* **2008**, *108*, 4475–4482. [CrossRef]
62. Dauphin, Y.; Cuif, J.-P.; Doucet, J.; Salomé, M.; Susini, J.; Terry Willams, C. In Situ Chemical Speciation of Sulfur in Calcitic Biominerals and the Simple Prism Concept. *J. Struct. Biol.* **2003**, *142*, 272–280. [CrossRef]
63. Dauphin, Y.; Cuif, J.; Doucet, J.; Salomé, M.; Susini, J.; Williams, C. In Situ Mapping of Growth Lines in the Calcitic Prismatic Layers of Mollusc Shells Using X-ray Absorption near-Edge Structure (XANES) Spectroscopy at the Sulphur K-Edge. *Mar. Biol.* **2003**, *142*, 299–304. [CrossRef]
64. Guzman, N.; Ball, A.D.; Cuif, J.-P.; Dauphin, Y.; Denis, A.; Ortlieb, L. Subdaily Growth Patterns and Organo-Mineral Nanostructure of the Growth Layers in the Calcitic Prisms of the Shell of Concholepas Concholepas Bruguière, 1789 (Gastropoda, Muricidae). *Microsc. Microanal. Off. J. Microsc. Soc. Am. Microbeam Anal. Soc. Microsc. Soc. Can.* **2007**, *13*, 397–403. [CrossRef]
65. Addadi, L.; Raz, S.; Weiner, S. Taking Advantage of Disorder: Amorphous Calcium Carbonate and Its Roles in Biomineralization. *ChemInform* **2003**, *34*, 959–970. [CrossRef]
66. Ren, D.; Feng, Q.; Bourrat, X. Effects of Additives and Templates on Calcium Carbonate Mineralization in Vitro. *Micron* **2011**, *42*, 228–245. [CrossRef]
67. Dong, W.; Huang, J.; Liu, C.; Wang, H.; Zhang, G.; Xie, L.; Zhang, R. Characterization of the Myostracum Layers in Molluscs Reveals a Conservative Shell Structure. *Front. Mar. Sci.* **2022**, *9*, 544. [CrossRef]
68. Dicko, H.; Grünewald, T.A.; Ferrand, P.; Vidal-Dupiol, J.; Teaniniuraitemoana, V.; Koua, M.S.; le Moullac, G.; Le Luyer, J.; Saulnier, D.; Chamard, V.; et al. Sub-Micrometric Spatial Distribution of Amorphous and Crystalline Carbonates in Biogenic Crystals Using Coherent Raman Microscopy. *J. Struct. Biol.* **2022**, *214*, 107909. [CrossRef]
69. Duboisset, J.; Ferrand, P.; Baroni, A.; Grünewald, T.A.; Dicko, H.; Grauby, O.; Vidal-Dupiol, J.; Saulnier, D.; Gilles, L.M.; Rosenthal, M.; et al. Amorphous-to-Crystal Transition in the Layer-by-Layer Growth of Bivalve Shell Prisms. *Acta Biomater.* **2022**, *142*, 194–207. [CrossRef]
70. Grünewald, T.A.; Checchia, S.; Dicko, H.; Le Moullac, G.; Sham Koua, M.; Vidal-Dupiol, J.; Duboisset, J.; Nouet, J.; Grauby, O.; Di Michiel, M.; et al. Structure of an Amorphous Calcium Carbonate Phase Involved in the Formation of Pinctada Margaritifera Shells. *Proc. Natl. Acad. Sci. USA* **2022**, *119*, e2212616119. [CrossRef] [PubMed]

71. Taylor, M.; Simkiss, K.; Greaves, G.N. Amorphous Structure of Intracellular Mineral Granules. *Biochem. Soc. Trans.* **1986**, *14*, 549–552. [CrossRef] [PubMed]
72. Blue, C.R.; Dove, P.M. Chemical Controls on the Magnesium Content of Amorphous Calcium Carbonate. *Geochim. Cosmochim. Acta* **2015**, *148*, 23–33. [CrossRef]
73. Mancuso, A.; Stagioni, M.; Prada, F.; Scarponi, D.; Piccinetti, C.; Goffredo, S. Environmental Influence on Calcification of the Bivalve Chamelea Gallina along a Latitudinal Gradient in the Adriatic Sea. *Sci. Rep.* **2019**, *9*, 11198. [CrossRef] [PubMed]
74. Suzuki, M.; Nagasawa, H. Mollusk Shell Structures and Their Formation Mechanism. *Can. J. Zool.* **2013**, *91*, 349–366. [CrossRef]
75. Moss, D.K.; Ivany, L.C.; Jones, D.S. Fossil Bivalves and the Sclerochronological Reawakening. *Paleobiology* **2021**, *47*, 551–573. [CrossRef]
76. Hallmann, N.; Burchell, M.; Schöne, B.R.; Irvine, G.V.; Maxwell, D. High-Resolution Sclerochronological Analysis of the Bivalve Mollusk Saxidomus Gigantea from Alaska and British Columbia: Techniques for Revealing Environmental Archives and Archaeological Seasonality. *J. Archaeol. Sci.* **2009**, *36*, 2353–2364. [CrossRef]
77. Louis, V.; Besseau, L.; Lartaud, F. Step in Time: Biomineralisation of Bivalve's Shell. *Front. Mar. Sci.* **2022**, *9*, 1–16. [CrossRef]
78. Lutz, R.; Rhoads, D.C. Anaerobiosis and a Theory of Growth Line Formation. Available online: https://www.science.org/doi/10.1126/science.198.4323.1222 (accessed on 21 February 2023).
79. Crenshaw, M.A. The Inorganic Composition of Molluscan Extrapallial Fluid. *Biol. Bull.* **1972**, *143*, 506–512. [CrossRef] [PubMed]
80. Littlewood, D.T.J.; Young, R.E. The Effect of Air-Gaping Behaviour on Extrapallial Fluid pH in the Tropical Oyster Crassostrea Rhizophorae. *Comp. Biochem. Physiol. A Physiol.* **1994**, *107*, 1–6. [CrossRef]
81. Clark, G.R. Daily Growth Lines in Some Living Pectens (Mollusca: Bivalvia), and Some Applications in a Fossil Relative: Time and Tide Will Tell. *Palaeogeogr. Palaeoclimatol. Palaeoecol.* **2005**, *228*, 26–42. [CrossRef]
82. Rodríguez-Tovar, F.J. Orbital Climate Cycles in the Fossil Record: From Semidiurnal to Million-Year Biotic Responses. *Annu. Rev. Earth Planet. Sci.* **2014**, *42*, 69–102. [CrossRef]
83. Richardson, C.A.; Crisp, D.J.; Runham, N.W. An Endogenous Rhythm in Shell Deposition in Cerastoderma Edule. *J. Mar. Biol. Assoc. U. K.* **1980**, *60*, 991–1004. [CrossRef]
84. Poulain, C.; Lorrain, A.; Flye-Sainte-Marie, J.; Amice, E.; Morize, E.; Paulet, Y.-M. An Environmentally Induced Tidal Periodicity of Microgrowth Increment Formation in Subtidal Populations of the Clam Ruditapes Philippinarum. *J. Exp. Mar. Biol. Ecol.* **2011**, *397*, 58–64. [CrossRef]
85. Richardson, C.A. Exogenous and Endogenous Rhythms of Band Formation in the Shell of the Clam Tapes Philippinarum (Adams et Reeve, 1850). *J. Exp. Mar. Biol. Ecol.* **1988**, *122*, 105–126. [CrossRef]
86. Chapman, E.C.; Bonsor, B.J.; Parsons, D.R.; Rotchell, J.M. Influence of Light and Temperature Cycles on the Expression of Circadian Clock Genes in the Mussel Mytilus Edulis. *Mar. Environ. Res.* **2020**, *159*, 104960. [CrossRef]
87. Ditty, J.L.; Williams, S.B.; Golden, S.S. A Cyanobacterial Circadian Timing Mechanism. *Annu. Rev. Genet.* **2003**, *37*, 513–543. [CrossRef]
88. Partch, C.L.; Green, C.B.; Takahashi, J.S. Molecular Architecture of the Mammalian Circadian Clock. *Trends Cell Biol.* **2014**, *24*, 90–99. [CrossRef]
89. Tan, Y.; Merrow, M.; Roenneberg, T. Photoperiodism in Neurospora Crassa. *J. Biol. Rhythms* **2004**, *19*, 135–143. [CrossRef]
90. Comeau, L.A.; Babarro, J.M.F.; Longa, A.; Padin, X.A. Valve-Gaping Behavior of Raft-Cultivated Mussels in the Ría de Arousa, Spain. *Aquac. Rep.* **2018**, *9*, 68–73. [CrossRef]
91. Tran, D.; Perrigault, M.; Ciret, P.; Payton, L. Bivalve Mollusc Circadian Clock Genes Can Run at Tidal Frequency. *Proc. R. Soc. B* **2020**, *287*, 20192440. [CrossRef]
92. Aschoff, J. Freerunning and Entrained Circadian Rhythms. In *Biological Rhythms*; Aschoff, J., Ed.; Springer: Boston, MA, USA, 1981; pp. 81–93. [CrossRef]
93. Dunlap, J.C. Molecular Bases for Circadian Clocks. *Cell* **1999**, *96*, 271–290. [CrossRef] [PubMed]
94. Connor, K.M.; Gracey, A.Y. Circadian Cycles Are the Dominant Transcriptional Rhythm in the Intertidal Mussel *Mytilus Californianus*. *Proc. Natl. Acad. Sci. USA* **2011**, *108*, 16110–16115. [CrossRef] [PubMed]
95. Perrigault, M.; Tran, D. Identification of the Molecular Clockwork of the Oyster Crassostrea Gigas. *PLoS ONE* **2017**, *12*, e0169790. [CrossRef]
96. Pairett, A.N.; Serb, J.M. De Novo Assembly and Characterization of Two Transcriptomes Reveal Multiple Light-Mediated Functions in the Scallop Eye (Bivalvia: Pectinidae). *PLoS ONE* **2013**, *8*, e69852. [CrossRef] [PubMed]
97. Perrigault, M.; Andrade, H.; Bellec, L.; Ballantine, C.; Camus, L.; Tran, D. Rhythms during the Polar Night: Evidence of Clock-Gene Oscillations in the Arctic Scallop Chlamys Islandica. *Proc. R. Soc. B* **2020**, *287*, 20201001. [CrossRef] [PubMed]
98. Surge, D.; Lohmann, K.C.; Dettman, D.L. Controls on Isotopic Chemistry of the American Oyster, Crassostrea Virginica: Implications for Growth Patterns. *Palaeogeogr. Palaeoclimatol. Palaeoecol.* **2001**, *172*, 283–296. [CrossRef]
99. Tynan, S.; Dutton, A.; Eggins, S.; Opdyke, B. Oxygen Isotope Records of the Australian Flat Oyster (Ostrea Angasi) as a Potential Temperature Archive. *Mar. Geol.* **2014**, *357*, 195–209. [CrossRef]
100. Owen, R.; Kennedy, H.; Richardson, C. Isotopic Partitioning between Scallop Shell Calcite and Seawater: Effect of Shell Growth Rate. *Geochim. Cosmochim. Acta* **2002**, *66*, 1727–1737. [CrossRef]
101. Huyghe, D.; de Rafelis, M.; Ropert, M.; Mouchi, V.; Emmanuel, L.; Renard, M.; Lartaud, F. New Insights into Oyster High-Resolution Hinge Growth Patterns. *Mar. Biol.* **2019**, *166*, 48. [CrossRef]

102. Trofimova, T.; Alexandroff, S.J.; Mette, M.J.; Tray, E.; Butler, P.G.; Campana, S.E.; Harper, E.M.; Johnson, A.L.A.; Morrongiello, J.R.; Peharda, M.; et al. Fundamental Questions and Applications of Sclerochronology: Community-Defined Research Priorities. *Estuar. Coast. Shelf Sci.* **2020**, *245*, 106977. [CrossRef]
103. Jones, D.S. Annual Cycle of Shell Growth Increment Formation in Two Continental Shelf Bivalves and Its Paleoecologic Significance. *Paleobiology* **1980**, *6*, 331–340. [CrossRef]
104. Epstein, S.; Buchsbaum, R.; Lowenstam, H.A.; Urey, H.C. Revised carbonate-water isotopic temperature scale. *GSA Bull.* **1953**, *64*, 1315–1326. [CrossRef]
105. Jones, D.S.; Quitmyer, I.R. Marking Time with Bivalve Shells; Oxygen Isotopes and Season of Annual Increment Formation. *Palaios* **1996**, *11*, 340–346. [CrossRef]
106. Burchell, M.; Cannon, A.; Hallmann, N.; Schwarcz, H.P.; Schöne, B.R. Refining Estimates for the Season of Shellfish Collection on the Pacific Northwest Coast: Applying High-Resolution Stable Oxygen Isotope Analysis and Sclerochronology. *Archaeometry* **2013**, *55*, 258–276. [CrossRef]
107. Chute, A.S.; Wainright, S.C.; Hart, D.R. Timing of Shell Ring Formation and Patterns of Shell Growth in the Sea Scallop *Placopecten Magellanicus* Based on Stable Oxygen Isotopes. *J. Shellfish Res.* **2012**, *31*, 649–662. [CrossRef]
108. Kennedy, H.; Richardson, C.; Duarte, C.; Kennedy, D. Oxygen and Carbon Stable Isotopic Profiles of the Fan Mussel, Pinna Nobilis, and Reconstruction of Sea Surface Temperatures in the Mediterranean. *Mar. Biol.* **2001**, *139*, 1115–1124. [CrossRef]
109. Klein, R.T.; Lohmann, K.C.; Thayer, C.W. Bivalve Skeletons Record Sea-Surface Temperature and δ18O via Mg/Ca and 18O/16O Ratios. *Geology* **1996**, *24*, 415–418. [CrossRef]
110. Krantz, D.E.; Jones, D.S.; Williams, D.F. Growth Rates of the Sea Scallop, Placopecten Magellanicus, Determined from the 18o/16o Record in Shell Calcite. *Biol. Bull.* **1984**, *167*, 186–199. [CrossRef]
111. Tan, F.C.; Cai, D.; Roddick, D.L. Oxygen Isotope Studies on Sea Scallops, Placopecten Magellanicus, from Browns Bank, Nova Scotia. *Can. J. Fish. Aquat. Sci.* **1988**, *45*, 1378–1386. [CrossRef]
112. Balestra, B.; Rose, T.; Fehrenbacher, J.; Knobelspiesse, K.D.; Huber, B.T.; Gooding, T.; Paytan, A. In Situ Mg/Ca Measurements on Foraminifera: Comparison between Laser Ablation Inductively Coupled Plasma Mass Spectrometry and Wavelength-Dispersive X-ray Spectroscopy by Electron Probe Microanalyzer. *Geochem. Geophys. Geosyst.* **2021**, *22*, e2020GC009449. [CrossRef]
113. Poitevin, P.; Chauvaud, L.; Pécheyran, C.; Lazure, P.; Jolivet, A.; Thébault, J. Does Trace Element Composition of Bivalve Shells Record Utra-High Frequency Environmental Variations? *Mar. Environ. Res.* **2020**, *158*, 104943. [CrossRef]
114. Soldati, A.L.; Jacob, D.E.; Schöne, B.R.; Bianchi, M.M.; Hajduk, A. Seasonal Periodicity of Growth and Composition in Valves of Diplodon Chilensis Patagonicus (d'Orbigny, 1835). *J. Molluscan Stud.* **2009**, *75*, 75–85. [CrossRef]

Chapter 2.

Investigating the impacts of seawater acidification on juvenile Pacific littleneck clams (*Leukoma staminea*): can shell hash promote growth by altering pore water chemistry?

Abstract

Marine organisms that build calcium carbonate shells and skeletons are perhaps the most at-risk from ocean acidification, and adaptation strategies may be needed to keep coastal populations healthy. It can be energetically costly for marine invertebrates to mineralize under low pH conditions, and acidification can lead to shell dissolution. If shellfish populations decline, coastal ecosystems, commercial aquaculture, as well as communities dependent on shellfish for food security will suffer. Adding calcium carbonate shell hash beach sediments may mitigate negative effects of acidification by altering the chemistry of pore fluids, thus providing a potential strategy to protect infaunal calcifiers in the future. We tested the hypothesis that mixing shell hash into the sediment increases the pH and alkalinity of pore fluids, and enhances calcification in Pacific littleneck clams (*Leukoma staminea*). Juvenile clams were raised in four experimental conditions for 90 days: control seawater, acidified seawater, control seawater with shell hash, and acidified seawater with shell hash. Pore water and overlying seawater were sampled three times a week for pH, alkalinity, salinity, temperature, and dissolved oxygen. Clam shell weight, soft tissue weight, and new shell growth were measured. The presence of shell hash increased the pH, alkalinity and aragonite saturation state of pore fluids across all treatments. For example, the average pore water pH in acidified treatments was 7.06 +/- 0.084, and 7.48 +/- 0.034 in acidified treatments with shell hash. Clams grown in the presence of shell hash showed greater shell growth on average, although growth was variable across and within treatments, and shell hash did not have a statistically-significant effect on growth. This study suggests that adding shell hash to coastal sediments alters the chemistry of pore fluids, thus buffering against acidic conditions that could deleteriously affect mineralization of infaunal organisms.

1. Introduction

1.1 Ocean acidification and its impacts on shellfish

In seawater, inorganic carbon cycles through the carbonate system, which regulates acidity (pH) and contributes to the circulation of carbon among the atmosphere, lithosphere, hydrosphere and biosphere (Zeebe and Wolf-Gladrow 2001; Caldeira and Wickett 2003; Sabine et al. 2004; Millero 2005). Anthropogenic activities are actively disrupting this system, as the acid buffering capacity of the oceans (associated with weathering of continental rock and carbonate marine sediments) occurs on timescales too slow to balance out the effects of modern anthropogenic CO_2 inputs (Caldeira and Wickett 2003; Zachos et al. 2008; Doney et al. 2009; Hönisch et al. 2012). This imbalance is leading to the swift acidification of the world's oceans, posing risks to shellfish and other marine organisms (Caldeira and Wickett 2005; Orr et al. 2005; Gazeau et al. 2007; Doney et al. 2020). This occurs because ocean acidification (OA) leads to a net gain in hydrogen ions and net loss of carbonate ions, an important building block for shells and hard parts composed of calcium carbonate (Millero 2005; Orr et al. 2005; Cusack and Freer 2008).

Average global surface water pH levels have already declined by ~0.1 units since the Industrial Revolution (1760-1840), and are predicted to drop between 0.3 - 0.5 units by the year 2100 (Caldeira and Wickett 2005; Orr et al. 2005; Stocker et al. 2013). Given the myriad threats OA poses to humans and global ecosystems (e.g., Wallace et al. 2014; Waldbusser et al. 2015; Doney et al. 2020), mitigation strategies are of growing interest to both scientific and non-scientific communities (Renforth and Henderson 2017; Saderne et al. 2019; Macreadie et al. 2019; Curtin et al. 2022; Mackenzie et al. 2022). OA makes it energetically costly for marine invertebrates, including economically important species like shellfish, to build shells and skeletons, and low saturation conditions can lead to shell dissolution (Orr et al. 2005; Green et al.

2004; 2009; Waldbusser et al. 2015; Doney et al. 2020). Interestingly, adding pulverized bivalve shells (i.e., shell hash) to coastal habitats could lessen the effects of local acidification by buffering the chemistry of pore fluids, thus providing a potential adaptation strategy for infaunal organisms (Salter 2018; Ericson and Ragg 2021; Curtin et al. 2022; Doyle and Bendell 2022). Acid buffering capacity of seawater is measured by its alkalinity, which is affected by acid-base additions, redox reactions and mineral dissolution and precipitation (Middelburg et al. 2020). Alkalinity is of increasing interest to those interested in Blue Carbon ecosystems and climate change mitigation (Renforth and Henderson 2017; Middelburg et al. 2020).

Coastal ecosystems are perhaps the most at-risk of anthropogenically-induced OA due to additional acidification stressors including river runoff and increased nutrient loads (Smith et al. 1991; Salisbury et al. 2008; Wallace et al. 2014; Laurent et al. 2017; Kessouri et al. 2021). Pore water chemistry is related to the overlying seawater chemistry, but more complex and variable (Widdicombe et al. 2011). While overlying water chemistry affects the pore waters, additional processes including microbially-mediated redox reactions, abiotic mineral formation/dissolution, and mixing of sediments by macrofauna, are largely responsible for the amount and distribution of carbon dioxide in marine sediments (Burdige et al. 2008; Dashfield et al. 2008; Widdicombe et al. 2011; Kindeberg et al. 2020). Therefore, the precise impacts of anthropogenically-induced acidification of surface waters on infaunal organisms (i.e., those that live within the sediment) remains elusive (Andersson and Mackenzie 2011; Widdicombe et al. 2011). Infaunal organisms like *L. staminea* can be affected by acidification in two ways: taking in overlying water through the siphon at the sediment-water interface and processing it physiologically, and via the potential dissolution of shell material once mineralized via undersaturated pore fluids. Some recent studies demonstrate that seawater acidification can deleteriously alter infaunal adult bivalve shell

structure, growth and survival over the course of 40-120 days (Green et al. 2009; Cummings et al. 2011; Zhao et al. 2017). If shellfish within these settings fail to cope with the rapid pace of anthropogenic climate change, coastal ecosystems, commercial aquaculture, and communities dependent on shellfish for food security will suffer (Doney et al. 2020). Critical evaluations of how OA affects infaunal shellfish growth and survival can help predict future outcomes and manage current coastal populations.

1.2 Chemical buffering as a localized acidification mitigation strategy

In the 1990s, researchers first explored the potentially deleterious effects of ocean acidification on calcification in coral reefs, and acidic conditions have continued to negatively impact mineralizing organisms in a variety of marine habitats around the world (Kleypas et al. 1999; Kleypas et al. 2006; Ries et al. 2009). In the early 2000s, Pacific Northwest commercial oyster hatcheries experienced widespread collapse associated with coastal acidification (Feely et al. 2012; Barton et al. 2015). In response, hatchery, government and academic scientists began to explore methods to buffer seawater used in shellfish culture, including adding soda ash (Na_2CO_3) to larval rearing tanks (Barton et al. 2015; Clements and Chopin 2017; Mackenzie et al. 2022). In the northeastern United States, adding crushed bivalve shells (i.e., "shell hash") to mudflat was shown to increase the pH of sediment pore waters, decrease juvenile clam mortality, and increase settlement (Green et al. 2009; 2013). Similarly, Ericson and Ragg (2021), demonstrated that larval rearing tanks enriched with mussel shell hash improves larval shell development exposed to acidified conditions (Ericson and Ragg 2021). Under acidified conditions, the addition of soda ash (Na_2CO_3) and/or crushed shell ($CaCO_3$) increases the alkalinity and pH of the water, thus chemically buffering against the effects of OA (Clements and Chopin 2017; Ericson and Ragg 2021; Mackenzie et al. 2022). Chemical buffering of acidification to improve growth and

survival under future conditions will have varying success, depending on species' habitat preferences (i.e., epifaunal oysters and mussels vs. infaunal clams). Furthermore, the addition of shell hash can lead to additional physical changes in the substrate, like increasing the interstitial spaces in sediments, that promote juvenile clam recruitment and higher overall biodiversity (Jackley et al. 2016; Greiner et al. 2018).

Adding shell material back into intertidal sediments is not a novel management technique; this practice is part of some Indigenous mariculture systems built on millenia of knowledge (Lepofsky et al. 2015; Toniello et al. 2019; Tadlock 2019), particularly along the Northwest coast of North America. Although the precise management techniques vary by location, Indigenous sea gardens are intended to promote healthy populations and provide food security (Deur et al. 2015; Lepofsky et al. 2015; Jackley et al. 2016; Toniello et al. 2019). The existing published research on sea gardens demonstrates that they host larger clam populations (Toniello et al. 2019), greater intertidal biodiversity (Jackley et al. 2016), and promote public health, sovereignty, and sense of place and well-being for Indigenous citizens (Tadlock 2019). Sea garden tending sometimes involves the purposeful addition of pulverized shell material, or "shell hash," into beach sediments (Groesbeck et al. 2014; Deur et al. 2015; Greiner et al. 2018). Adding shell hash to beach sediments has known benefits for clam populations, but may also mitigate anticipated future changes to marine habitats and species.

We investigated the effects of experimentally acidified water on growth of infaunal juvenile Pacific littleneck clams (*L. staminea*), and determined if adding shell hash (i.e., pulverized clam shells) to the sediment mitigates the effects of acidic conditions over the course of three months. **We hypothesized that mixing shell hash into sediment increases the pH,**

alkalinity and saturation state of pore fluids, and enhances calcification in juvenile *L. staminea* exposed to experimental acidification.

1.3 Leukoma staminea as a study organism

The Pacific littleneck clam (*L. staminea*) is an excellent focal species because it is geographically widespread, relatively abundant and easily collected, and ecologically and culturally significant (Fraser and Smith 1928; Lepofsky et al. 2015; Schneider et al. 2018). *L. staminea* is an infaunal marine venerid bivalve that burrows 5-15 cm beneath the sediment surface along nearly the entire coast of western North America, ranging from Baja California, Mexico to Alaska (Fraser and Smith 1928) (Figure 2.1). Found in wide-ranging habitats, including exposed rocky beaches to low-energy mudflats, *L. staminea* have been managed and harvested by Indigenous peoples across the northeastern Pacific coast for millenia (Lepofsky et al. 2015; Schneider et al. 2018), and remain commonly collected and eaten by humans today. *L. staminea* is also an important food source within intertidal food webs, and is preyed on by drilling gastropods, sea stars, crabs, birds, and sea otters (Feder et al. 1979; Hiebert 2015). *L. staminea* is a suspension feeder, metabolizing ambient water that they take in with their siphons, while living in an infaunal environment where pore fluids affect their development once mineralized (Fraser and Smith 1928). Sexual maturity occurs at around 2-3 years, with broadcast spawning taking place in late-spring and early summer (Fraser and Smith 1928; Feder et al. 1979). Larvae remain pelagic for about 3-4 weeks, after which they settle on the substrate (Hiebert 2015). *L. staminea* biomineralizes a shell composed of the calcium carbonate polymorph aragonite, and contains light and dark banding patterns in the outer shell layers (Takesue and van Geen 2004; Fraser and Smith 1928). *L staminea* shells' banding patterns correspond with geochemical and microstructural changes in the shell, and significant size

variability can exist within populations of the same age (Kempf et al. 2023). Recent research has documented *L. staminea* population decline in some areas, perhaps due to competition with invasive species (Bendell 2014). Additional research suggests that some *L. staminea* populations have declined at least partly in response to oceanographic changes in salinity and temperature (Barber et al. 2019), but information regarding the impacts of acidification on *L. staminea* is lacking.

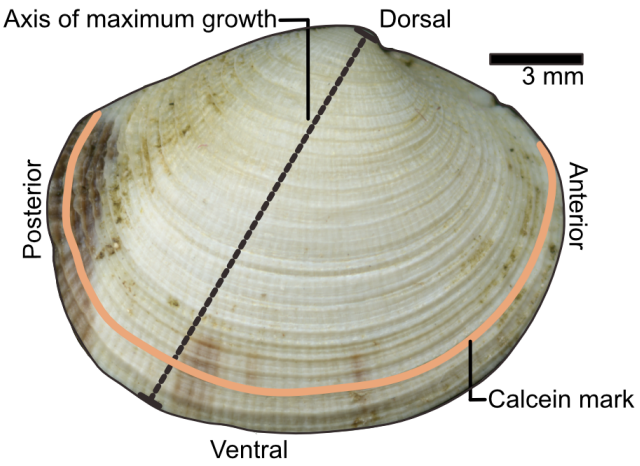

Figure 2.1 Juvenile *Leukoma staminea* left valve, exterior morphology.

2. Materials and Methods

2.1 Oceanographic setting of broodstock collection

Juvenile clams used in this study were from the same genetic cohort from a controlled spawn in the lab, with parent individuals collected live from Bodega Harbor in Bodega Bay, CA (Kempf et al. 2023). Bodega Bay is located approximately 60 miles north of San Francisco on the coast of California, and oceanographically sits within the California Current System (CCS)

(Hickey and Banas 2003; Checkley and Barth 2009; Davis et al. 2018; Largier 2020). The CCS is composed of the dominant south-flowing California Current, the north-flowing subsurface California Undercurrent, and the north-flowing Davidson Current that occurs seasonally in the winter (e.g., Hickey and Banas 2003). Along the CCS, distinct oceanographic conditions occur over varying spatiotemporal scales due to both physical and climate-related processes (Feely et al. 2008; García-Reyes and Largier 2012; Davis et al. 2018). For example, north of Point Conception, CA the CCS runs approximately parallel to the coastline, which yields strong seasonal upwelling associated with alongshore winds and Ekman transport, and lower sea surface temperatures than off the coast of southern California (Feely et al. 2008; Checkley and Barth 2009) . The coastal waters around Bodega Bay experience this seasonal upwelling during the spring-early summer months, with temperatures from ~10 to 12°C, followed by autumn relaxation periods with temperatures around ~13 to 15°C, and wet, moderate winters with seawater temperatures ~11°C (García-Reyes and Largier 2010; 2012). Average seawater pH varies widely from ~7.6 to ~8.0 throughout the region due to seasonally-influenced physical processes including upwelling, which lowers pH, as well as diel cycles of photosynthesis and respiration (Arp et al. 1992; García-Reyes and Largier 2012; Silbiger and Sorte 2018; Ricart et al. 2021). While dissolved inorganic carbon, total alkalinity and aragonite saturation state in coastal pore waters are heterogenous, and vary from overlying seawater (Widdicombe et al. 2011; Greiner et al. 2018; Kindeberg et al. 2020), the biogeochemical properties of the Bodega Bay region pore waters have not been extensively studied.

2.2 Broodstock conditioning and mass spawn protocol

We tested if acidification reduces the shell growth of juvenile *L. staminea* from the same reproductive cohort at the Bodega Marine Laboratory (Bodega Bay, CA, USA). Adult

broodstock *L. staminea* collected from Bodega Harbor during the winter of 2021 (n = 22) were brought to the Bodega Marine Lab for conditioning. Seawater is supplied to the lab via intake lines approximately 200 ft offshore in Horseshoe Cove. Intake elevation is approximately six feet below mean low tide, and water is sand-filtered to ~30 um before being gravity-fed to the facilities. Broodstock were placed in an open plastic basket (10" x 6") and set within a sea table filled with circulating seawater. During the 6-week conditioning period clams were fed twice a day with a dense mixture of *Nannochloropsis oculata* and *Isochrysis* algae (*personal communication* Jeff Hetrick, January 2021). During the first week, seawater temperature gradually increased to 17°C from 11°C using a gentle heater. The system was maintained with a steady influx of filtered seawater, and waste was siphoned from the holding containers daily. To check if clams were gravid, two clams were sacrificed and the visceral mass was gently scraped with a scalpel. The gonadal fluid from the sacrificed clams was pipetted onto a microscope slide and mixed with a small amount of seawater, and checked for the presence of eggs and sperm.

Once both males and females were gravid, all conditioned clams (n=20) were gently rinsed with warm seawater (~20 °C) and put in clean plastic baskets. Baskets were then placed in a single open 10 gallon shallow container containing seawater adjusted to approximately 24 °C. As the water was raised to 24 °C using a heated stirring rod, we gently added 30 L of dense *Nannochloropsis oculata* algae to the container. After the seawater algae mix reached 24°C, the clams were left in this set-up for one hour and allowed to feed and adjust to room temperature (~18 °C). A second round of algae was heated to 30 °C then added to the clams approximately one hour after the first feeding. Clams were left to eat and return to ambient temperature before a third round of 30 °C algae was added an hour later. The clams fed for 2 hours, with the lights off. Since clams had still not spawned after the third feeding, we flushed out the water/algae mix, and

sacrificed one clam, checked for sperm, and then pipetted its gonadal fluid into the setup to induce spawning. After two more hours at ~24 C, clams were fed one last time with 10 L of *N.oculata* and *Isochrysis*, and were left together in the experimental setup overnight and the system was allowed to gradually return to the ambient temperature of the room (~20 °C). Clams (n=19) spawned overnight.

Planktonic larvae were removed from the spawning container the following morning via siphoning, and transported into 400 L tanks in the Bodega Marine Laboratory Shellfish Hatchery. They remained in the hatchery at a temperature of 18-20 °C until the start of the experiment. Once some larvae began to settle at the bottom of the tank (three weeks post-fertilization), larvae were transferred onto a 250 micron settling screen and placed in a shallow water table supplied with filtered seawater in the same hatchery room (18-20 °C). Lights were kept on during the day and turned off at night, and salinity was maintained between 33-36 ppt and checked approximately every 3 days. The entire cohort was fed twice weekly with a 30 L mixture of *N. oculata* and *Isochrysis* algae. All individuals were kept in identical laboratory conditions during the juvenile rearing period (200 days). At 200 days old, juveniles were transported to the experimental conditions outlined below.

2.3 Experimental design and treatments

Juvenile clams were raised in four experimental conditions for 90 days where the pH of the overlying fluids was maintained in the following ways: (1) control filtered seawater (pH=7.76 +/- 0.054), (2) experimentally acidified seawater (pH=7.38 +/- 0.055), (3) control seawater with shell hash (pH=7.76 +/- 0.049), and (4) acidified seawater with shell hash (pH=7.38 +/- 0.056) (Figure 2.2). Treatments were run in technical duplicate, totalling eight

~22.7 L food-grade plastic buckets. Buckets were fed with filtered seawater held in header tanks, in which pH conditions were controlled using PinPoint pH controllers and regulators and a cylinder of compressed air with 1% CO2 (Airgas) (Figure 2.1). Probes were briefly removed every Monday and Friday in order to recalibrate using PinPoint recalibration fluids (pH = 4.0 and pH = 10.0). Each header tank was supplied with air via an airstone.

The buckets were filled with filtered seawater for three days prior to the start of the experiment. At the start of the experiment, buckets were filled with 5 L volume of unconsolidated medium-grained quartz sand (AquaQuartz) (porosity of 38.8%) prior to adding seawater. A silica-based substrate was chosen to minimize confounding variables of other substrates (such as sand collected *in situ* in Bodega Bay) that could more drastically affect the carbonate chemistry of the pore fluids via dissolution and microbial processes. Disarticulated clam shells were gathered in Bodega Bay, CA, bleached in 6 vol% NaOCl for 30 min to minimize the effects of microorganisms, rinsed thoroughly with fresh water, and air dried for 48 hours. Shells were then crushed using a mortar and pestle, and shell hash pieces were size-graded to 0.25-0.5 cm. All treatments with shell hash contained quartz sand with 10 wt% pulverized *L. staminea* and *Saxidomus nuttalli*, species native to Bodega Bay. We used two species to ensure enough shell material was available for the experimental setup, and because *Saxidomus spp.* and *L. staminea* are both managed in sea garden settings. Juvenile clams (n=30 per bucket) were placed in each bucket at the beginning of the experiment. We ran a research experiment simultaneously to examine gene expression in juvenile clams, which required sampling. Therefore, at the end of the experiment, 18 clams were sampled from each bucket for the shell growth analysis presented herein.

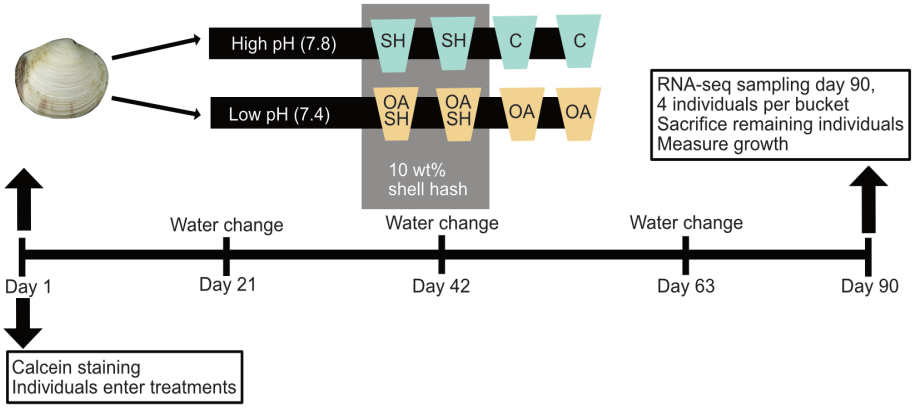

Figure 2.2. Experimental design of 90-day experiment. SH = shell hash, C = control, OASH = acidified with shell hash, OA = acidified.

2.4 Clam diet during the 90-day experimental period

N. oculata algae (8 L) was added every Monday and Friday to the header tanks to feed the animals. Although the decomposition of algae and waste likely altered the overlying water chemistry in the header tanks via respiration, the pH probes and CO_2 regulators detected that change and corrected for it by controlling the amount of CO_2 put into the system (see Results). Seawater changes in the header tanks were conducted approximately every three weeks (days 21, 42, 63, and 80).

2.5 Calcein staining and fluorescence

All individuals were fluorescently stained with calcein immediately before exposure to experimental treatments to mark the animals' shell length at the start of the experiment. Following the protocols of Moran and Marko (2005), calcein powder and DI water were combined to make a concentrated stock solution of 6.25g/L calcein, and the pH of the stock was adjusted to ~7.5 using sodium bicarbonate to increase the solubility of the calcein in seawater

(Moran and Marko 2005). The stock was added to 1L of filtered seawater (final concentration of 100 mg/L) (Moran and Marko 2005). After spending 24 hours in this solution, clams were transported to the experimental buckets and the 90 day experiment began.

2.6 Seawater chemistry

Throughout the duration of the 90 day experiment, seawater in the buckets was sampled for salinity, temperature, pH, and dissolved oxygen every Monday, Wednesday, and Friday using a Pinpoint® pH probe, a Pinpoint® dissolved oxygen probe, a thermometer, and a VeeGee refractometer for salinity. Pore water (i.e. water within the sediment grains) in each bucket was sampled for chemical analyses once per week using pore water wells (MHE products). Samples were taken from 8 cm depth in the substrate, approximately the depth at which *L. staminea* clams burrow. Pore water was sampled less frequently than overlying fluids to allow the pore fluids more time to interact with shell hash before removing them for sampling.

In addition to probe measurements, water samples for total pH and alkalinity were collected for pore water and overlying water in 125 mL glass bottles with a positive meniscus once per week to characterize water chemistry. Total pH samples were immediately poisoned with mercuric chloride to stop microbial respiration, and stored at 4°C unless analyzed immediately. pH samples were run in duplicate on an Ocean Optics Jaz Spectrophotometer EL200 (SD +/- 0.003) using m-cresol purple dye (Dickson et al., 2007). A calibration regression was produced for *m-cresol* and calibrated against Tris for a <0.1 pH offset. Prior to calculating the rest of the carbonate system, duplicate sample pH values were averaged (SD +/- 0.0088). At the same time, total alkalinity (TA) samples were collected in 250 mL Nalgene with a small amount of headspace, and frozen at -20°C, and later analyzed on an automated Gran titration on

a Metrohm 809 Titrando in triplicates. Measured TA was corrected for drift due to changes in temperature with drift catchers every twelve samples, and certified reference materials were analyzed at the beginning of each run (SD +/- 25.63 μmol/kg). Salinity, pH and alkalinity, and temperature were used to calculate aragonite saturation state using the "seacarb" package with the Shiny web application 'ScarFace' in R (vers. 4.1.3).

2.7 Shell morphology and growth

On day 90, juvenile clams (n=138) were sacrificed. Soft tissues were removed, immediately frozen at -20 ℃ and later freeze-dried. Shells were gently cleaned with fresh water and air-dried. We measured the following traits of clam shells: 1) total axis of maximum growth (AMG), 2) new growth along the AMG from the calcein mark, 3) shell dry weight and 4) freeze-dried soft tissue weight (Figure 2.1). Furthermore, in order to account for differences in shell sizes and growth rates, we calculated the percentage of AMG represented by new growth during the experiment as 5) % new growth = [(new growth (mm) / total axis maximum growth (mm))*100]. We also standardized the tissue and shell weights by calculating 6 and 7) weight per unit length [weight (mg)/total AMG(mm)] for each individual. Shell weight and soft tissue dry weight were then measured using a Mettler Toledo ME104E scale (0.0001 g). Shell length and AMG were measured using digital calipers (0.001 mm). New growth along the axis of maximum growth was measured in Fiji (formerly ImageJ) using images taken on a Nikon AZ100 fluorescent microscope (Schindelin et al. 2012) (Supplemental Figure 2.1).

2.8 Statistical analyses

Two-way analysis of variance (ANOVA) tests were performed to evaluate the statistical relationships between shell growth, carbonate chemistry and treatment types. ANOVA tests for

statistical significance using an *F* test, which compares variances of each group mean to the overall variance of the dependent variable. Here, two-way ANOVAs tested whether the overlying water pH (independent variable 1) and/or shell hash (independent variable 2) affected the pore water pH, pore water alkalinity and pore water saturation state (dependent variables). For morphological characteristics, we tested whether overlying water pH (independent variable 1) and shell hash (independent variable 2) affected the percent of new growth and shell weight (dependent variables). When data were not normally distributed, we transformed them using a log function. For all comparisons, we ran three ANOVAs: an additive two-way ANOVA (without any interaction or blocking variable), 2) two-way ANOVA with interaction (sediment type and pH level) but with no blocking variable (bucket ID), and 3) a two-way ANOVA with interaction (sediment type and pH level) and a blocking variable (bucket ID). We then calculated Akaike information criterion (AIC) to determine which ANOVA model best fit the data and reported F-statistics and *p*-values from that model. Lastly, to investigate bucket effects on growth, a linear mixed effects model was applied using restricted maximum likelihood in the lme4 package in R. The model predicted the percent new growth with treatment as a fixed-effect parameter and bucket ID as a nested random-effect within treatment. The call for this model in lme4 was: percent_new_growth ~ treatment + (1 | bucket.id/treatment). All statistical tests were performed in R (version 3.5.3).

3. Results

3.1 Seawater chemistry

Salinity, temperature and dissolved oxygen remained relatively constant over the course of the 90-day experiment (Table 2.1; Supplemental Table 2.1). Total pH values of the overlying

water demonstrate the experimental design was successful in maintaining the desired values around 7.4 and 7.8, with OA and OASH treatments maintaining overlying average pH values 7.38 and our C and SH treatments maintaining average values 7.76 (Figure 2.3, Supplemental Table 2.1). pH values did not vary significantly between technical replicates (T-test: $p > 0.05$), and we therefore pooled replicate data for calculating means and standard deviations (Supplemental Table 2.1). Using two-way ANOVA tests, we found statistically-significant differences in pore water alkalinity, pH and saturation states across treatments due to the presence of shell hash and overlying pH (Figures 2.3-2.6). Pore water alkalinity varied significantly by both overlying pH [$F(1)=457.89$, $p < 0.001$] and by presence/absence of shell hash [$F(2)=29.29$, $p < 0.001$], and the interaction between these these was significant ($p < 0.001$). Pore water pH also varied significantly by both overlying pH [$F(1)=74.34$, $p < 0.001$] and by presence/absence of shell hash [$F(2)=196.99$, $p < 0.001$], and the interaction between these was statistically significant ($p = 0.039$). Pore water saturation state also varied significantly by both overlying pH [$F(1)=34.66$, $p < 0.001$] and by presence/absence of shell hash [$F(2)=372.88$, $p < 0.001$], and the interaction between these was statistically significant ($p < 0.001$). Tukey post-hoc tests for all carbonate chemistry parameters revealed significant pairwise differences between many treatments based on presence/absence of shell hash and overlying pH (Table 2.2). pH in the pore waters remained relatively constant over time for all treatments except for the control treatment, which decreased over time (Figure 2.6).

Header tank	**Salinity (ppt)**	**Temperature (ºC)**	**Dissolved Oxygen (mg/L)**	**pH (in situ)**
Acidified	34.58 +/- 0.50	15.7 +/- 0.49	8.22 +/- 0.569	7.80 +/- 0.039
Control	34.57 +/- 0.51	15.7 +/- 0.49	8.25 +/- 0.471	7.31 +/- 0.028

Table 2.1. Means and standard deviations for salinity, temperature, dissolved oxygen, and pH measured in the header tanks (acidified and control) over the course of the 90-day experiment.

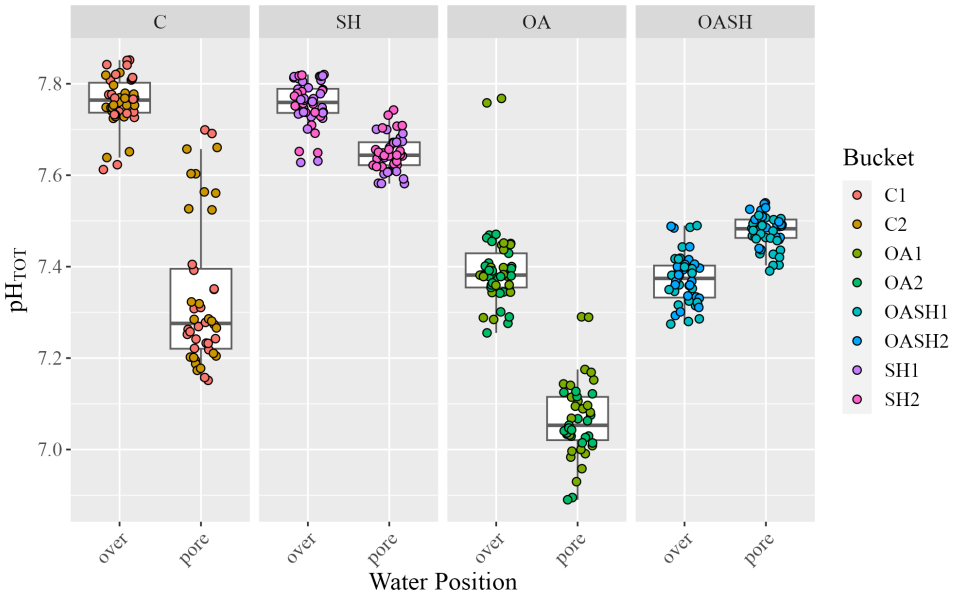

Figure 2.3. Box plots depicting pH_{TOT} for all treatments' pore water and overlying water. C = control; SH = shell hash; OA = acidified; OASH = acidified + shell hash.

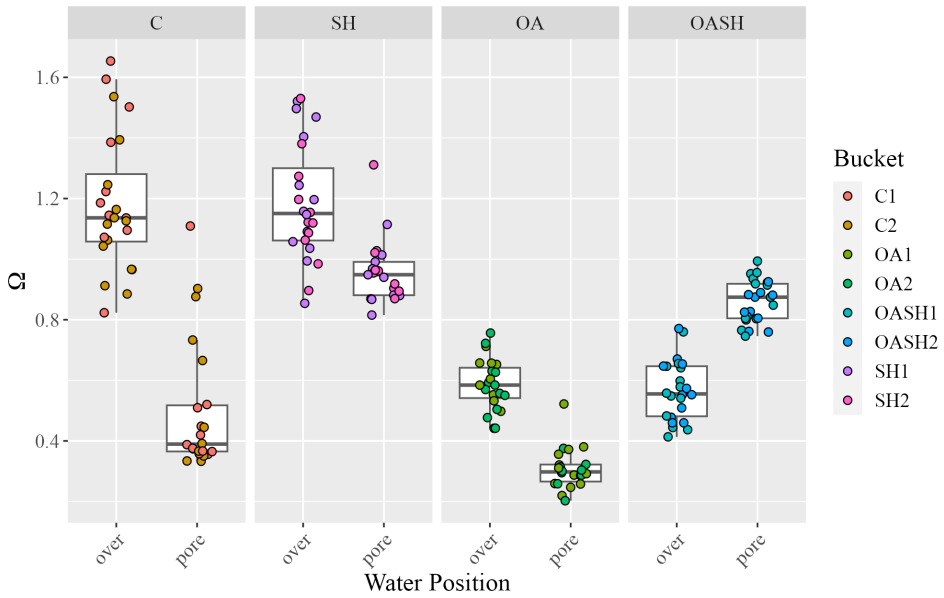

Figure 2.4. Boxplots depicting pooled aragonite saturation state (**Ω**) data for all treatments' pore water and overlying water. For saturation state data, values over one favor aragonite precipitation, and less than one favor dissolution. C = control; SH = shell hash; OA = acidified; OASH = acidified + shell hash.

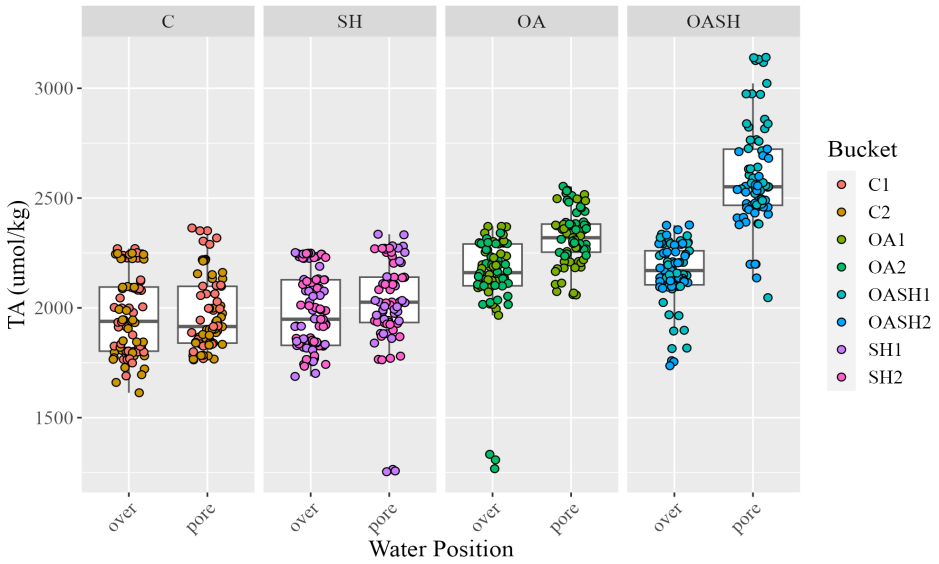

Figure 2.5. Boxplots depicted pooled total alkalinity (TA) data for all treatments' pore water and overlying water. C = control; SH = shell hash; OA = acidified; OASH = acidified + shell hash.

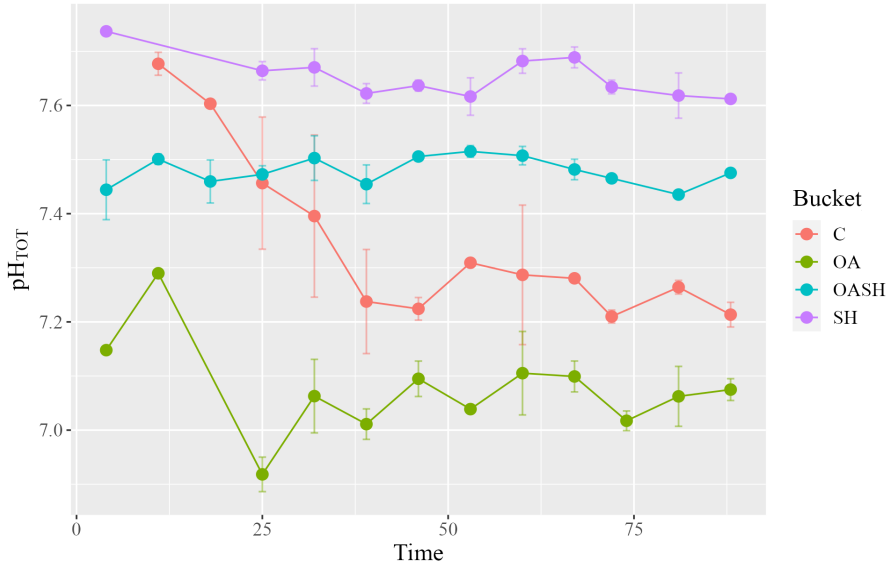

Figure 2.6. Pore water pH_{TOT} over time. Points on the plot show the mean values, and lines denote standard deviation. A set of samples from the beginning of the experiment are missing due to sampling error. C = normal pH conditions, SH= normal conditions with shell hash, OA = ocean acidification, OASH = ocean acidification + shell hash.

Tukey HSD Results for Pore Water Chemistry ($p < 0.001$)		
pH	**Alkalinity**	**Saturation State**
SH:C	SH:C	SH:C
OA:C	OA:C	OA:C
OASH:C	OASH:C	OASH:C
OA:SH	OA:SH	OA:SH
OASH:SH	OASH:SH	OASH:OA
SH:OA	OASH:OA	

Table 2.2. Tukey post-hoc tests for all pore water carbonate chemistry parameters analyzed with two-way ANOVA. Significant pairwise differences between treatments based on presence/absence of shell hash (sand vs. sand with shell hash) and overlying pH (low vs. high) are shown for pH, alkalinity and aragonite saturation state.

3.2 Shell morphology and growth

Calcein stains were reliably produced in most individuals (n=136), with only a small subset lacking distinct lines (n=7). Furthermore, one clam died in the SH treatment, and a subset of clams were removed from the SH treatment for a genetic study by the first author (n=6). Therefore, a total of 130 clams were measured and compared statistically at the end of the experiment. Growth metrics within the population varied within each treatment, regardless of exposure to low pH seawater and/or shell hash. Average percent new growth varied across treatments (Table 2.3; Figure 2.7), with those growing in shell hash treatments the most and

those in the low pH treatments the least. Two-way ANOVAs revealed that, when viewing all data, differences were statistically-significant by overlying pH [$F(1)=5.82$, $p = 0.0173$], but not presence/absence of shell hash [$F(1)=3.01$, $p = 0.085$], and the interaction between these metrics was not statistically significant ($p = 0.066$). This difference in size may be caused by the size variability in the juvenile animals at the beginning of the experiment. Tukey HSD post-hoc tests for percent new growth revealed significant pairwise differences between the following levels: OA vs. C ($p = 0.0157$), OA vs. SH ($p = 0.0258$), and OASH vs. OA ($p = 0.0487$). Two-way ANOVAs and Tukey HSDs did not identify statistically significant differences in shell weight or tissue weight across treatments by overlying pH or sediment type ($p > 0.05$). Bucket effects did not affect growth metrics, with only 0.154% variance explained by bucket ID (Supplemental Table 2.2).

	Shell length (mm)	**Total AMG (mm)**	**Growth on AMG (mm)**	**% New growth**	**Shell weight (g)**	**Tissue dry weight (mg)**
C	12.4 +/- 4.21	11.5 +/- 3.76	1.05 +/- 0.815	8.30 +/- 4.24	0.604 +/- 0.485	47.5 +/- 39.7
SH	13.2 +/- 4.33	11.1 +/- 3.45	1.13 +/- 0.963	9.38 +/- 7.24	0.611 +/- 0.538	49.7 +/- 44.3
OA	12.8 +/- 3.53	10.7 +/- 2.91	0.670 +/- 0.51	5.65 +/- 3.5	0.468 +/- 0.374	35.7 +/- 27.9
OASH	12.8 +/- 3.97	11.0 +/- 3.15	0.873 +/- .50	7.46 +/- 3.35	0.486 +/- 0.414	37.5 +/- 31.5

Table 2.3. Morphological metrics measured on day 90. Averages and standard deviations are shown. C = normal pH conditions, SH= normal conditions with shell hash, OA = ocean acidification, OASH = ocean acidification + shell hash.

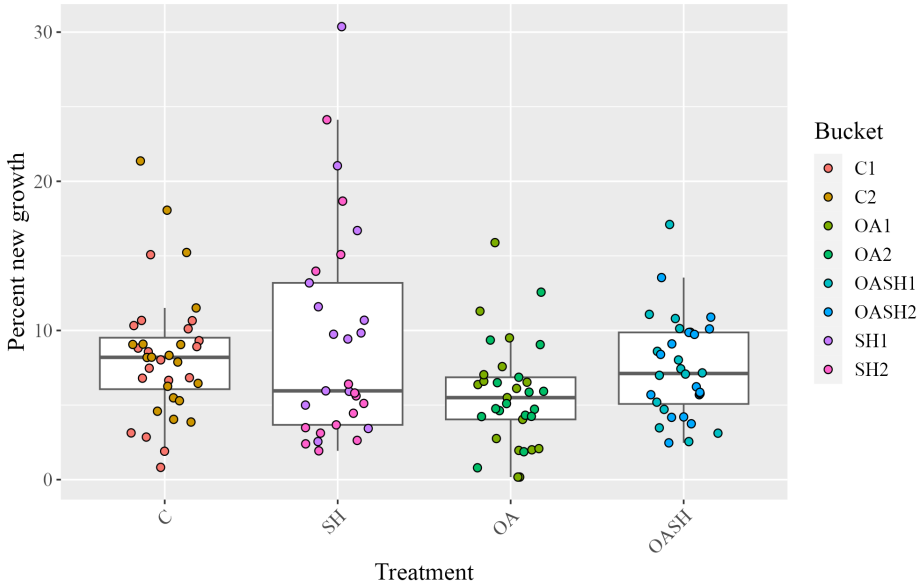

Figure 2.7. Box plots depicting percent new growth for clams in different treatments at day 90. C = normal pH conditions, SH= normal conditions with shell hash, OA = ocean acidification, OASH = ocean acidification + shell hash.

4. Discussion

Shell hash added to the sediment had a clear and statistically-significant effect on pore water chemistry. Specifically, shell hash increased alkalinity, pH, and the aragonite saturation state of pore fluids, thus buffering experimental acidification ($p < 0.01$). The effect of shell hash on shell growth, however, was less clear. While significant *p*-values (typically 0.05) have been criticized as overly strict for biological comparisons (Holland 2019), we present results herein based on this cutoff. Percent new growth was on average the highest in shell hash treatments, and lowest in the low pH treatments. However, two-way ANOVAs did not reveal statistically-significant effects of shell hash on clam growth ($p = 0.085$). However, it is possible that our sample size was too small to detect and statistically-significant result (Holland 2019). For

percent new growth, differences were statistically-significant due to overlying pH (i.e. acidified vs. non-acidified treatments) ($p = 0.0173$), suggesting clam growth is deleteriously affected by overlying seawater acidification. Post-hoc Tukey tests revealed statistically significant pairwise differences in percent new growth between the following treatments: control vs. OA treatments, OA vs. SH treatments, and OA vs. OASH treatments. Growth rate varied within and across treatments, despite using individuals from the same reproductive cohort (Kempf et al. 2023). Size (and genetic) variability within the population is one possible explanation for the lack of statistically-significant differences in growth in the presence of shell hash. In the future, additional studies using animals of both the same age, genetic cohort and *size* may help disentangle the effects of OA on shell growth.

In all, our results demonstrate that shell hash can significantly affect pore water chemistry under experimentally acidified conditions, and warrants future research investigating the scalability of this mitigation strategy. Ocean acidification reduces alkalinity, saturation state and pH of both overlying and pore fluids, which, as demonstrated here, deleteriously affect mineralizing organisms like clams. However, biomineralizing species have varying responses to ocean acidification (e.g., Ries et al. 2009; Cummings et al. 2011; Zhao et al. 2017; Dodd et al. 2021), and shell hash is likely not a panacea for all infaunal organisms experiencing this stressor. As this laboratory study is limited in its scope, additional research is needed to manage *L. staminea* populations in the future. For example, the vulnerability of planktonic *L. staminea* larvae to corrosive conditions while in the water column is unknown. Further research on the ability of shell hash to buffer acidic conditions at the water-sediment interface where larvae first settle could help protect the youngest, most vulnerable life stages (Green et al. 2009; Waldbusser et al. 2015). This research is needed for many species in coastal settings, where the compounding

stressors of ocean acidification, eutrophication and infaunal respiration could yield conditions that are too corrosive for larval settlement and development (Green et al. 2009; Waldbusser et al. 2015; Doyle and Bendell 2022).

Further, the existing field research on the role that shell hash plays in moderating pore water chemistry has variable results (Green et al. 2009; 2013; Greiner et al. 2018; Beal et al. 2020; Curtin et al. 2022; Doyle and Bendell 2022). In the wild, local variability is most likely large and difficult to characterize accurately. Our experimental results oppose the findings of Beal et al. (2020), which identified no significant difference in mean pH of sediment pore waters in Freeport, Maine, regardless of presence/absence of shell hash ($p = .115$). Interestingly, though, Green et al. (2009) found that the saturation state increased significantly from 0.25 in control plots to 0.53 in plots buffered with shell hash in the nearby West Bath, Maine. Greiner et al. (2018) demonstrated that adding shell hash to field settings in the Pacific Northwest led to higher pore-water pH and aragonite saturation state ($p < 0.05$), corroborating our results, but identified no measured effect on the recruitment or survival of the venerid *Ruditapes philippinarum* (Greiner et al. 2018). In the Burrat Islet of British Columbia, Doyle and Bendell (2021) found that the presence of shell hash did not clearly mitigate corrosive pH conditions, but did correlate with a reduction in pore water chemistry variability in a site with a high quantity of organic matter associated with tidal cycles, suggesting that using shell hash as an OA mitigation strategy is likely site-dependent (Doyle and Bendell 2022). The size of shell hash particles, and timescale of experiment varied amongst these studies, which may explain some of the differences in results. Shell hash may also have additional effects on the benthos that are not explored in these studies, including increased settlement cues for predators like crab (Palacios et al. 2000;

Moksnes 2002), although increasing structural complexity in soft-bottom mudflats generally increases prey refugia (Irlandi and Peterson 1991; Grabowski 2004).

In coastal settings, biological processes like respiration and bioturbation can alter pore water carbonate chemistry parameters (Mackenzie and Andersson 2011; Kindeberg et al. 2020), which may explain some of the water chemistry variability observed in our laboratory experiment. Interestingly, pore fluids in all treatments had a lower pH than the overlying fluids, except for the OASH treatment, and this decreased over time, especially in the control condition (Figure 2.6). We suspect that this is related to the microbially-mediated decomposition of organic matter (fecal matter, uneaten algae) that accumulated in the buckets and substrate, as well as respiration from the clams themselves, both processes that would lead to increased carbon dioxide in the system. In the absence of shell hash, the pH was thus driven down. Additionally, the clams may have moved up and down as they fed, potentially mixing the sediments around their burrows and introducing water from above. All of these biological factors likely affected the measured chemical properties of the pore water. In all, we observed statistically-significant differences in water chemistry within the pore fluids of our experimental treatments. Our results demonstrate that, at a very localized level, shell hash increases total alkalinity (i.e., buffering capacity), pH and saturation state in pore fluids, but further research is needed to demonstrate how these values could scale differently in field settings. As the oceans increase in total inorganic carbon and dissolved carbon dioxide, and decrease in pH and carbonate concentration (i.e., OA), investigating the use of shell hash (from varying species) to increase localized buffering capacity and promote shellfish growth, both epifaunal and infaunal, is warranted (Middelburg et al. 2020).

5. Conclusions

Ocean acidification had a negative effect on clam growth, and this result was statistically significant. Furthermore, on average, clam shell weight, soft tissue weight, and new growth were higher in treatments in which shell hash was added, but the effect of shell hash on growth was not statistically significant, potentially due to significant size variability within the experimental, young juvenile population. Although we observed variability in growth metrics, our results clearly demonstrate that mixing shell hash into the sediments reduces corrosive conditions in pore waters exposed to future-predicted overlying seawater conditions. The presence of shell hash increased the pH, alkalinity, and saturation state of pore fluids across all treatments, and this was statistically significant. Interestingly, pore fluids were more acidic than the overlying fluids in all treatments except for the OASH, which had pore fluids with a higher pH and saturation state than the overlying fluid. We suspect the lower pH and saturation state of three of the four treatments' pore fluids relative to the overlying water was related to microbial decomposition of organic matter. In all, this study suggests that adding shell hash to sediments can alter the chemistry of pore fluids, thus buffering against acidic conditions that could harm the growth, mineralization and potential shell dissolution of infaunal organisms. Implementation of this technique in coastal settings, however, should be considered on a site-by-site basis and will require more research on additional species. Nonetheless, this experiment provides significant evidence of shell hash buffering capacity, and provides promising results to prompt future research on localized acidification mitigation.

References

Andersson, A. J., and F. T. Mackenzie. 2011. “Effects of Ocean Acidification on Benthic Processes, Organisms, and Ecosystems.” In *Ocean Acidification*, edited by Jean-Pierre Gattuso and Lina Hansson, 0. Oxford University Press. https://doi.org/10.1093/oso/9780199591091.003.0012.

Arp, A. J., B. M. Hansen, and D. Julian. 1992. “Burrow Environment and Coelomic Fluid Characteristics of the Echiuran Worm Urechis Caupo from Populations at Three Sites in Northern California.” *Marine Biology* 113 (4): 613–23. https://doi.org/10.1007/BF00349705.

Barber, J. S., C. P. Ruff, J. T. McArdle, L. L. Hunter, C. A. Speck, D. W. Rogers, and C. M. Greiner. 2019. “Intertidal Clams Exhibit Population Synchrony across Spatial and Temporal Scales.” *Limnology and Oceanography* 64 (S1): S284–300. https://doi.org/10.1002/lno.11085.

Barton, A., G. Waldbusser, R. Feely, S. Weisberg, J. Newton, B. Hales, S. Cudd. 2015. “Impacts of Coastal Acidification on the Pacific Northwest Shellfish Industry and Adaptation Strategies Implemented in Response.” *Oceanography* 25 (June): 146–59. https://doi.org/10.5670/oceanog.2015.38.

Beal, B. F., C. R. Coffin, S. F. Randall, C. A. Goodenow, K. E. Pepperman, and B. W. Ellis. 2020. “Interactive Effects of Shell Hash and Predator Exclusion on 0-Year Class Recruits of Two Infaunal Intertidal Bivalve Species in Maine, USA.” *Journal of Experimental Marine Biology and Ecology* 530–531 (September): 151441. https://doi.org/10.1016/j.jembe.2020.151441.

Bendell, L. 2014. “Evidence for Declines in the Native Leukoma Staminea as a Result of the Intentional Introduction of the Non-Native Venerupis Philippinarum in Coastal British Columbia, Canada.” *Estuaries and Coasts*, 12.

Burdige, D. J., R. C. Zimmerman, and X. Hu. 2008. “Rates of Carbonate Dissolution in Permeable Sediments Estimated from Pore-Water Profiles: The Role of Sea Grasses.” *Limnology and Oceanography* 53 (2): 549–65. https://doi.org/10.4319/lo.2008.53.2.0549.

Caldeira, K., and M.E. Wickett. 2003. “Anthropogenic Carbon and Ocean pH.” *Nature* 425 (6956): 365–365. https://doi.org/10.1038/425365a.

———. 2005. “Ocean Model Predictions of Chemistry Changes from Carbon Dioxide Emissions to the Atmosphere and Ocean.” *Journal of Geophysical Research: Oceans* 110 (C9). https://doi.org/10.1029/2004JC002671.

Checkley, D., and J. Barth. 2009. “Patterns and Processes in the California Current System.” *Progress In Oceanography* 83 (December): 49–64. https://doi.org/10.1016/j.pocean.2009.07.028.

Clements, J.C., and T. Chopin. 2017. “Ocean Acidification and Marine Aquaculture in North America: Potential Impacts and Mitigation Strategies.” *Reviews in Aquaculture* 9 (4): 326–41. https://doi.org/10.1111/raq.12140.

Cummings, V., J.Hewitt, A.Van Rooyen, K. Currie, S. Beard, S. Thrush, J.Norkko. 2011. “Ocean Acidification at High Latitudes: Potential Effects on Functioning of the Antarctic Bivalve Laternula Elliptica.” *PLOS ONE* 6 (1): e16069. https://doi.org/10.1371/journal.pone.0016069.

Curtin, T. P., N. Volkenborn, I. P. Dwyer, R. C. Aller, Q. Zhu, and C. J. Gobler. 2022. "Buffering Muds with Bivalve Shell Significantly Increases the Settlement, Growth, Survival, and Burrowing of the Early Life Stages of the Northern Quahog, Mercenaria Mercenaria, and Other Calcifying Invertebrates." *Estuarine, Coastal and Shelf Science* 264 (January): 107686. https://doi.org/10.1016/j.ecss.2021.107686.

Cusack, M., and A. Freer. 2008. "Biomineralization: Elemental and Organic Influence in Carbonate Systems." *Chemical Reviews* 108 (11): 4433–54. https://doi.org/10.1021/cr078270o.

Dashfield, S. L., P. J. Somerfield, S. Widdicombe, M. C. Austen, and M. Nimmo. 2008. "Impacts of Ocean Acidification and Burrowing Urchins on Within-Sediment pH Profiles and Subtidal Nematode Communities." *Journal of Experimental Marine Biology and Ecology* 365 (1): 46–52. https://doi.org/10.1016/j.jembe.2008.07.039.

Davis, C.V., K. Hewett, T. M. Hill, J. L. Largier, B. Gaylord, and J. Jahncke. 2018. "Reconstructing Aragonite Saturation State Based on an Empirical Relationship for Northern California." *Estuaries and Coasts* 41 (7): 2056–69. https://doi.org/10.1007/s12237-018-0372-0.

Deur, D., A. Dick, K. Recalma-Clutesi, and N. J. Turner. 2015. "Kwakwaka'wakw 'Clam Gardens.'" *Human Ecology* 43 (2): 201–12. https://doi.org/10.1007/s10745-015-9743-3.

Dodd, L. F., J. H. Grabowski, M. F. Piehler, I. Westfield, and J. B. Ries. 2021. "Juvenile Eastern Oysters More Resilient to Extreme Ocean Acidification than Their Mud Crab Predators." *Geochemistry, Geophysics, Geosystems* 22 (2): e2020GC009180. https://doi.org/10.1029/2020GC009180.

Doney, S. C., D. S. Busch, S. R. Cooley, and K. J. Kroeker. 2020. “The Impacts of Ocean Acidification on Marine Ecosystems and Reliant Human Communities.” *Annual Review of Environment and Resources* 45 (1): 83–112. https://doi.org/10.1146/annurev-environ-012320-083019.

Doney, S. C., V. J. Fabry, R. A. Feely, and J. A. Kleypas. 2009. “Ocean Acidification: The Other CO2 Problem.” *Annual Review of Marine Science* 1 (1): 169–92. https://doi.org/10.1146/annurev.marine.010908.163834.

Doyle, B., and L. I. Bendell. 2022. “An Evaluation of the Efficacy of Shell Hash for the Mitigation of Intertidal Sediment Acidification.” *Ecosphere* 13 (3): e4003. https://doi.org/10.1002/ecs2.4003.

Ericson, J. A., and N. L. C. Ragg. 2021. “Effects of Crushed Mussel, Perna Canaliculus, Shell Enrichment on Seawater Carbonate Buffering and Development of Conspecific Larvae Exposed to near-Future Ocean Acidification.” *Journal of the World Aquaculture Society* n/a (n/a). https://doi.org/10.1111/jwas.12779.

Feder, H. M., J. C. Hendee, P. Holmes, G. J. Mueller, and A. J. Paul. 1979. “Examination of a Reproductive Cycle of Protothaca Staminea Using Histology, We Weight-Dry Weight Ratios, and Condition Indices.” *Veliger* 22 (2): 182–87.

Feely, R. A., T. Klinger, J. A. Newton, and M. Chadsey. 2012. “Scientific Summary of Ocean Acidification in Washington State Marine Waters.” NOAA OAR Special Report.

Feely, R. A., C.L. Sabine, J. M. Hernandez-Ayon, D. Ianson, and B. Hales. 2008. “Evidence for Upwelling of Corrosive ‘Acidified’ Water onto the Continental Shelf.” *Science* 320

(5882): 1490–92. https://doi.org/10.1126/science.1155676.

Fraser, C.M., and G. M. Smith. 1928. “Notes on the Ecology of the Little Neck Clam. Paphia Staminea Conrad.” *Trans. R. Soc. Can. Ser.* 3: 249–69.

García-Reyes, M., and J. Largier. 2010. “Observations of Increased Wind-Driven Coastal Upwelling off Central California.” *Journal of Geophysical Research: Oceans* 115 (C4). https://doi.org/10.1029/2009JC005576.

García-Reyes, M., and J. L. Largier. 2012. “Seasonality of Coastal Upwelling off Central and Northern California: New Insights, Including Temporal and Spatial Variability.” *Journal of Geophysical Research: Oceans* 117 (C3). https://doi.org/10.1029/2011JC007629.

Gazeau, F., C. Quiblier, J. M. Jansen, J. Gattuso, J. J. Middelburg, and C. H. R. Heip. 2007. “Impact of Elevated CO2 on Shellfish Calcification.” *Geophysical Research Letters* 34 (7). https://doi.org/10.1029/2006GL028554.

Grabowski, J. H. 2004. “Habitat Complexity Disrupts Predator–Prey Interactions but Not the Trophic Cascade on Oyster Reefs.” *Ecology* 85 (4): 995–1004. https://doi.org/10.1890/03-0067.

Green, M. A., M. E. Jones, C. L. Boudreau, R. L. Moore, and B. A. Westman. 2004. “Dissolution Mortality of Juvenile Bivalves in Coastal Marine Deposits.” *Limnology and Oceanography* 49 (3): 727–34. https://doi.org/10.4319/lo.2004.49.3.0727.

Green, M. A., G. G. Waldbusser, L. Hubazc, E. Cathcart, and J. Hall. 2013. “Carbonate Mineral Saturation State as the Recruitment Cue for Settling Bivalves in Marine Muds.” *Estuaries and Coasts* 36 (1): 18–27. https://doi.org/10.1007/s12237-012-9549-0.

Green, M. A., G. G. Waldbusser, S. L. Reilly, K. Emerson, and S. O'Donnell. 2009. "Death by Dissolution: Sediment Saturation State as a Mortality Factor for Juvenile Bivalves." *Limnology and Oceanography* 54 (4): 1037–47. https://doi.org/10.4319/lo.2009.54.4.1037.

Greiner, C. M., T. Klinger, J. L. Ruesink, J. S. Barber, and M. Horwith. 2018. "Habitat Effects of Macrophytes and Shell on Carbonate Chemistry and Juvenile Clam Recruitment, Survival, and Growth." *Journal of Experimental Marine Biology and Ecology* 509 (December): 8–15. https://doi.org/10.1016/j.jembe.2018.08.006.

Groesbeck, Amy, K. Rowell, D. Lepofsky, and A. Solomon. 2014. "Ancient Clam Gardens Increased Shellfish Production: Adaptive Strategies from the Past Can Inform Food Security Today." *PLoS One* 9 (3).

Hickey, B. M., and N. S. Banas. 2003. "Oceanography of the U.S. Pacific Northwest Coastal Ocean and Estuaries with Application to Coastal Ecology." *Estuaries* 26 (4): 1010–31. https://doi.org/10.1007/BF02803360.

Hiebert, T.C. 2015. "Leukoma Staminea." In *Oregon Estuarine Invertebrates: Rudys' Illustrated Guide to Common Species*, 3rd ed. Charleston, OR: University of Oregon Libraries and Oregon Institute of Marine Biology. https://scholarsbank.uoregon.edu/xmlui/bitstream/handle/1794/12918/L_staminea_2016_final.pdf?sequence=3.

Holland, S. M. 2019. "Estimation, Not Significance." *Paleobiology* 45 (1): 1–6. https://doi.org/10.1017/pab.2018.43.

Hönisch, B., A. Ridgwell, D. N. Schmidt, E. Thomas, S. J. Gibbs, A. Sluijs, R. Zeebe. 2012. "The Geological Record of Ocean Acidification." *Science* 335 (6072): 1058–63. https://doi.org/10.1126/science.1208277.

Irlandi, E. A., and C. H. Peterson. 1991. "Modification of Animal Habitat by Large Plants: Mechanisms by Which Seagrasses Influence Clam Growth." *Oecologia* 87 (3): 307–18. https://doi.org/10.1007/BF00634584.

Jackley, J., L. Gardner, A. Djunaedi, and A. Salomon. 2016. "Ancient Clam Gardens, Traditional Management Portfolios, and the Resilience of Coupled Human-Ocean Systems." *Ecology and Society* 21 (4). https://doi.org/10.5751/ES-08747-210420.

Kempf, H. L., D. A. Gold, and S. J. Carlson. 2023. "Investigating the Relationship between Growth Rate, Shell Morphology, and Trace Element Composition of the Pacific Littleneck Clam (Leukoma Staminea): Implications for Paleoclimate Reconstructions." *Minerals* 13 (6): 814. https://doi.org/10.3390/min13060814.

Kessouri, F., J.C. McWilliams, D. Bianchi, M. Sutula, L. Renault, C. Deutsch, R. A. Feely. 2021. "Coastal Eutrophication Drives Acidification, Oxygen Loss, and Ecosystem Change in a Major Oceanic Upwelling System." *Proceedings of the National Academy of Sciences* 118 (21): e2018856118. https://doi.org/10.1073/pnas.2018856118.

Kindeberg, T., N. R. Bates, T. A. Courtney, T. Cyronak, A. Griffin, F. T. Mackenzie, M. Paulsen, and A. J. Andersson. 2020. "Porewater Carbonate Chemistry Dynamics in a Temperate and a Subtropical Seagrass System." *Aquatic Geochemistry* 26 (4): 375–99. https://doi.org/10.1007/s10498-020-09378-8.

Kleypas, J. A., R. W. Buddemeier, D. Archer, J. Gattuso, C.Langdon, and B. N. Opdyke. 1999. "Geochemical Consequences of Increased Atmospheric Carbon Dioxide on Coral Reefs." *Science* 284 (5411): 118–20. https://doi.org/10.1126/science.284.5411.118.

Kleypas, J., R. Feely, V. Fabry, C. Langdon, S. Chris, and L. Robbins. 2006. "Impacts of Ocean Acidification on Coral Reefs and Other Marine Calcifiers: A Guide for Future Research." *Report of a Workshop Held* Vol. 18 (January).

Largier, J. L. 2020. "Upwelling Bays: How Coastal Upwelling Controls Circulation, Habitat, and Productivity in Bays." *Annual Review of Marine Science* 12 (1): 415–47. https://doi.org/10.1146/annurev-marine-010419-011020.

Laurent, A., K. Fennel, W. Cai, W. Huang, L. Barbero, and R. Wanninkhof. 2017. "Eutrophication-Induced Acidification of Coastal Waters in the Northern Gulf of Mexico: Insights into Origin and Processes from a Coupled Physical-Biogeochemical Model." *Geophysical Research Letters* 44 (2): 946–56. https://doi.org/10.1002/2016GL071881.

Lepofsky, D., N. Smith, N. Cardinal, J. Harper, M. Morris, G. Elroy White, R. Bouchard. 2015. "Ancient Shellfish Mariculture on the Northwest Coast of North America." *American Antiquity* 80 (2): 236–59.

Mackenzie, C. L., C. M. Pearce, S. Leduc, D. Roth, C.T. E. Kellogg, R. B. G. Clemente-Carvalho, and T. J. Green. 2022a. "Impacts of Seawater pH Buffering on the Larval Microbiome and Carry-Over Effects on Later-Life Disease Susceptibility in Pacific Oysters." *Applied and Environmental Microbiology* 88 (22): e01654-22. https://doi.org/10.1128/aem.01654-22.

Mackenzie, F. T., and A. J. Andersson. 2011. “Biological Control on Diagenesis: Influence of Bacteria and Relevance to Ocean Acidification.” In *Encyclopedia of Geobiology*, edited by Joachim Reitner and Volker Thiel, 137–43. Encyclopedia of Earth Sciences Series. Dordrecht: Springer Netherlands. https://doi.org/10.1007/978-1-4020-9212-1_73.

Macreadie, P. I., A. Anton, J. A. Raven, N. Beaumont, R. M. Connolly, D. A. Friess, J. J. Kelleway, et al. 2019. “The Future of Blue Carbon Science.” *Nature Communications* 10 (September): 3998. https://doi.org/10.1038/s41467-019-11693-w.

Middelburg, J. J., K. Soetaert, and M. Hagens. 2020. “Ocean Alkalinity, Buffering and Biogeochemical Processes.” *Reviews of Geophysics* 58 (3): e2019RG000681. https://doi.org/10.1029/2019RG000681.

Millero, F. J. 2005. *Chemical Oceanography, Third Edition*. CRC Press.

Moksnes, P. 2002. “The Relative Importance of Habitat-Specific Settlement, Predation and Juvenile Dispersal for Distribution and Abundance of Young Juvenile Shore Crabs Carcinus Maenas L.” *Journal of Experimental Marine Biology and Ecology* 271 (1): 41–73. https://doi.org/10.1016/S0022-0981(02)00041-2.

Moran, A. and P Marko. 2005. “A Simple Technique for Physical Marking of Larvae of Marine Bivalves.” *Journal of Shellfish Research* 24 (2): 567–71. https://doi.org/10.2983/0730-8000(2005)24[567:ASTFPM]2.0.CO;2.

Orr, J. C., V. J. Fabry, O. Aumont, L. Bopp, S. C. Doney, R. A. Feely, A. Gnanadesikan. 2005. “Anthropogenic Ocean Acidification over the Twenty-First Century and Its Impact on Calcifying Organisms.” *Nature* 437 (7059): 681–86. https://doi.org/10.1038/nature04095.

Palacios, R., D.A. Armstrong, and J. Orensanz. 2000. “Fate and Legacy of an Invasion: Extinct and Extant Populations of the Soft-Shell Clam (Mya Arenaria) in Grays Harbor (Washington).” *Aquatic Conservation: Marine and Freshwater Ecosystems* 10 (4): 279–303. https://doi.org/10.1002/1099-0755(200007/08)10:4<279::AID-AQC412>3.0.CO;2-I.

Renforth, P., and G. Henderson. 2017. “Assessing Ocean Alkalinity for Carbon Sequestration.” *Reviews of Geophysics* 55 (3): 636–74. https://doi.org/10.1002/2016RG000533.

Ricart, A. M., M.Ward, T. M. Hill, E. Sanford, K. J. Kroeker, Y.Takeshita, S. Merolla. 2021. “Coast-Wide Evidence of Low pH Amelioration by Seagrass Ecosystems.” *Global Change Biology* 27 (11): 2580–91. https://doi.org/10.1111/gcb.15594.

Ries, J.B., A. L. Cohen, and D.C. McCorkle. 2009. “Marine Calcifiers Exhibit Mixed Responses to CO2-Induced Ocean Acidification.” *Geology* 37 (12): 1131–34. https://doi.org/10.1130/G30210A.1.

Sabine, C. L., R. A. Feely, N. Gruber, R. M. Key, K. Lee, J. L. Bullister, R.Wanninkhof. 2004. “The Oceanic Sink for Anthropogenic CO2.” *Science* 305 (5682): 367–71. https://doi.org/10.1126/science.1097403.

Saderne, V., N. R. Geraldi, P. I. Macreadie, D. T. Maher, J. J. Middelburg, O. Serrano, H. Almahasheer, et al. 2019. “Role of Carbonate Burial in Blue Carbon Budgets.” *Nature Communications* 10 (1): 1106. https://doi.org/10.1038/s41467-019-08842-6.

Salisbury, J., M. Green, C. Hunt, and J. Campbell. 2008. “Coastal Acidification by Rivers:A Threat to Shellfish?” *Eos, Transactions American Geophysical Union* 89 (50): 513–513. https://doi.org/10.1029/2008EO500001.

Salter, N. 2018. “Ancient Clam Gardens Magnify Bivalve Production by Moderating Ambient Temperature and Enhancing Sediment Carbonate.” Burnaby, British Columbia, CA: Simon Fraser University.

Schindelin, J., I.Arganda-Carreras, E. Frise, V. Kaynig, M. Longair, T. Pietzsch, S.Preibisch. 2012. “Fiji: An Open-Source Platform for Biological-Image Analysis.” *Nature Methods* 9 (7): 676–82. https://doi.org/10.1038/nmeth.2019.

Schneider, T., G. DeAntoni, A. Hill, and A. Apodaca. 2018. “Indigenous Persistence and Foodways at the Toms Point Trading Post (CA-MRN-202), Tomales Bay, California.” *Journal of California and Great Basin Anthropology* 38 (1): 51–73.

Silbiger, N. J., and C. J. B. Sorte. 2018. “Biophysical Feedbacks Mediate Carbonate Chemistry in Coastal Ecosystems across Spatiotemporal Gradients.” *Scientific Reports* 8 (1): 796. https://doi.org/10.1038/s41598-017-18736-6.

Smith, S.V., J.T. Hollibaugh, S.J. Dollar, and S. Vink. 1991. “Tomales Bay Metabolism: C, N, P Stoichiometry and Ecosystem Heterotrophy at the Land-Sea Interface.” *Estuarine, Coastal and Shelf Science* 33 (3): 223–57. https://doi.org/10.1016/0272-7714(91)90055-G.

Stocker, T. F, D. Qin, G. K. Plattner, M. Tignor, S. K. Allen, J. Boschung, A. Nauels, Y. Xia, V. Bex, and P. M. Midgley. 2013. “IPCC, Climate Change 2013: The Physical Science Basis.” In *Working Group I Contribution to the Fifth Assessment Report of the Intergovernmental Panel on Climate Change*, 1552. Cambridge, U.K./New York, U.S.A: Cambridge.

Tadlock, S. 2019. "'One Day You're Gonna Know You Won't Starve Here':" *Thesis for Masters of Public Health, University of Washington*.

Takesue, R. K., and A. van Geen. 2004. "Mg/Ca, Sr/Ca, and Stable Isotopes in Modern and Holocene Protothaca Staminea Shells from a Northern California Coastal Upwelling Region." *Geochimica et Cosmochimica Acta* 68 (19): 3845–61. https://doi.org/10.1016/j.gca.2004.03.021.

Toniello, G., D. Lepofsky, G. Lertzman-Lepofsky, A. Salomon, and K. Rowell. 2019. "11,500 y of Human–Clam Relationships Provide Long- Term Context for Intertidal Management in the Salish Sea, British Columbia." *PNAS* 116 (44): 22106–14.

Waldbusser, G. G., B. Hales, C. J. Langdon, B. A. Haley, P. Schrader, E. L. Brunner, M. W. Gray, C.A. Miller, and I. Gimenez. 2015. "Saturation-State Sensitivity of Marine Bivalve Larvae to Ocean Acidification." *Nature Climate Change* 5 (3): 273–80. https://doi.org/10.1038/nclimate2479.

Wallace, R. B., H. Baumann, J. S. Grear, R. C. Aller, and C. J. Gobler. 2014. "Coastal Ocean Acidification: The Other Eutrophication Problem." *Estuarine, Coastal and Shelf Science* 148 (July): 1–13. https://doi.org/10.1016/j.ecss.2014.05.027.

Widdicombe, S., J. Spicer, and V. Kitidis. 2011. "Effects of Ocean Acidification on Sediment Fauna." *Ocean Acidification*, June, 176–91.

Zachos, J. C., G. R. Dickens, and R. E. Zeebe. 2008. "An Early Cenozoic Perspective on Greenhouse Warming and Carbon-Cycle Dynamics." *Nature* 451 (7176): 279–83. https://doi.org/10.1038/nature06588.

Zeebe, R. E., and D. Wolf-Gladrow. 2001. *CO2 in Seawater: Equilibrium, Kinetics, Isotopes*. Gulf Professional Publishing.

Zhao, X., W. Shi, Y. Han, S. Liu, C. Guo, W. Fu, X. Chai, and G. Liu. 2017. "Ocean Acidification Adversely Influences Metabolism, Extracellular pH and Calcification of an Economically Important Marine Bivalve, Tegillarca Granosa." *Marine Environmental Research* 125 (April): 82–89. https://doi.org/10.1016/j.marenvres.2017.01.007.

Chapter 3.

Utilizing RNA-sequencing to test if shell hash buffers the effects of experimental acidification on *Leukoma staminea* gene expression

Abstract

For calcifying organisms, it can be energetically costly to mineralize under acidic conditions. Here, I continue my investigation of juvenile Pacific littleneck clams' (*Leukoma staminea*) response to ocean acidification, and study the buffering capacity of shell hash using RNA-sequencing technology. Since adding calcium carbonate shell hash to sediments significantly alters the chemistry of pore fluids (see Chapter 2), I hypothesized that gene expression profiles in clams exposed to acidification would change when shell hash is present in their infaunal habitat. We assembled the first mantle transcriptome for *L. staminea*, and tested the hypotheses that 1) experimental acidification leads to the downregulation of genes involved in biomineralization, and 2) overall gene expression profiles of clams in the acidified + shell hash (pH = 7.4) treatment are more similar to the control (pH = 7.8) treatment. Juvenile clams were raised in four experimental conditions for 90 days: control seawater, acidified seawater, control seawater with shell hash, and acidified seawater with shell hash. Clam mantle tissue was sampled at day 90 for analysis of gene expression. Although few of the differentially expressed genes were successfully functionally-annotated (n=20), the data presented herein demonstrate that adding shell hash to sediments in which clams burrow yields gene expression profiles more similar to those in non-acidified conditions, supporting our hypothesis. Furthermore, this study identifies a suite of genetic markers that will be useful for future research on the biological impacts of ocean acidification on infaunal marine calcifiers.

1. Introduction

1.1. Using gene expression to test if shell hash can mitigate acidification effects

The oceans are acidifying as a result of rising anthropogenic carbon dioxide in the atmosphere, and coastal areas are at increased risk to acidification due to nutrient runoff, algal blooms and microbial decay (Orr et al. 2005; Gazeau et al. 2007; Feely et al. 2008; Wallace et al. 2014; Barton et al. 2015; Laurent et al. 2017; Doney et al. 2020; Kessouri et al. 2021). Mean global surface water pH levels have declined by ~0.1 units since the late 18th century, and will likely drop another 0.3 - 0.5 pH units by 2100 (Caldeira and Wickett 2005; Orr et al. 2005; Stocker et al. 2013). This poses risks to shellfish, including culturally, economically and ecologically important species like clams (Orr et al. 2005; Feely et al. 2012; Waldbusser et al. 2015; Schwaner et al. 2023). Here, I further test whether shell hash can buffer ocean acidification effects on infaunal clam biomineralization by investigating the gene expression of *Leukoma staminea* using RNA-sequencing (RNA-seq) technology. **We construct the first mantle transcriptome for *L. staminea* and test the hypothesis that gene expression profiles of clams raised in acidified seawater (pH = 7.4) buffered with shell hash are more similar to clams grown in control (pH = 7.8) conditions.** Clams grown in non-acidified and shell hash conditions may upregulate (i.e., produce more copies) of genes involved in shell formation, and/or have lower energetic demands than those in low pH conditions (Li et al. 2016; De Wit et al. 2018; Strader et al. 2020). Alternatively, clams exposed to shell hash may up/downregulate distinct genes from those in the other experimental conditions. Either way, RNA-sequencing of the mantle tissue can elucidate the genetic mechanisms underlying the species' biomineralization response to ocean acidification. Given the negative impact of experimental acidification on *L. staminea* shell growth ($p < 0.05$, see Chapter 2), we hypothesize that acidification leads to the downregulation of biomineralization genes expressed in the mantle.

1.2 Marine invertebrates have varying genetic responses to acidification

Clams and other molluscs secrete their shells using a specialized tissue called the mantle (Hüning et al. 2013; Wanninger and Wollesen 2019). A mantle transcriptome is the collection of RNA transcripts produced in the mantle tissue at a given time, and reveals *which* genes are actively being transcribed (or expressed) and *how much* transcription is occuring for each gene. Transcriptomes (whole-organism, cellular, and/or tissue-specific) change throughout an organism's life; they reveal how gene expression shifts in different environmental conditions and throughout ontogeny. In the context of rapid global change, transcriptomics can elucidate the molecular underpinnings of species-level responses to different environmental stressors (Strader et al. 2020, and references therein). Impacts of ocean acidification include: a decreased ability to biomineralize (as evidenced by deformed, thinner, and/or weaker shells or skeletons) (Stumpp et al. 2011; Moya et al. 2012; Moya et al. 2016; Li et al. 2016; De Wit et al. 2018; Zhao et al. 2020) and regulate acid-base ion transport (Kurihara et al. 2012; Davies et al. 2016; Li et al. 2016; Michael et al. 2016; Lee et al. 2019), metabolic depression (Todgham and Hofmann 2009; Hüning et al. 2013; Li et al. 2016; Peng et al. 2017; Zhao et al. 2017), reduced immunity (Schwaner et al. 2023), increased cellular stress response (Moya et al. 2015), and altered neural function and behavior (Peng et al. 2017; Johnson and Hofmann 2017; Porteus et al. 2018). Over time, marine organisms will exhibit varying levels of resilience to ocean acidification, depending on their abilities to both rapidly adapt and acclimate to new conditions (Ries et al. 2009; Ries 2011; Davies et al. 2016; Dodd et al. 2021; Gold and Vermeij 2023). Understanding species' ability to acclimate to acute stressors is helpful for predicting their long-term resilience in the face of environmental change. One method for investigating the molecular underpinnings of acclimation involves tracking organisms' transcriptomic response to laboratory-controlled changes in their environment (Davies et al. 2016; Johnson and Hofmann 2017). In an

evolutionary context, phenotypic plasticity in the face of acute, rapid environmental shifts can have a strong selective advantage, and thus be important for long term resilience.

The existing research on marine invertebrates' genetic response to ocean acidification is limited, and non-existent for *L. staminea*. Peng et al. (2017) documented that experimentally acidified seawater (pH = 7.4) affects adult razor clams (*Sinonovacula constricta)* via decreased metabolism and burrowing depth. Then, using quantitative real-time PCR, they argued that the changes in physiology and behavior were associated with an upregulation of "energy-producing genes" associated with the tricarboxylic acid pathway, such as citrate synthase genes, which are hypothesized to provide energy for foot movement (Peng et al. 2017). In pteropods, small free-swimming shelled molluscs, even a relatively small lowering in pH (pH = 7.71) caused the down-regulation of metabolism-related genes that produce carbonic anhydrase, glucose dehydrogenase and malate dehydrogenase (Johnson and Hofmann 2017). These genes are central to ATP production in metabolic pathways, the integrity of which may confer tolerance to environmental change (Johnson and Hofmann 2017). In sea urchins, the expression of *msp130*, a gene involved in transporting calcium ions to the site of calcification, has been suppressed under acidified (pCO_2 = 2,000 ppm) conditions (Kurihara et al. 2012). A number of candidate biomineralization genes have been identified in marine calcifiers in addition to *msp130*, including calmodulin-like protein, chitin synthases, C-type lectins, perlucin, and collagen associated transcripts (Kaniewska et al. 2012; Liu et al. 2012; Moya et al. 2012; Moya et al. 2016; De Wit et al. 2018). The cellular response to acidification involves many genes/pathways, is species-specific, and warrants further study, particularly among calcifying marine invertebrates (Johnson and Hofmann 2017; De Wit et al. 2018; Strader et al. 2020).

2. Methods

2.1 Experimental acidification experiment

Clams were raised in the following experimental conditions for 90 days prior to sampling for RNA-seq: (1) control seawater (overlying seawater pH=7.76 +/- 0.054), (2) experimentally acidified seawater (overlying seawater pH=7.38 +/- 0.055), (3) control seawater with shell hash added to the substrate (overlying seawater pH=7.76 +/- 0.049), and (4) acidified seawater with shell hash added to the substrate (overlying pH=7.38 +/- 0.056) (Kempf et al. *in prep*). Each treatment was run in technical duplicate in 22.7 L food-grade buckets. Buckets were filled with 5 L volume of unconsolidated medium-grained quartz sand with a porosity of 38.8% (AquaQuartz). Disarticulated clam shells were gathered in Bodega Bay, CA, bleached in 6 vol% NaOCl for 30 minutes, rinsed thoroughly with fresh water, and air dried for 48 hours. Cleaned shells were then crushed using a mortar and pestle, and size-graded to 0.25-0.5 cm. All shell hash treatments consisted of sand with 10 wt% pulverized *L. staminea* and *Saxidomus nuttalli*.

Treatment buckets were supplied with filtered seawater held in header tanks. Header tank pH conditions were controlled using PinPoint pH controllers and regulators connected to a cylinder of compressed air with 1% CO2 (Airgas). Every Monday and Friday, probes were recalibrated using PinPoint recalibration fluids (pH = 4.0 and pH = 10.0). Header tanks were supplied with air via an airstone to maintain oxygen levels. Once a week, samples for spectrophotometric total pH analyses were collected from the pore water and overlying water in each bucket. Water was collected in 125 mL glass bottles with a positive meniscus, immediately poisoned with mercuric chloride, and stored at 4°C unless analyzed immediately. Total pH samples were run in duplicate on an Ocean Optics Jaz Spectrophotometer EL200 (SD +/- 0.003) using m-cresol purple dye (Dickson et al., 2007). A calibration regression was produced for *m-cresol* and calibrated against Tris for a <0.1 pH offset (Kempf et al. *in prep*).

2.1 RNA extraction and quality control protocol

Total RNA was extracted from clam mantle tissue on day 90 of the experiment to test a possible linkage between the genetic effects of acidification to measurable differences in shell growth (Kempf et al. *in prep*). To extract RNA, a total of four biological replicates (i.e., four individuals) were sacrificed from each of the eight buckets at day 90 (n = 32). Total RNA was extracted from the mantle tissue using a TRIzol protocol (Figure 3.1). From each clam, approximately 50-100 mg of mantle tissue was removed from the mantle edge (i.e., the ridge of tissue near the ventral margin of the shell) using a surgical scalpel equipped with a new blade for each animal. Extractions were performed at ambient room temperature (~19°C) in a hood to avoid contamination. TRIzol (an acid guanidinium-phenol based reagent) was first added to each tissue sample within five minutes of sacrificing the animal, and homogenized using an electric pestle. Next, chloroform was added and the samples were centrifuged to separate the molecular phases. The top aqueous layer was transferred to a new sample tube, and an equal volume of isopropyl alcohol and 1 µl glycol blue was added. After centrifuging the samples again, the resulting RNA precipitate was washed with 100% ethanol and air dried before being dissolved in RNase free water (Figure 3.1).

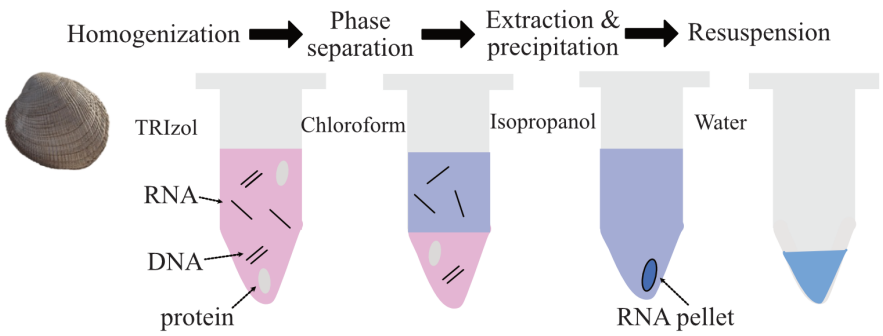

Figure 3.1. Simplified TRIzol protocol adapted from Chomczynski and Sacchi (2006).

Concentration and quality of extracted RNA were first evaluated using a NanoDrop spectrophotometer and QuBit fluorometer. Once assessed, samples were sent to the UC Davis DNA Technologies and Expression Analysis Core Laboratory, where the raw RNA was then run on an Agilent BioAnalyzer 2100, a microcapillary-based machine that uses electrophoresis, to evaluate quantity and quality of the RNA more rigorously. The highest quality samples (i.e., those with BioAnalyzer RNA integrity numbers > 7) were used for cDNA library prep and sequenced using Illumina High Throughput Sequencing (n=24 total, three per bucket). Samples were run on a NovaSeq 6000 S4 flow cell to produce ~25 million 150 base pair paired-end reads per sample for all 24 individuals. The quality of raw sequencing data (in .fastq format) was evaluated using fastQC to identify whether adapter sequences were present ("FastQC" 2015). Because adapters were present, we then used Trimmomatic to trim the first 15 base pairs from each read to remove adapters (Bolger et al. 2014) (Figures 3.2 and 3.3).

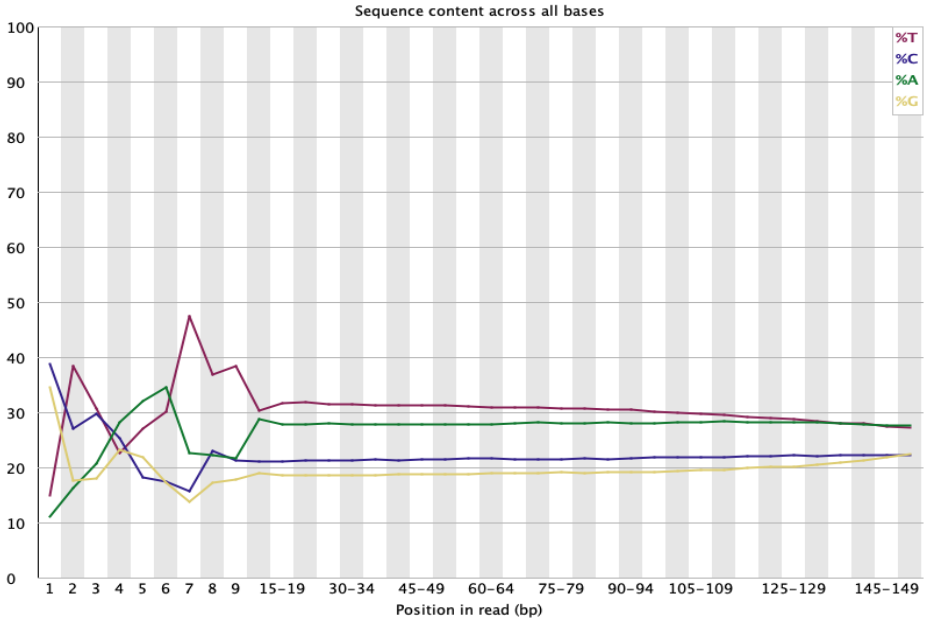

Figure 3.2. Example sequence from Illumina output before adapter trimming, visualized using FastQC. This sample is C1_B1. Colors depict the relative percentage of each of the nucleotides (A, T, C, G). The % of nucleotides should be relatively constant throughout the fragment; when they are not, adapters are present (i.e., position 1-15).

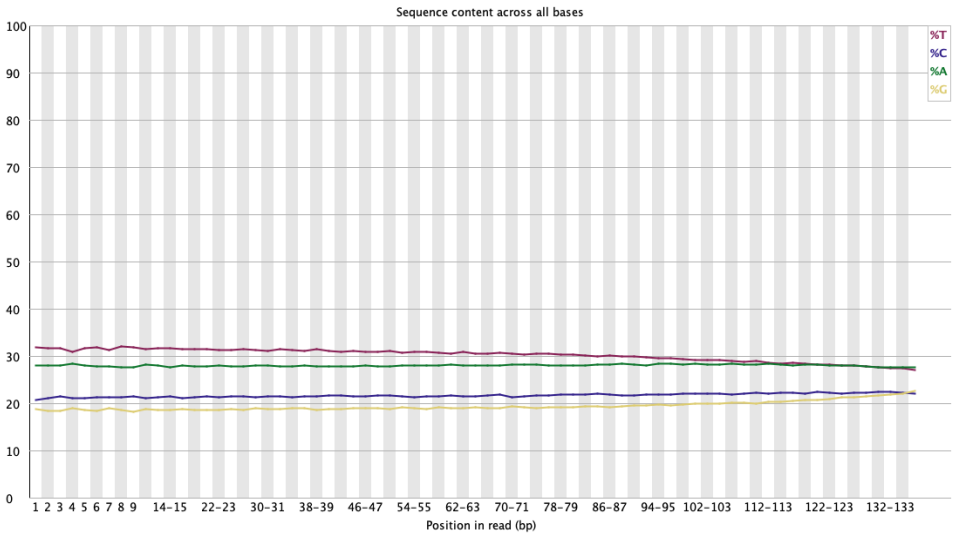

Figure 3.3. Post-adapter-removal sequence content, visualized using FastQC. Colors depict the relative percentage of each of the nucleotides (A, T, C, G). This sample is C1_B1, after removing the first 15 base pairs. This step was done for all sequences before building the mantle transcriptome in Trinity.

2.2. Mantle transcriptome assembly

As there is no published reference genome for *L. staminea*, we assembled *de novo* (i.e., reference-free) transcriptomes with the raw Illumina reads in Trinity (Grabherr et al. 2011). The amount of data produced from sequencing made it infeasible to create a reference transcriptome from all data (i.e., by combining multiple samples). Therefore, we tested multiple transcriptomes using individual paired-end datasets. We then used the sample with the most mapped reads as our reference transcriptome assembly for mapping (see below). Trinity implements three software modules (Inchworm, Chrysalis and Butterfly) to build a full transcriptome using de Bruijn graphs, a dynamic programming method based on overlap between sequences. The transcriptome was then functionally annotated using Trinotate (Bryant et al. 2017), a

comprehensive annotation suite designed for *de novo* transcriptomes, including a sequence similarity search (Uniprot/SwissProt), protein domain identification (HMMER and PFAM), protein signal peptides and transmembrane domain predictions (signalP and tmHMM), and eggNog mapper (Cantalapiedra et al. 2021).

2.3 Differential gene expression analysis

To determine which genes were differentially expressed across replicates and treatments, we used the R package edgeR (Robinson et al. 2010), which is part of the Trinity pipeline. Pairwise comparisons of gene expression were performed for all genes in all samples, and correlation heatmaps were produced to compare overall gene expression profile similarity across biological replicates. Genes were considered "differentially expressed" if there was a logarithm of fold change (logFC) $>|2|$ (i.e., a four-fold change in gene expression between experimental conditions) and a false-discovery rate adjusted p-value < 0.001. The logFC measures the relative expression of a gene, with positive numbers indicating a gene is upregulated in sample A relative to sample B, and negative numbers indicating downregulation of that gene in sample A relative to sample B. Differentially expressed genes were extracted from edgeR results and cross-referenced to the Trinotate annotation report. Differentially expressed genes were also annotated using the program Blast2Go (OmicsBox 3.1.9) to run BlastX, which searches the National Center for Biotechnology Information (NCBI) protein database using a translated nucleotide sequence, and identified the top 100 protein hits for each of our differentially expressed transcripts.

3. Results

3.1 Mantle transcriptome assembly and mapping results

Our reference *de novo* transcriptome was built using the SH2_B2 (i.e., shell hash bucket 2) sample. Samples were mapped and transcripts quantified via the alignment-free quantification method "kallisto" (Bray et al. 2016). All 24 samples, including SH2_B2, successfully mapped between 63.7-69.9 % reads, with average fragment lengths between 160-173 bp (Table 3.1). Illumina Technologies recommends 2-25 million reads/sample for analyses aimed at identifying highly expressed genes (see https://knowledge.illumina.com/library-preparation/rna-library-prep/library-preparation-rna-library-prep-reference_material-list/000001243) . As shown in Table 3.1, we observed 16-23 million reads mapped per sample, falling within this range. Future analyses will yield an improved transcriptome, which will likely increase our percent reads mapped, and help identify additional genes in downstream analyses.

Sample	Sample Name	Reads	Reads Mapped	% Mapped	Average fragment length
SRR25907743	C1_B1	30,918,626	21,261,655	68.80%	168.958
SRR25907726	C1_B2	30,041,091	20,746,147	69.10%	169.923
SRR25907742	C2_B1	34,980,982	22,522,740	64.40%	160.985
SRR25907725	C2_B2	34,198,240	23,382,574	68.40%	169.362
SRR25907731	C3_B1	28,455,643	19,895,781	69.90%	169.845
SRR25907724	C4_B2	29,708,902	19,578,869	65.90%	162.842
SRR25907739	OA2_B1	28,495,864	19,360,800	67.90%	164.695
SRR25907736	OA2_B2	20,636,968	13,728,781	66.50%	169.77
SRR25907738	OA3_B1	33,184,148	23,077,323	69.50%	163.252
SRR25907735	OA3_B2	30,025,393	20,198,139	67.30%	167.075
SRR25907737	OA4_B1	30,889,286	20,957,799	67.80%	170.346
SRR25907734	OA4_B2	29,244,674	19,841,571	67.80%	168.167
SRR25907733	OASH1_B1	24,314,306	16,065,973	66.10%	165.545
SRR25907729	OASH1_B2	25,711,404	17,205,721	66.90%	165.293
SRR25907732	OASH2_B1	32,102,419	21,696,268	67.60%	163.865
SRR25907728	OASH2_B2	29,774,393	19,947,844	67.00%	164.228
SRR25907730	OASH4_B1	32,545,028	20,717,851	63.70%	161.668
SRR25907727	OASH4_B2	24,684,861	17,251,875	69.90%	170.073
SRR25907723	SH1_B1	31,105,262	21,316,181	68.50%	165.817
SRR25907720	SH2_B2	36,046,389	24,433,874	67.80%	173.807
SRR25907741	SH3_B2	32,069,259	21,317,521	66.50%	166.862
SRR25907721	SH4_B1	29,217,347	19,649,177	67.30%	164.544
SRR25907740	SH4_B2	28,617,606	19,797,884	69.20%	167.535
SRR25907722	SH2_B1	31,114,042	20,709,014	66.60%	163.538

Table 3.1. Mapping results for our transcriptome. Sample SH2_B2 was used for transcriptome assembly. All samples (n=24) were mapped to the mantle transcriptome to identify any evidence of bias. All samples mapped to the reference transcriptome at 63.7-69.9%.

3.2 Differential gene expression

When including all 24 samples in the differential expression analysis, biological replicates cluster together except for two shell hash samples (SH3_B2 and SH1_B1), which plot with the control treatments in the logFC correlation matrix (Supplemental Figure 3.1). The gene expression of these samples may have truly been indistinguishable from the control treatment, and/or the shell hash may have had a small effect on gene expression in the mantle in these samples. However, this pattern could be due to other confounding variables. Therefore, we ultimately excluded these two samples from the following analysis (see "Discussion" for potential causes and directions for future work). After excluding these two samples, we observe an increase in the number of differentially expressed transcripts from 72 to 97. Of the 97, a total of 20 genes were successfully annotated via BlastX in the Blast2Go program (Table 3.2). As shown in Figure 3.4, gene expression profiles from samples in the same treatments generally cluster together, demonstrating that the four treatments (OA, OASH, SH, C) differentially affected *L. staminea* gene expression.

The OASH samples have gene expression profiles most like the C samples, with only four genes differentially expressed between them out of the 97 differentially expressed across all samples (Table 3.3; Figure 3.4). These results support our hypothesis that the presence of shell hash in an acidified environment would yield gene expression profiles more like clams in non-acidified conditions. These four genes were upregulated in the control relative to the OASH treatment, but lacked annotation (Tables 3.3 and 3.4). The SH and OA treatments had the

greatest number of differentially expressed genes, with 33 genes differentially expressed (Table 3.3). Of those 33 genes, 28 genes were downregulated in the OA treatment relative to the SH treatment, and 5 genes were upregulated in the OA treatment relative to the SH treatment (Table 3.4). When comparing C to SH treatments, 23 genes were differentially expressed, with 20 downregulated in the control relative to the SH, and 3 upregulated in the control relative to the SH treatment (Supplemental Sheet 3.2).

Of the genes that were differentially-expressed, few had functional annotations. Of the annotations available, many were understudied and uncharacterized proteins (Supplemental Sheet 3.2). For example in the OA vs. SH comparison, TRINITY_DN107511_c0_g1 (Hypothetical predicted protein) was downregulated, and in the OA vs. OASH comparison, TRINITY_DN13247_c0_g1 (Uncharacterized protein LOC123526437) was downregulated. In the OASH vs. SH comparison, TRINITY_DN17470_c0_g3 (Insoluble matrix shell protein 2-like) was upregulated. Insoluble proteins serve as a surface for crystal growth and serve as the scaffold upon which biominerals nucleate and develop, while soluble shell matrix proteins determine the mineralogical properties of the shell (Song et al. 2019; Rivera-Perez et al. 2020).

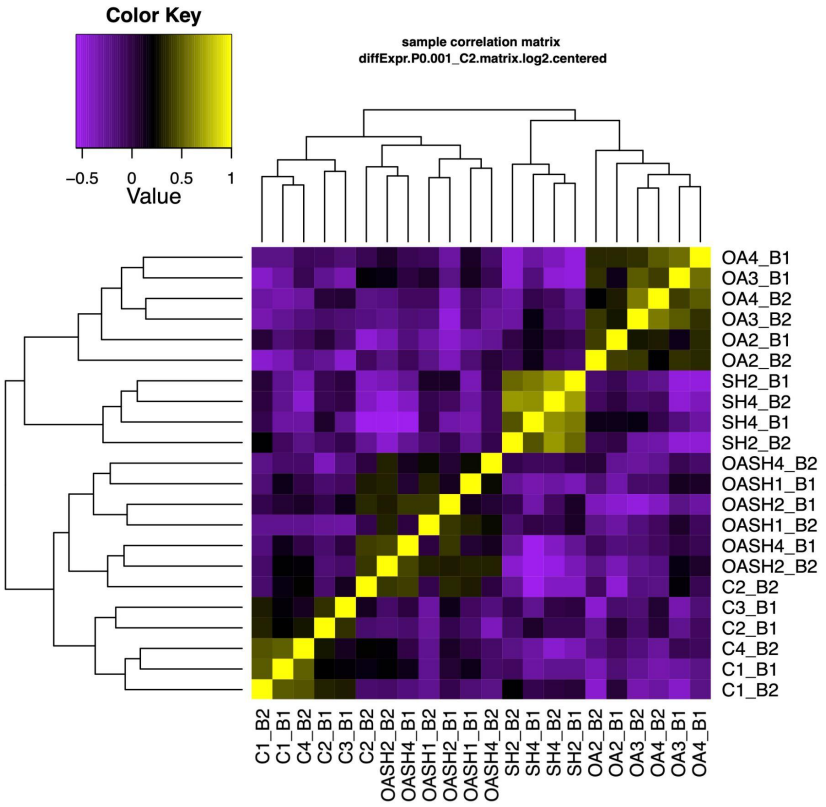

Figure 3.4. Sample correlation matrix heat map. Each row and column represents a single biological sample (i.e., one animal).Warmer colors (yellow) represent a positive correlation in expression profiles (i.e., value of 1 means the samples are identical), and cooler colors (purple) indicate a negative correlation. Black represents neutral or no correlation. Dendrograms on the x and y axes depict clustering of samples, where samples that cluster together have holistically more similar gene expression profiles.

Trancript Name	Description	Length (bp)	#BlastX Hits	Mollusc-specific?
TRINITY_DN71273_c0_g1_i1	Cubilin	203	100	no
TRINITY_DN102907_c0_g1_i1	uncharacterized protein LOC123537936	207	100	no
TRINITY_DN15969_c0_g1_i1	E3 ubiquitin-protein ligase HERC2-like	209	100	no
TRINITY_DN107511_c0_g1_i1	Hypothetical predicted protein	209	100	no
TRINITY_DN91018_c0_g1_i1	Hypothetical predicted protein	312	100	no
TRINITY_DN2701_c0_g1_i1	E3 ubiquitin-protein ligase rnf213-alpha-like isoform X1	1577	100	no
TRINITY_DN2197_c0_g1_i2	Serine/threonine-protein kinase/endoribonuclease IRE1 isoform X1	1916	100	no
TRINITY_DN81556_c0_g1_i1	Para-nitrobenzyl esterase-like	297	63	no
TRINITY_DN19940_c0_g2_i1	Uncharacterized protein LOC123554133	201	41	no
TRINITY_DN17470_c0_g3_i1	Insoluble matrix shell protein 2-like	431	9	yes
TRINITY_DN13247_c0_g1_i1	Uncharacterized protein LOC123526437	658	7	yes
TRINITY_DN32447_c0_g1_i2	CorA family divalent cation transporter	207	4	no
TRINITY_DN97679_c0_g1_i1	WP_207305327.1DUF5983 family protein	271	3	no
TRINITY_DN93036_c0_g1_i1	Hypothetical protein MAR_005918, partial	207	2	yes
TRINITY_DN68078_c0_g1_i1	Golgin subfamily A member 6-like protein 22 isoform X1	259	2	yes
TRINITY_DN28814_c6_g1_i1	Hypothetical protein DPMN_054990	261	2	yes
TRINITY_DN70406_c0_g1_i1	Hypothetical protein, partial	209	1	no
TRINITY_DN2376_c1_g3_i1	WAR18128.1XFIN-like protein	210	1	yes
TRINITY_DN1590_c0_g1_i3	WP_207305327.1DUF5983 family protein	263	1	no
TRINITY_DN9047_c0_g1_i1	Uncharacterized protein LOC123538794	621	1	yes

Table 3.2. List of differentially expressed genes with BlastX hits (n=20).

	C	OA	OASH	SH
C	0	13	4	23
OA	13	0	17	33
OASH	4	17	0	19
SH	23	33	19	0

Table 3.3. Matrix showing pairwise relationship in differentially expressed genes between treatments. For example, C vs. OA has 13 genes that are differentially expressed. Transcript names and their up/down-regulation patterns can be found in Supplemental Sheet 3.2.

Transcript Name	sampleA	sampleB	logFC	PValue	Annotation
TRINITY_DN887_c16_g1	OA	SH	-10.805043	5.74E-08	NA
TRINITY_DN3612_c0_g4	OA	SH	-8.9955051	6.23E-18	NA
TRINITY_DN23098_c1_g1	OA	SH	-8.8351966	3.35E-12	NA
TRINITY_DN1195_c5_g1	OA	SH	-8.5444688	4.76E-08	NA
TRINITY_DN65559_c0_g1	OA	SH	-8.5163191	7.98E-09	NA
TRINITY_DN10706_c0_g1	OA	SH	-8.4677864	1.37E-12	NA
TRINITY_DN74692_c0_g1	OA	SH	-8.3761786	4.94E-08	NA
TRINITY_DN12008_c1_g2	OA	SH	-8.3565195	1.73E-13	NA
TRINITY_DN867_c12_g1	OA	SH	-8.3181613	1.04E-07	NA
TRINITY_DN81556_c0_g1	OA	SH	-8.2348529	1.39E-10	Para-nitrobenzyl esterase-like
TRINITY_DN107511_c0_g1	OA	SH	-8.0115808	4.23E-10	Hypothetical predicted protein
TRINITY_DN463_c39_g1	OA	SH	-7.8927725	2.78E-08	NA
TRINITY_DN7580_c1_g1	OA	SH	-7.8382446	8.94E-09	NA
TRINITY_DN40151_c3_g1	OA	SH	-7.8340614	1.20E-07	NA
TRINITY_DN88036_c0_g1	OA	SH	-7.8098929	7.09E-09	NA
TRINITY_DN31954_c0_g1	OA	SH	-7.8047194	2.15E-08	NA
TRINITY_DN28714_c0_g2	OA	SH	-7.7894216	7.89E-09	NA
TRINITY_DN20933_c5_g1	OA	SH	-7.7840239	2.34E-07	NA
TRINITY_DN1382_c3_g1	OA	SH	-7.7729943	2.27E-08	NA
TRINITY_DN29520_c1_g2	OA	SH	-7.7586879	6.32E-08	NA
TRINITY_DN39274_c1_g1	OA	SH	-7.7423529	5.28E-08	NA
TRINITY_DN8976_c3_g1	OA	SH	-7.7086849	1.59E-07	NA
TRINITY_DN48436_c0_g1	OA	SH	-7.6330118	1.27E-07	NA
TRINITY_DN80892_c0_g1	OA	SH	-7.597563	2.85E-08	NA
TRINITY_DN78746_c0_g1	OA	SH	-7.5731837	7.88E-08	NA
TRINITY_DN10425_c4_g1	OA	SH	-7.4882725	2.27E-07	NA
TRINITY_DN73126_c0_g1	OA	SH	-7.4757229	4.85E-08	NA
TRINITY_DN119343_c0_g1	OA	SH	2.26532628	1.84E-07	NA
TRINITY_DN51632_c0_g1	OA	SH	6.94163104	1.30E-10	NA
TRINITY_DN28814_c6_g1	OA	SH	7.46394672	1.06E-07	Hypothetical protein DPMN_054990
TRINITY_DN16265_c0_g2	OA	SH	8.07128819	1.23E-08	NA
TRINITY_DN3939_c2_g1	OA	SH	8.90384527	3.07E-10	NA
TRINITY_DN29822_c0_g2	OA	SH	9.9306222	5.35E-08	NA

Table 3.4. Transcripts differentially expressed between SH (pH = 7.8) and OA treatments (pH = 7.4), which had 33 genes differentially expressed. The logarithm of fold change (logFC) measures the relative expression of a gene, with positive numbers indicating the gene is upregulated in sampleA (C) relative to sampleB (OA), and negative numbers indicate downregulation of that gene in C relative to OA. Annotations from Blast2Go.

4. Discussion

The RNA-seq data presented here suggests that adding shell hash to sediments can mitigate the molecular, in addition to the geochemical, effects of ocean acidification. Despite limited information on the functions of the differentially expressed genes presented here, our results support the hypothesis that clams exposed to acidification buffered with shell hash have gene expression profiles more similar to those in non-acidified conditions, as measured via

logFC differences in gene expression (Figure 3.4). These results support our findings that clams grown with shell hash have higher mean growth rate during a 90-day experimental acidification experiment (see Chapter 2). Some of the differentially expressed genes are "uncharacterized" proteins that appear restricted to molluscs (Supplemental Figure 3.2; Supplemental Sheet 3.1).

Because we specifically targeted the mantle tissue (i.e., the tissue that secretes the shell), at least some of these proteins may be shell matrix proteins, which are understudied, but required for biomineralization and serve as the scaffold upon which mineralized structures are built (Weiner and Dove 2003; Addadi et al. 2006). Recent studies have used various techniques to characterize and study shell matrix proteins including: gene cloning, *in situ* hybridization, immunohistochemistry, isolation by chromatography, antibody staining, and mass spectrometry-based protein analyses, coupled with high-throughput genomic, proteomic, transcriptomic data (Mann et al. 2012; C. Liu et al. 2015; Song et al. 2019 and references therein). A general lack of data on shell matrix proteins in calcifying marine invertebrates, and molluscs in particular, presents a barrier not only to understanding these organisms' responses to contemporary global change, but also their phylogenetic histories and how biomineralization has evolved over geologic history (Strader et al. 2020; Yarra et al. 2021). By identifying transcripts that lack annotation but are clearly affected by experimental acidification, and linking them with differences in growth, this project will motivate research focused on understanding the specific role of these novel transcripts, and molluscan biomineralization more broadly.

Our genetic data reveals distinct biological responses to the four experimental conditions (OA, OASH, C and SH), adding to our data on measured growth. As discussed in Chapter 2, the mean percent new shell growth was lowest in the OA treatment (5.65 +/- 3.5), followed by OASH (7.46 +/- 3.35), then C (8.30 +/- 4.24), and finally SH (9.38 +/- 7.24). Two-way

ANOVAs revealed that these differences were driven primarily by the overlying pH (p = 0.0173), not presence/absence of shell hash (p = 0.085), suggesting that growth is deleteriously affected by acidification, but not buffered by shell hash in a statistically-significant manner (but see Holland 2019). Our genetic results presented here generally corroborate these trends, with the OA and SH treatments showing the most distinct gene expression profiles. Further, clams from the OA treatment experienced both the lowest growth rates and the largest number of downregulated genes (n=28). The lack of statistical difference in measurable shell growth in the presence of shell hash may be caused by the starting size variability in the animals. In other words, the underlying genetic variability within the population may have had a larger effect on growth rate than the presence of shell hash. In the future, studying individuals of the same *size*– as well as age and genetic cohort–may address these questions.

Some studies using RNA-seq to examine whole-organism acidification response have revealed thousands of annotatable transcripts when a reference genome is available (Johnson and Hofmann 2017), while others have yielded results more similar to ours (i.e., less than 100 annotations) (De Wit et al. 2018). Because this study investigated a specific tissue (the mantle, rather than the whole organism) a relatively small number of transcripts (n=97) drove the differences in the gene expression profiles observed here. Samples here mapped at a rate of ~63-70% to the reference transcriptome, which may be missing lowly-expressed and/or sample-specific transcripts. Further, as mentioned above, samples SH3_B2 and SH1_B1 were excluded from differential expression analyses due to their gene expression profiles plotting separately from the other shell hash samples in edgeR (Supplemental Figure 3.1). These samples likely plotted away from other SH samples due to minor differences in the amount of mantle tissue sampled during the RNA extraction protocol. In the future, an improved transcriptome in which

we combine one sample from each experimental treatment, may address some of these complications, and provide a better understanding of *L. staminea* genetic response to acidification and shell hash.

Future research should also document how gene expression varies across life stages in response to ocean acidification (i.e., planktonic larvae vs. infaunal adults). While post-settlement juveniles were studied here, more research on ocean acidification response is needed on planktonic larval stages, given their small, thin shells and increased vulnerability to ocean acidification (De Wit et al. 2018; Bashevkin et al. 2020). Future work should also incorporate population-level studies and field observations to link experimental acidification results with field data. As discussed in Chapter 2, field studies investigating the role that shell hash plays in moderating pore water chemistry have varying results (Green et al. 2009; 2013; Greiner et al. 2018; Beal et al. 2020; Doyle and Bendell 2022; Curtin et al. 2022), and population-level responses to this mitigation strategy (and ocean acidification more broadly) have not been investigated using genetic tools for *L. staminea.* The California Current System contains a complex mosaic of oceanographic conditions, and clam populations are likely locally adapted to their unique environmental conditions (i.e., low upwelling vs. seasonally high upwelling sites), which could yield differential responses to acidification (Hickey and Banas 2003; Griffiths et al. 2019; Largier 2020). Comparative transcriptomics studies using animals from naturally variable environmental settings may provide more insight to population-level responses. In all, the implementation of shell hash as a localized ocean acidification mitigation strategy should be considered on a site-by-site basis and will require more research to be scaled regionally. The California coastline, given its variable oceanographic conditions and widespread presence of *L.*

staminea populations, could be an ideal study system to investigate these questions in the future, particularly for infaunal species.

5. Conclusions

Adding shell hash to juvenile clams' infaunal environment mitigated the biological effects of experimental acidification, as evidenced by a holistic analysis of their gene expression. Clams grown in OASH conditions and C conditions had only four genes differentially expressed, all of which were upregulated in the C relative to the OASH samples, and the percent new growth between these conditions was not statistically different ($p > 0.05$). SH and OA gene expression profiles were the most distinct from each other with 33 genes differentially expressed, 28 of which were downregulated in the OA condition. These results support the data presented in Chapter 2, which demonstrate that growth is deleteriously affected by acidification in a statistically-significant manner. Some of the differentially genes, extracted from the mantle (which mineralizes the shell), especially those downregulated in OA conditions, may be shell matrix proteins, but further work is needed. We expect an improved *L. staminea* mantle transcriptome will yield more genes that can be annotated in ongoing studies, which will provide more information on the specific physiological effects of acidification on *L. staminea*. Furthermore, implementation of shell hash buffering in coastal settings will require more information on site-specific biogeochemical properties, and population-level responses to acidification. In all, this study provides novel insight into the genetic mechanisms of infaunal clam biomineralization in a rapidly changing ocean.

References

Addadi, L., D. Joester, F. Nudelman, and S. Weiner. 2006. "Mollusk Shell Formation: A Source of New Concepts for Understanding Biomineralization Processes." *Chemistry – A European Journal* 12 (4): 980–87. https://doi.org/10.1002/chem.200500980.

Barton, A., G. Waldbusser, R. Feely, S. Weisberg, J. Newton, B. Hales, S.Cudd, et al. 2015. "Impacts of Coastal Acidification on the Pacific Northwest Shellfish Industry and Adaptation Strategies Implemented in Response." *Oceanography* 25 (June): 146–59. https://doi.org/10.5670/oceanog.2015.38.

Bashevkin, S. M., C. D. Dibble, R. P. Dunn, J. A. Hollarsmith, G. Ng, E. V. Satterthwaite, and S. G. Morgan. 2020. "Larval Dispersal in a Changing Ocean with an Emphasis on Upwelling Regions." *Ecosphere* 11 (1): 1–29.

Beal, B. F., C. R. Coffin, S. F. Randall, C. A. Goodenow, K. E. Pepperman, and B. W. Ellis. 2020. "Interactive Effects of Shell Hash and Predator Exclusion on 0-Year Class Recruits of Two Infaunal Intertidal Bivalve Species in Maine, USA." *Journal of Experimental Marine Biology and Ecology* 530–531 (September): 151441. https://doi.org/10.1016/j.jembe.2020.151441.

Bolger, A. M., M. Lohse, and B. Usadel. 2014. "Trimmomatic: A Flexible Trimmer for Illumina Sequence Data." *Bioinformatics* 30 (15): 2114–20. https://doi.org/10.1093/bioinformatics/btu170.

Bray, N. L., H. Pimentel, P. Melsted, and L. Pachter. 2016. "Near-Optimal Probabilistic RNA-Seq Quantification." *Nature Biotechnology* 34 (5): 525–27.

Bryant, D. M., K. Johnson, T. DiTommaso, T. Tickle, M. Brian Couger, D. Payzin-Dogru, T. J. Lee, et al. 2017. “A Tissue-Mapped Axolotl De Novo Transcriptome Enables Identification of Limb Regeneration Factors.” *Cell Reports* 18 (3): 762–76. https://doi.org/10.1016/j.celrep.2016.12.063.

Caldeira, K., and M. E. Wickett. 2005. “Ocean Model Predictions of Chemistry Changes from Carbon Dioxide Emissions to the Atmosphere and Ocean.” *Journal of Geophysical Research: Oceans* 110 (C9). https://doi.org/10.1029/2004JC002671.

Cantalapiedra, C. P, A. Hernández-Plaza, I. Letunic, P. Bork, and J. Huerta-Cepas. 2021. “eggNOG-Mapper v2: Functional Annotation, Orthology Assignments, and Domain Prediction at the Metagenomic Scale.” *Molecular Biology and Evolution* 38 (12): 5825–29. https://doi.org/10.1093/molbev/msab293.

Chomczynski, P. and N. Sacchi. 2006. “The Single-Step Method of RNA Isolation by Acid Guanidinium Thiocyanate-Phenol-Chloroform Extraction: Twenty-Something Years On.” *Nature Protocols* 1 (2): 581–85. https://doi.org/10.1038/nprot.2006.83.

Curtin, T. P., N.Volkenborn, I. P. Dwyer, R. C. Aller, Q. Zhu, and C. J. Gobler. 2022. “Buffering Muds with Bivalve Shell Significantly Increases the Settlement, Growth, Survival, and Burrowing of the Early Life Stages of the Northern Quahog, Mercenaria Mercenaria, and Other Calcifying Invertebrates.” *Estuarine, Coastal and Shelf Science* 264 (January): 107686. https://doi.org/10.1016/j.ecss.2021.107686.

Davies, S.W., A. Marchetti, J. B. Ries, and K. D. Castillo. 2016. “Thermal and pCO2 Stress Elicit Divergent Transcriptomic Responses in a Resilient Coral.” *Frontiers in Marine Science* 3. https://www.frontiersin.org/articles/10.3389/fmars.2016.00112.

De Wit, P., E. Durland, A. Ventura, and C. J. Langdon. 2018. “Gene Expression Correlated with Delay in Shell Formation in Larval Pacific Oysters (Crassostrea Gigas) Exposed to Experimental Ocean Acidification Provides Insights into Shell Formation Mechanisms.” *BMC Genomics* 19 (1): 160. https://doi.org/10.1186/s12864-018-4519-y.

Dodd, L. F., J. H. Grabowski, M. F. Piehler, I. Westfield, and J. B. Ries. 2021. “Juvenile Eastern Oysters More Resilient to Extreme Ocean Acidification than Their Mud Crab Predators.” *Geochemistry, Geophysics, Geosystems* 22 (2): e2020GC009180. https://doi.org/10.1029/2020GC009180.

Doney, S. C., D. S. Busch, S. R. Cooley, and K. J. Kroeker. 2020. “The Impacts of Ocean Acidification on Marine Ecosystems and Reliant Human Communities.” *Annual Review of Environment and Resources* 45 (1): 83–112. https://doi.org/10.1146/annurev-environ-012320-083019.

Doyle, B., and L. I. Bendell. 2022. “An Evaluation of the Efficacy of Shell Hash for the Mitigation of Intertidal Sediment Acidification.” *Ecosphere* 13 (3): e4003. https://doi.org/10.1002/ecs2.4003.

Andrews, S. (2010). FastQC: A Quality Control Tool for High Throughput Sequence Data [Online]. Available online at: http://www.bioinformatics.babraham.ac.uk/projects/fastqc/

Feely, R. A, T. Klinger, J. A Newton, and M. Chadsey. 2012. “Scientific Summary of Ocean Acidification in Washington State Marine Waters.” NOAA OAR Special Report.

Feely, R. A., C. L. Sabine, J. M.Hernandez-Ayon, D. Ianson, and B. Hales. 2008. “Evidence for Upwelling of Corrosive ‘Acidified’ Water onto the Continental Shelf.” *Science* 320

(5882): 1490–92. https://doi.org/10.1126/science.1155676.

Gazeau, F., C.Quiblier, J. M. Jansen, J. Gattuso, J. J. Middelburg, and C. H. R. Heip. 2007. "Impact of Elevated CO2 on Shellfish Calcification." *Geophysical Research Letters* 34 (7). https://doi.org/10.1029/2006GL028554.

Gold, D. A., and G. J. Vermeij. 2023. "Deep Resilience: An Evolutionary Perspective on Calcification in an Age of Ocean Acidification." *Frontiers in Physiology* 14. https://www.frontiersin.org/articles/10.3389/fphys.2023.1092321.

Grabherr, M., G. Brian, J. Haas, M. Yassour, J. Z. Levin, D. A. Thompson, I. Amit, X. Adiconis, et al. 2011. "Full-Length Transcriptome Assembly from RNA-Seq Data without a Reference Genome." *Nature Biotechnology* 29 (7): 644–52. https://doi.org/10.1038/nbt.1883.

Green, M. A., G. G. Waldbusser, L. Hubazc, E. Cathcart, and J. Hall. 2013. "Carbonate Mineral Saturation State as the Recruitment Cue for Settling Bivalves in Marine Muds." *Estuaries and Coasts* 36 (1): 18–27. https://doi.org/10.1007/s12237-012-9549-0.

Green, M. A., G. G. Waldbusser, S. L. Reilly, K. Emerson, and S. O'Donnell. 2009. "Death by Dissolution: Sediment Saturation State as a Mortality Factor for Juvenile Bivalves." *Limnology and Oceanography* 54 (4): 1037–47.

Greiner, C. M., T. Klinger, J. L. Ruesink, J. S. Barber, and M. Horwith. 2018. "Habitat Effects of Macrophytes and Shell on Carbonate Chemistry and Juvenile Clam Recruitment, Survival, and Growth." *Journal of Experimental Marine Biology and Ecology* 509 (December): 8–15. https://doi.org/10.1016/j.jembe.2018.08.006.

Griffiths, J. S., T. Francis Pan, and M. W. Kelly. 2019. “Differential Responses to Ocean Acidification between Populations of Balanophyllia Elegans Corals from High and Low Upwelling Environments.” *Molecular Ecology* 28 (11): 2715–30. https://doi.org/10.1111/mec.15050.

Hickey, B. M., and N. S. Banas. 2003. “Oceanography of the U.S. Pacific Northwest Coastal Ocean and Estuaries with Application to Coastal Ecology.” *Estuaries* 26 (4): 1010–31. https://doi.org/10.1007/BF02803360.

Holland, S. M. 2019. “Estimation, Not Significance.” *Paleobiology* 45 (1): 1–6. https://doi.org/10.1017/pab.2018.43.

Hüning, A. K., F. Melzner, J. Thomsen, M. A. Gutowska, L. Krämer, S. Frickenhaus, P. Rosenstiel, H. Pörtner, E. E. R. Philipp, and M. Lucassen. 2013. “Impacts of Seawater Acidification on Mantle Gene Expression Patterns of the Baltic Sea Blue Mussel: Implications for Shell Formation and Energy Metabolism.” *Marine Biology*, 160(8), 1845-1861, Https://Doi.Org/10.1007/S00227-012-1930-9.

Johnson, K. M., and G. E. Hofmann. 2017. “Transcriptomic Response of the Antarctic Pteropod Limacina Helicina Antarctica to Ocean Acidification.” *BMC Genomics* 18 (1): 812. https://doi.org/10.1186/s12864-017-4161-0.

Kaniewska, P., P. R. Campbell, D. I. Kline, M. Rodriguez-Lanetty, D. J. Miller, S. Dove, and O. Hoegh-Guldberg. 2012. “Major Cellular and Physiological Impacts of Ocean Acidification on a Reef Building Coral.” *PLOS ONE* 7 (4): e34659. https://doi.org/10.1371/journal.pone.0034659.

Kessouri, F., J. C. McWilliams, D. Bianchi, M. Sutula, L. Renault, C. Deutsch, R. A. Feely, et al. 2021. “Coastal Eutrophication Drives Acidification, Oxygen Loss, and Ecosystem Change in a Major Oceanic Upwelling System.” *Proceedings of the National Academy of Sciences* 118 (21): e2018856118. https://doi.org/10.1073/pnas.2018856118.

Kurihara, H., Y. Takano, D. Kurokawa, and K.Akasaka. 2012. “Ocean Acidification Reduces Biomineralization-Related Gene Expression in the Sea Urchin, Hemicentrotus Pulcherrimus.” *Marine Biology* 159 (12): 2819–26. https://doi.org/10.1007/s00227-012-2043-1.

Largier, J. L. 2020. “Upwelling Bays: How Coastal Upwelling Controls Circulation, Habitat, and Productivity in Bays.” *Annual Review of Marine Science* 12 (1): 415–47. https://doi.org/10.1146/annurev-marine-010419-011020.

Laurent, A., K. Fennel, W. Cai, W. Huang, L. Barbero, and R. Wanninkhof. 2017. “Eutrophication-Induced Acidification of Coastal Waters in the Northern Gulf of Mexico: Insights into Origin and Processes from a Coupled Physical-Biogeochemical Model.” *Geophysical Research Letters* 44 (2): 946–56. https://doi.org/10.1002/2016GL071881.

Lee, H., M. Stumpp, J. Yan, Y. Tseng, S. Heinzel, and M. Yong-An Hu. 2019. “Tipping Points of Gastric pH Regulation and Energetics in the Sea Urchin Larva Exposed to CO2 - Induced Seawater Acidification.” *Comparative Biochemistry and Physiology. Part A, Molecular & Integrative Physiology* 234 (August): 87–97. https://doi.org/10.1016/j.cbpa.2019.04.018.

Li, S., J. Huang, C. Liu, Y. Liu, G. Zheng, L. Xie, and R. Zhang. 2016. “Interactive Effects of Seawater Acidification and Elevated Temperature on the Transcriptome and

Biomineralization in the Pearl Oyster Pinctada Fucata." *Environmental Science & Technology* 50 (3): 1157–65. https://doi.org/10.1021/acs.est.5b05107.

Liu, C., S. Li, J. Kong, Y. Liu, T. Wang, L. Xie, and R. Zhang. 2015. "In-Depth Proteomic Analysis of Shell Matrix Proteins of Pinctada Fucata." *Scientific Reports* 5 (1): 17269. https://doi.org/10.1038/srep17269.

Liu, W., X. Huang, J. Lin, and M. He. 2012. "Seawater Acidification and Elevated Temperature Affect Gene Expression Patterns of the Pearl Oyster Pinctada Fucata." *PLOS ONE* 7 (3): e33679. https://doi.org/10.1371/journal.pone.0033679.

Mann, K., E. Edsinger-Gonzales, and M. Mann. 2012. "In-Depth Proteomic Analysis of a Mollusc Shell: Acid-Soluble and Acid-Insoluble Matrix of the Limpet Lottia Gigantea." *Proteome Science* 10 (1): 28. https://doi.org/10.1186/1477-5956-10-28.

Michael, K., C. M. Kreiss, M. Y. Hu, N. Koschnick, U. Bickmeyer, S. Dupont, H. Pörtner, and M. Lucassen. 2016. "Adjustments of Molecular Key Components of Branchial Ion and pH Regulation in Atlantic Cod (Gadus Morhua) in Response to Ocean Acidification and Warming." *Comparative Biochemistry and Physiology. Part B, Biochemistry & Molecular Biology* 193 (March): 33–46. https://doi.org/10.1016/j.cbpb.2015.12.006.

Moya, A., L. Huisman, E. E. Ball, D. C. Hayward, L. C. Grasso, C. M. Chua, H. N. Woo, J.-P. Gattuso, S. Foret, and D. J. Miller. 2012. "Whole Transcriptome Analysis of the Coral Acropora Millepora Reveals Complex Responses to CO2-Driven Acidification during the Initiation of Calcification." *Molecular Ecology* 21 (10): 2440–54. https://doi.org/10.1111/j.1365-294X.2012.05554.x.

Moya, A., L. Huisman, S. Forêt, J.-P. Gattuso, D. C. Hayward, E. E. Ball, and D. J. Miller. 2015. "Rapid Acclimation of Juvenile Corals to CO2 -Mediated Acidification by Upregulation of Heat Shock Protein and Bcl-2 Genes." *Molecular Ecology* 24 (2): 438–52. https://doi.org/10.1111/mec.13021.

Moya, A., E. L. Howes, T. Lacoue-Labarthe, S. Forêt, B. Hanna, M. Medina, P. L. Munday, et al. 2016. "Near-Future pH Conditions Severely Impact Calcification, Metabolism and the Nervous System in the Pteropod Heliconoides Inflatus." *Global Change Biology* 22 (12): 3888–3900. https://doi.org/10.1111/gcb.13350.

Orr, J. C., V. J. Fabry, O. Aumont, L. Bopp, S. C. Doney, R. A. Feely, A. Gnanadesikan, et al. 2005. "Anthropogenic Ocean Acidification over the Twenty-First Century and Its Impact on Calcifying Organisms." *Nature* 437 (7059): 681–86. https://doi.org/10.1038/nature04095.

Peng, C., X. Zhao, S. Liu, W. Shi, Y. Han, C. Guo, X. Peng, X. Chai, and G. Liu. 2017. "Ocean Acidification Alters the Burrowing Behaviour, Ca2+/Mg2+-ATPase Activity, Metabolism, and Gene Expression of a Bivalve Species, Sinonovacula Constricta." *Marine Ecology Progress Series* 575 (July): 107–17. https://doi.org/10.3354/meps12224.

Porteus, C. S., P. C. Hubbard, T. M. Uren Webster, R. van Aerle, A. V. M. Canário, E. M. Santos, and R. W. Wilson. 2018. "Near-Future CO2 Levels Impair the Olfactory System of a Marine Fish." *Nature Climate Change* 8 (8): 737–43. https://doi.org/10.1038/s41558-018-0224-8.

Ries, J. B. 2011. "A Physicochemical Framework for Interpreting the Biological Calcification Response to CO2-Induced Ocean Acidification." *Geochimica et Cosmochimica Acta* 75

(14): 4053–64. https://doi.org/10.1016/j.gca.2011.04.025.

Ries, J. B., A. L. Cohen, and D. C. McCorkle. 2009. “Marine Calcifiers Exhibit Mixed Responses to CO2-Induced Ocean Acidification.” *Geology* 37 (12): 1131–34. https://doi.org/10.1130/G30210A.1.

Rivera-Perez, C., I. A. Flores-Sánchez, J. J. O. Ramírez de Areyano, D. I. R. Posadas, and N. Y. Hernández-Saavedra. 2020. “A Shell Matrix Protein of Pinctada Mazatlanica Produces Nacre Platelets in Vitro.” *Scientific Reports* 10 (1): 20201. https://doi.org/10.1038/s41598-020-77320-7.

Robinson, M. D., D. J. McCarthy, and G. K. Smyth. 2010. “edgeR: A Bioconductor Package for Differential Expression Analysis of Digital Gene Expression Data.” *Bioinformatics* 26 (1): 139–40. https://doi.org/10.1093/bioinformatics/btp616.

Schwaner, C., S. Farhat, M. Barbosa, I. Boutet, A. Tanguy, E. Pales Espinosa, and B. Allam. 2023. “Molecular Features Associated with Resilience to Ocean Acidification in the Northern Quahog, Mercenaria Mercenaria.” *Marine Biotechnology* 25 (1): 83–99. https://doi.org/10.1007/s10126-022-10183-3.

Song, X., Z. Liu, L. Wang, and L. Song. 2019. “Recent Advances of Shell Matrix Proteins and Cellular Orchestration in Marine Molluscan Shell Biomineralization.” *Frontiers in Marine Science* 6. https://www.frontiersin.org/articles/10.3389/fmars.2019.00041.

Stocker, T. F., D. Qin, G. K. Plattner, M. Tignor, S. K. Allen, J. Boschung, A. Nauels, Y. Xia, V. Bex, and P. M. Midgley. 2013. “IPCC, Climate Change 2013: The Physical Science Basis.” In *Working Group I Contribution to the Fifth Assessment Report of the*

Intergovernmental Panel on Climate Change, 1552. Cambridge, U.K./New York, U.S.A: Cambridge.

Strader, M. E., J. M. Wong, and G. E. Hofmann. 2020. "Ocean Acidification Promotes Broad Transcriptomic Responses in Marine Metazoans: A Literature Survey." *Frontiers in Zoology* 17 (1): 7. https://doi.org/10.1186/s12983-020-0350-9.

Stumpp, M., J. Wren, F. Melzner, M. C. Thorndyke, and S. T. Dupont. 2011. "CO2 Induced Seawater Acidification Impacts Sea Urchin Larval Development I: Elevated Metabolic Rates Decrease Scope for Growth and Induce Developmental Delay." *Comparative Biochemistry and Physiology. Part A, Molecular & Integrative Physiology* 160 (3): 331–40. https://doi.org/10.1016/j.cbpa.2011.06.022.

Todgham, A. E., and G. E. Hofmann. 2009. "Transcriptomic Response of Sea Urchin Larvae Strongylocentrotus Purpuratus to CO2-Driven Seawater Acidification." *Journal of Experimental Biology* 212 (16): 2579–94. https://doi.org/10.1242/jeb.032540.

Waldbusser, G. G., B. Hales, C. J. Langdon, B. A. Haley, P. Schrader, E. L. Brunner, M. W. Gray, C. A. Miller, and I. Gimenez. 2015. "Saturation-State Sensitivity of Marine Bivalve Larvae to Ocean Acidification." *Nature Climate Change* 5 (3): 273–80. https://doi.org/10.1038/nclimate2479.

Wallace, R. B., H. Baumann, J. S. Grear, R. C. Aller, and C. J. Gobler. 2014. "Coastal Ocean Acidification: The Other Eutrophication Problem." *Estuarine, Coastal and Shelf Science* 148 (July): 1–13. https://doi.org/10.1016/j.ecss.2014.05.027.

Wanninger, A., and T. Wollesen. 2019. "The Evolution of Molluscs." *Biological Reviews* 94 (1):

102–15. https://doi.org/10.1111/brv.12439.

Weiner, S., and P. M. Dove. 2003. “An Overview of Biomineralization Processes and the Problem of the Vital Effect.” *Reviews in Mineralogy and Geochemistry* 54 (1): 1–29. https://doi.org/10.2113/0540001.

Yarra, T., M. Blaxter, and M. S. Clark. 2021. “A Bivalve Biomineralization Toolbox.” *Molecular Biology and Evolution* 38 (9): 4043–55. https://doi.org/10.1093/molbev/msab153.

Zhao, X., Y. Han, B. Chen, B. Xia, K. Qu, and G. Liu. 2020. “CO2-Driven Ocean Acidification Weakens Mussel Shell Defense Capacity and Induces Global Molecular Compensatory Responses.” *Chemosphere* 243 (March): 125415. https://doi.org/10.1016/j.chemosphere.2019.125415.

Zhao, X., W. Shi, Y. Han, S. Liu, C. Guo, W. Fu, X. Chai, and G. Liu. 2017. “Ocean Acidification Adversely Influences Metabolism, Extracellular pH and Calcification of an Economically Important Marine Bivalve, Tegillarca Granosa.” *Marine Environmental Research* 125 (April): 82–89. https://doi.org/10.1016/j.marenvres.2017.01.007.

Supplemental materials.

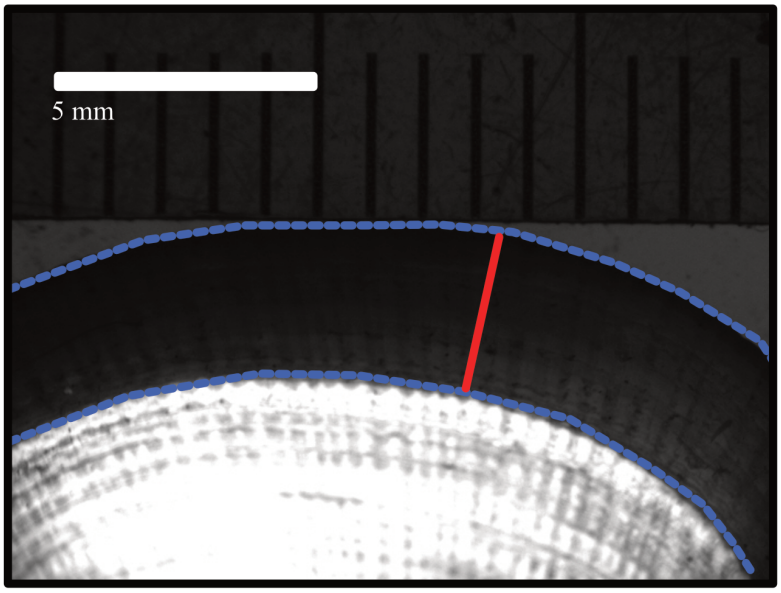

Supplemental Figure 2.1. Example fluorescent image of a calcein-stained shell. Area of the shell within the blue lines indicates shell growth during the duration of the experiment. Red line indicates the length of new growth.

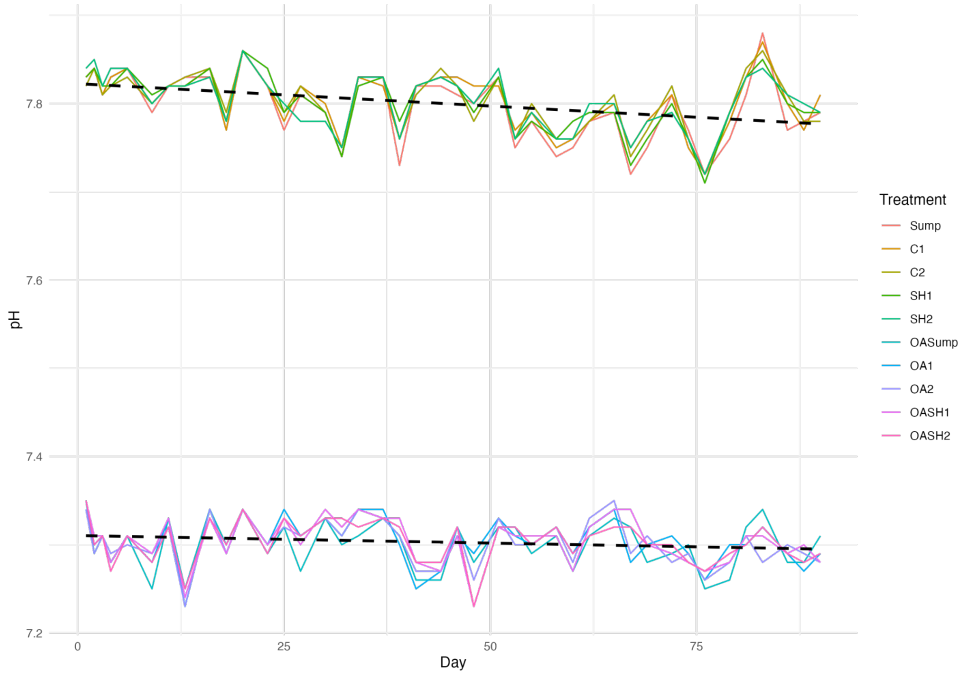

Supplemental Figure 2.2. pH measurements from PinPoint probes in the overlying water plotted over time for all buckets. Dotted lines show average for acidified and non-acidified treatments. OA = acidification, OASH = acidification + shell hash, C = control, and SH= control pH with shell hash.

	Overlying pH	**Pore pH**	**Overlying Ω**	**Pore Ω**	**DO**
OA	7.38 +/- 0.055	7.06 +/- 0.084	0.586 +/- 0.084	0.308 +/- 0.067	8.14 +/- 0.44
OASH	7.38 +/- 0.056	7.48 +/- 0.034	0.568 +/- 0.098	0.859 +/- 0.070	8.15 +/- 0.46
C	7.76 +/- 0.054	7.34 +/- 0.164	1.18 +/- 0.225	0.499 +/- 0.218	8.17 +/- 0.55
SH	7.76 +/- 0.049	7.65 +/- 0.040	1.19 +/- 0.193	0.958 +/- 0.107	8.14 +/- 0.55

Supplemental Table 2.1. Mean values and standard deviations for pH and aragonite saturation state (**Ω**) of overlying water and pore waters in the bucket treatments. Sample results here were taken once weekly for spectrophotometric pH analysis and alkalinity titrations. OA = acidification, OASH = acidification + shell hash, C = control, and SH= control pH with shell hash.

Fixed effects (treatment):				
Effect	**Estimate**	**Std. Error**	**t-value**	
Intercept (Control)	8.304	0.807	10.285	
OA	-2.656	1.166	-2.277	
OASH	-0.842	1.754	-0.716	
SH	1.075	1.206	0.891	
Random effects:				
Grouping	**Effect**	**Variance**	**%Variance**	**Std. Dev.**
Bucket ID	Intercept	0.03476	0.154	0.1864
Residual		22.49712	99.846	4.7431

Supplemental Table 2.2. Summary of linear mixed effects model fit to percent new shell for clams at the end of the 90-day experimental period. Fixed effects (i.e., treatment) have constant, systematic influence on the dependent variable (here, percent new shell). Random effects (i.e., bucket replicate ID) account for random variability not directly related to independent variables.

Supplemental Sheet 2.1. Complete list of raw total pH data.

Supplemental Sheet 2.2. Complete list of raw total alkalinity data.

Supplemental Sheet 2.3. Complete calculated carbonate system data using 'seacarb' in R.

Supplemental Sheet 2.4. Complete list of pH measurements using PinPoint probes.

Supplemental Sheet 2.5. Complete list of salinity measurements.

Supplemental Sheet 2.6. Complete list of dissolved oxygen measurements.

Supplemental Sheet 2.7. Complete list of temperature measurements.

Supplemental Sheet 2.8. Table with raw clam growth data measured day 90 of the experiment.

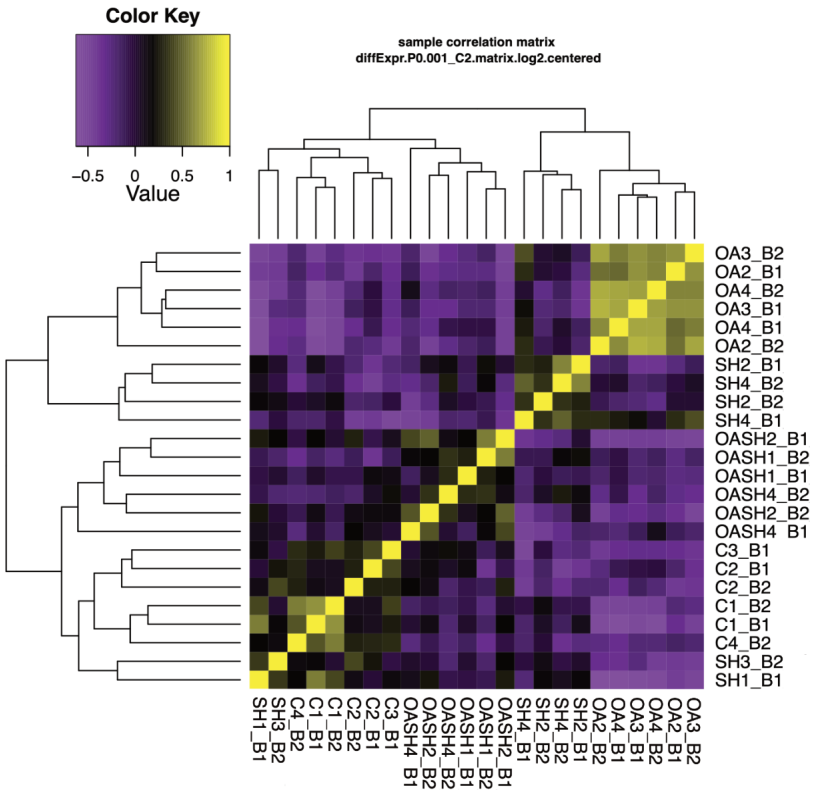

Supplemental Figure 3.1. Gene expression correlation matrix for all samples, including SH3_B2 and SH1_B1. Each row and column represent a biological sample. Color gradient represents the strength of the correlation, with warmer colors (yellow) representing a strong positive correlation, and cooler colors (purple) indicating a strong negative correlation. Black represents neutral or no correlation. Dendrograms depict clustering of samples, where samples that cluster together have more similar gene expression profiles.

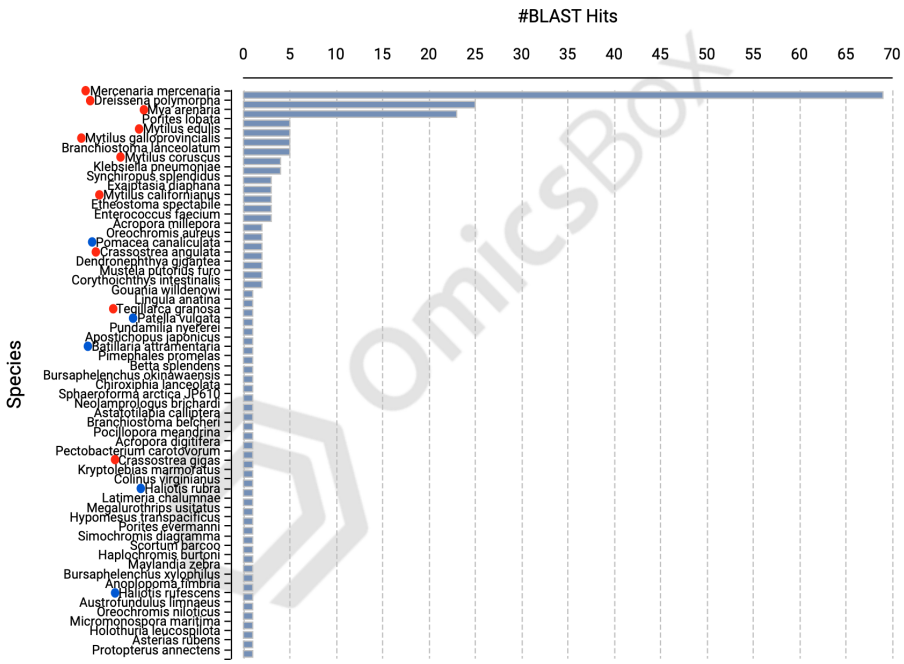

Supplemental Figure 3.2. Species with top 100 BlastX hits for differentially expressed genes. The species with the most hits, *Merceneria mercenaria*, is also a venerid clam. Species with a red dot are bivalve molluscs, and blue dots denote non-bivalve molluscs.

Supplemental Sheet 3.1. Complete list of differentially expressed transcripts and BlastX annotations, when available.

Supplemental Sheet 3.2. Log fold change in gene expression between all treatments. Red highlighted cells indicate replicate values. That is, these genes show up as differentially expressed in more than one pairwise comparison. Of those genes, six had BlastX hits.